The FERM protein EPB41L5 regulates actomyosin contractility and focal adhesion formation to maintain the kidney filtration barrier

Christoph Schell[a,b,1,2], Manuel Rogg[b,1], Martina Suhm[b,1], Martin Helmstädter[b], Dominik Sellung[b], Mako Yasuda-Yamahara[b,c], Oliver Kretz[b,d,e], Victoria Küttner[f,3], Hani Suleiman[g], Laxmikanth Kollipara[h], René P. Zahedi[h], Albert Sickmann[h,i,j], Stefan Eimer[d,k], Andrey S. Shaw[g], Albrecht Kramer-Zucker[b], Mariko Hirano-Kobayashi[l,4], Takaya Abe[m], Shinichi Aizawa[m], Florian Grahammer[b,e], Björn Hartleben[b,5], Jörn Dengjel[d,f,k,n], and Tobias B. Huber[b,d,k,e,2]

[a]Institute of Surgical Pathology, Medical Center - University of Freiburg, Faculty of Medicine, University of Freiburg, 79106 Freiburg, Germany; [b]Department of Medicine IV, Medical Center - University of Freiburg, Faculty of Medicine, University of Freiburg, 79106 Freiburg, Germany; [c]Department of Medicine, Shiga University of Medical Science, Otsu, Shiga 522-8522, Japan; [d]BIOSS Centre for Biological Signalling Studies, Albert-Ludwigs-University Freiburg, 79106 Freiburg, Germany; [e]III. Medizinische Klinik, Universitätsklinikum Hamburg-Eppendorf, 20251 Hamburg, Germany; [f]Department of Dermatology, Faculty of Medicine, Medical Center, University of Freiburg, 79106 Freiburg, Germany; [g]Department of Pathology, Washington University in St. Louis, MO 63130; [h]Leibniz-Institut für Analytische Wissenschaften – ISAS – e.V., 44139 Dortmund, Germany; [i]Department of Chemistry, College of Physical Sciences, University of Aberdeen, Aberdeen AB24 3FX, Scotland, United Kingdom; [j]Medizinische Proteom-Center, Ruhr-Universität Bochum, 44801 Bochum, Germany; [k]Center for Biological Systems Analysis (ZBSA) and Freiburg Institute for Advanced Studies, Albert-Ludwigs-University, 79106 Freiburg, Germany; [l]Laboratory for Vertebrate Body Plan, Center for Developmental Biology, RIKEN Kobe, Kobe 650-0047, Japan; [m]Genetic Engineering Team, RIKEN Center for Life Science Technologies, Kobe 650-0047, Japan; and [n]Department of Biology, University of Fribourg, 1700 Fribourg, Switzerland

Edited by Martin R. Pollak, Harvard University, Beth Israel Deaconess Medical Center, Brookline, MA, and approved April 27, 2017 (received for review October 27, 2016)

Podocytes form the outer part of the glomerular filter, where they have to withstand enormous transcapillary filtration forces driving glomerular filtration. Detachment of podocytes from the glomerular basement membrane precedes most glomerular diseases. However, little is known about the regulation of podocyte adhesion in vivo. Thus, we systematically screened for podocyte-specific focal adhesome (FA) components, using genetic reporter models in combination with iTRAQ-based mass spectrometry. This approach led to the identification of FERM domain protein EPB41L5 as a highly enriched podocyte-specific FA component in vivo. Genetic deletion of *Epb41l5* resulted in severe proteinuria, detachment of podocytes, and development of focal segmental glomerulosclerosis. Remarkably, by binding and recruiting the RhoGEF ARGHEF18 to the leading edge, EPB41L5 directly controls actomyosin contractility and subsequent maturation of focal adhesions, cell spreading, and migration. Furthermore, EPB41L5 controls matrix-dependent outside-in signaling by regulating the focal adhesome composition. Thus, by linking extracellular matrix sensing and signaling, focal adhesion maturation, and actomyosin activation EPB41L5 ensures the mechanical stability required for podocytes at the kidney filtration barrier. Finally, a diminution of EPB41L5-dependent signaling programs appears to be a common theme of podocyte disease, and therefore offers unexpected interventional therapeutic strategies to prevent podocyte loss and kidney disease progression.

focal adhesion | actomyosin | podocyte | FSGS

Glomerular epithelial cells or podocytes represent a pericyte-like cell type establishing the kidney filtration barrier in combination with endothelial cells and the basement membrane (1, 2). These cells exhibit a strictly polarized morphology characterized by a large cell body and extending primary and secondary foot processes, which enclose glomerular capillaries (3). The slit diaphragm, a specialized and unique cell–cell contact, connects interdigitating foot processes and confines the basolateral membrane compartment of podocytes (2, 4).

Because of the constant exposure of podocytes to filtration forces, tight adherence to the basement membrane is required to prevent detachment into Bowman's capsule. As a consequence, loss of podocytes from the glomerular basement membrane (GBM) is a major contributing factor to the progression of glomerular and chronic kidney disease (5–7).

On a molecular level, a multitude of adhesion receptors including heterodimeric integrins mediate interaction of cells with the surrounding extracellular matrix (ECM) or the basement membrane (8, 9). Integrin receptors are linked to an intracellular multiprotein complex, collectively named the integrin adhesome, constituting various adaptor proteins, GTPases, kinases, and phosphatases (9). One common form of integrin-mediated adhesion is focal adhesions (FAs), which have been extensively studied in cultured cells (9). Functionally, FAs support the physical interaction of cells to the ECM, establish connection to the actomyosin

Significance

Loss of podocyte adhesion is a hallmark of glomerular disease progression. Here we unravel the in vivo composition of the podocyte adhesion machinery by the use of quantitative proteomics and identify the FERM domain protein EPB41L5 as a selectively enriched novel podocyte focal adhesion protein. EPB41L5 is essential to maintaining podocyte adhesion in vivo by recruiting the Rho GEF ARHGEF18, initiating a signaling cascade and ultimately resulting in increased actomyosin activity and focal adhesion stabilization. As EPB41L5 is down-regulated in various glomerular pathologies, these findings offer a perspective for interventions aiming to prevent loss of podocytes in glomerular disease.

Author contributions: C.S., M.R., and T.B.H. designed research; C.S., M.R., M.S., M.H., D.S., M.Y.-Y., O.K., H.S., L.K., R.P.Z., and B.H. performed research; V.K., L.K., R.P.Z., A.S., S.E., A.S.S., A.K.-Z., M.H.-K., T.A., S.A., F.G., and J.D. contributed new reagents/analytic tools; C.S., M.R., H.S., and J.D. analyzed data; and C.S., M.R., and T.B.H. wrote the paper.

The authors declare no conflict of interest.

This article is a PNAS Direct Submission.

Freely available online through the PNAS open access option.

[1]C.S., M.R., and M.S. contributed equally to this work.

[2]To whom correspondence may be addressed. Email: t.huber@uke.de or christoph.schell@uniklinik-freiburg.de.

[3]Present address: Cold Spring Harbor Laboratory, Cold Spring Harbor, NY 11724.

[4]Present address: Vascular Biology Program, Boston Children's Hospital and Harvard Medical School, Boston, MA 02115.

[5]Present address: Institut für Pathologie, Medizinische Hochschule Hannover, Hannover 30625, Germany.

This article contains supporting information online at www.pnas.org/lookup/suppl/doi:10.1073/pnas.1617004114/-/DCSupplemental.

cytoskeleton, and provide a signaling hub to fine-tune regulatory cascades and cellular functions. The clinical relevance of the adhesome for podocyte function was recently demonstrated by the identification of mutations in the *Integrin alpha3* gene, causing glomerular and skin disease in affected patients (10). In addition, other focal adhesome components such as INTEGRIN-beta1 and INTEGRIN-LINKED KINASE (ILK), as well as other core focal adhesome components, were identified to be critical for podocyte maintenance (11–15).

Despite those previous advances, there is still no unifying pathophysiological concept of the role of FAs in podocyte biology, allowing for the design of targeted diagnostic, as well as therapeutic, approaches. In addition, a comprehensive description of podocyte-specific focal adhesome components is still lacking. To identify cell-specific adhesome modulators, we developed a method for large-scale isolation of highly purified podocyte cell populations from murine glomeruli (16). Using iTRAQ-based quantitative MS technology, we developed an unprecedented in vivo description of almost 3,500 podocyte proteins. We used these data and applied bioinformatic filtering approaches to identify components of the podocyte FA complex. This approach enabled the identification of the FERM-domain protein EPB41L5. Characterization of this podocyte-specific molecule offered unexpected insights into the biology, function, and disease mechanism of the kidney filtration barrier.

Results

Analysis of the Podocyte-Enriched Adhesome Identifies FERM-Domain Protein EBP41L5 as a Podocyte-Specific FA Component. One key feature of podocytes is the tightly regulated adhesion to the glomerular basement membrane (Fig. 1*A*) to maintain the filtration barrier (6). Detachment of podocytes from the glomerular basement membrane is a common hallmark of late-stage glomerular disease (Fig. 1*B*), suggesting an involvement of adhesome components (*SI Appendix*, Fig. S1). FAs are multiprotein complexes that sense the ECM environment, integrate incoming signals, and mediate required contractile forces for adhesion adjustment (Fig. 1*D*) (9). To identify podocyte adhesome-associated proteins, we made use of a genetically encoded reporter mouse system (Fig. 1*C*). After FACS sorting, GFP$^+$ podocyte cell populations were subjected to iTRAQ-based quantitative mass spectrometry (Fig. 1*C*). We identified nearly 3,500 proteins using this approach, and ranked those according to their detection rates (relative to nonpodocyte cells; Dataset S1). Pathway and process analysis revealed a high enrichment of integrin-mediated-signaling-associated proteins in podocytes compared with the nonpodocyte fraction (Fig. 1*E*, *SI Appendix*, Fig. S2, and Dataset S1). After selection for enriched proteins, a filtering step for FA gene ontology terms was implemented, resulting in a list of 56 enriched, presumptive FA proteins. In addition to previously described integrins (ITGA3, ITGB5, and ITGAV) and well-established actin-cross-linkers such

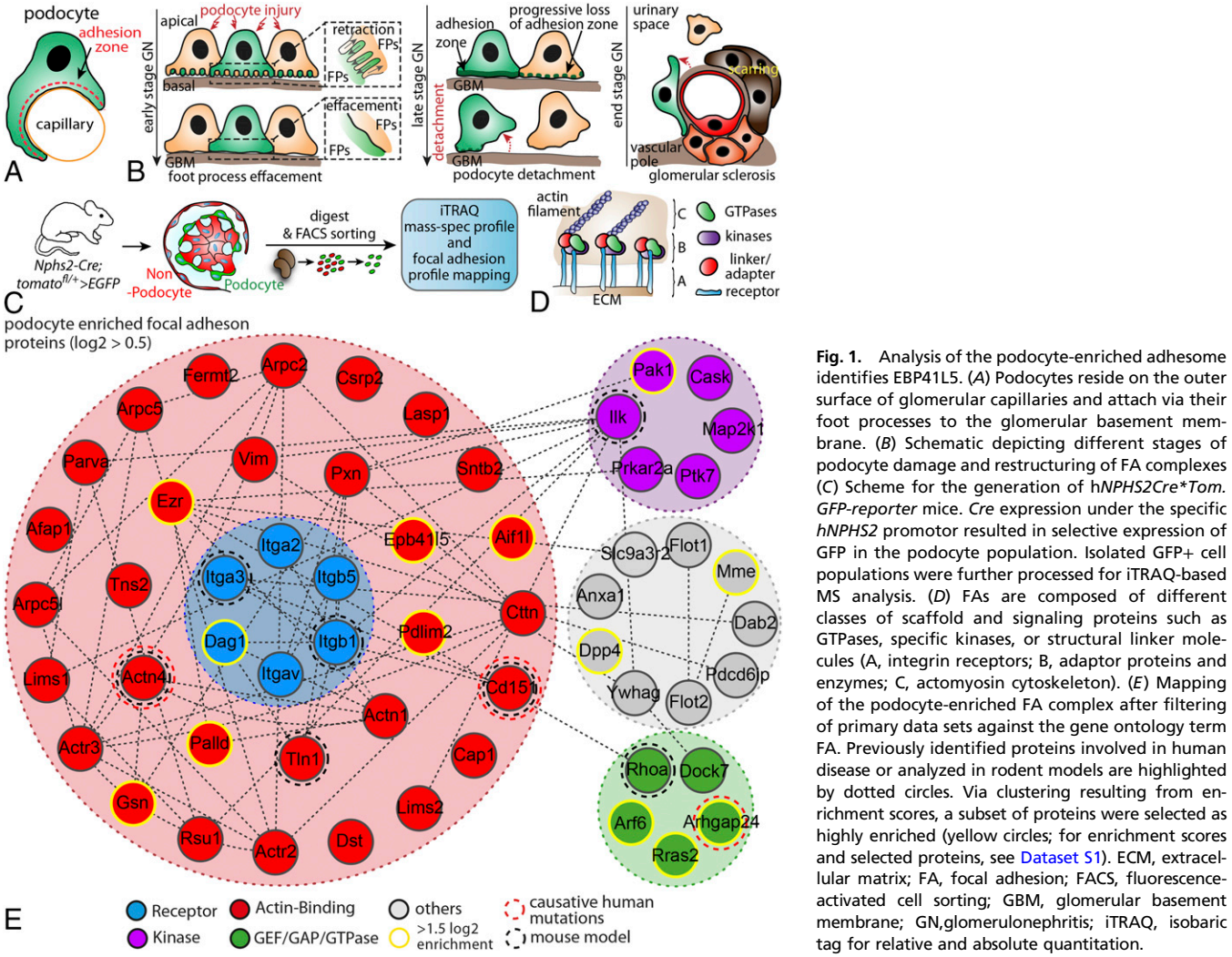

Fig. 1. Analysis of the podocyte-enriched adhesome identifies EBP41L5. (*A*) Podocytes reside on the outer surface of glomerular capillaries and attach via their foot processes to the glomerular basement membrane. (*B*) Schematic depicting different stages of podocyte damage and restructuring of FA complexes (*C*) Scheme for the generation of h*NPHS2Cre*Tom.GFP-reporter* mice. *Cre* expression under the specific *hNPHS2* promotor resulted in selective expression of GFP in the podocyte population. Isolated GFP+ cell populations were further processed for iTRAQ-based MS analysis. (*D*) FAs are composed of different classes of scaffold and signaling proteins such as GTPases, specific kinases, or structural linker molecules (A, integrin receptors; B, adaptor proteins and enzymes; C, actomyosin cytoskeleton). (*E*) Mapping of the podocyte-enriched FA complex after filtering of primary data sets against the gene ontology term FA. Previously identified proteins involved in human disease or analyzed in rodent models are highlighted by dotted circles. Via clustering resulting from enrichment scores, a subset of proteins were selected as highly enriched (yellow circles; for enrichment scores and selected proteins, see Dataset S1). ECM, extracellular matrix; FA, focal adhesion; FACS, fluorescence-activated cell sorting; GBM, glomerular basement membrane; GN,glomerulonephritis; iTRAQ, isobaric tag for relative and absolute quantitation.

as ACTININ-4, we identified recently discovered GTPase modulators such as ARHGAP24 (Fig. 1*E*) (17). We further refined our initial list by integrating recently published experimental data (18) and ended up with a list of 182 potential podocyte-enriched FA proteins (Dataset S1). EPB41L5 appeared as the top enriched protein in our candidate approach after applying different filtering steps for FA-associated protein domains (Dataset S1).

EPB41L5 Localizes to FAs in Vivo. To validate results of our proteome approach, we used mRNA in situ hybridization to develop a specific expression profile for the top candidate *Epb41l5* during murine development. Prenatally, *Epb41l5* expression was restricted to the brain, lung, and kidney (Fig. 2*A* and *SI Appendix*, Fig. S3). In the kidney, expression was particularly strong in the glomeruli at embryonic stage E14.5 (embryonic day 14.5) (Fig. 2*A* and *SI Appendix*, Fig. S3). Immunofluorescence of EPB41L5 further confirmed this expression in rodent as well as human podocytes (*SI Appendix*, Fig. S3). Glomerular epithelial cells undergo a dramatic change in cellular morphology during development (19, 20). To specifically localize EPB41L5 during this polarization process, we used a set of well-established polarity markers in combination with EPB41L5. Here, EPB41L5 showed a predominant colocalization with the basolateral marker SCRIBBLE, but not with the apical marker PODOCALYXIN or the tight junction marker PAR3 (*SI Appendix*, Fig. S4) (21). Using immunogold electron microscopy confirmed that bona fide FA components such as PAXILLIN and ZYXIN predominantly localized at a basal position of podocyte foot processes (Fig. 2 *B–D*). EPB41L5 showed an overlapping localization pattern in close proximity to the glomerular basement membrane (Fig. 2 *E* and *F*). Recently, the super resolution microscopy technique stochastic optical reconstruction microscopy was successfully applied to visualize the nanoscale composition of the glomerular basement membrane (22). Using this technique enabled the detection of EPB41L5 colocalizing with the bona fide FA component INTEGRIN-beta1, whereas no overlap was detectable with the apical marker protein PODOCALYXIN (Fig. 2 *G–L*). Altogether, these different imaging modalities highlight the basolateral, typical FA localization pattern for EPB41L5 in vivo. Remarkably, an altered localization and coarse intensity pattern was detected in biopsy samples from human patients with focal segmental glomerulosclerosis or diabetic nephropathy for EPB41L5 (*SI Appendix*, Fig. S5). These observations were furthermore corroborated by mRNA expression analysis for respective disease entities from open source databases, as well as experimental mouse models (*SI Appendix*, Figs. S5 and S6). Altogether, these data indicate that EPB41L5 is a highly sensitive FA component of podocytes and appears also to be drastically affected in human glomerular disease entities.

Loss of *Epb41l5* Causes Nephrotic Syndrome, Renal Failure, and Lethality. To test for the functional relevance of the loss of *Epb41l5* expression, we generated a conditional knockout model

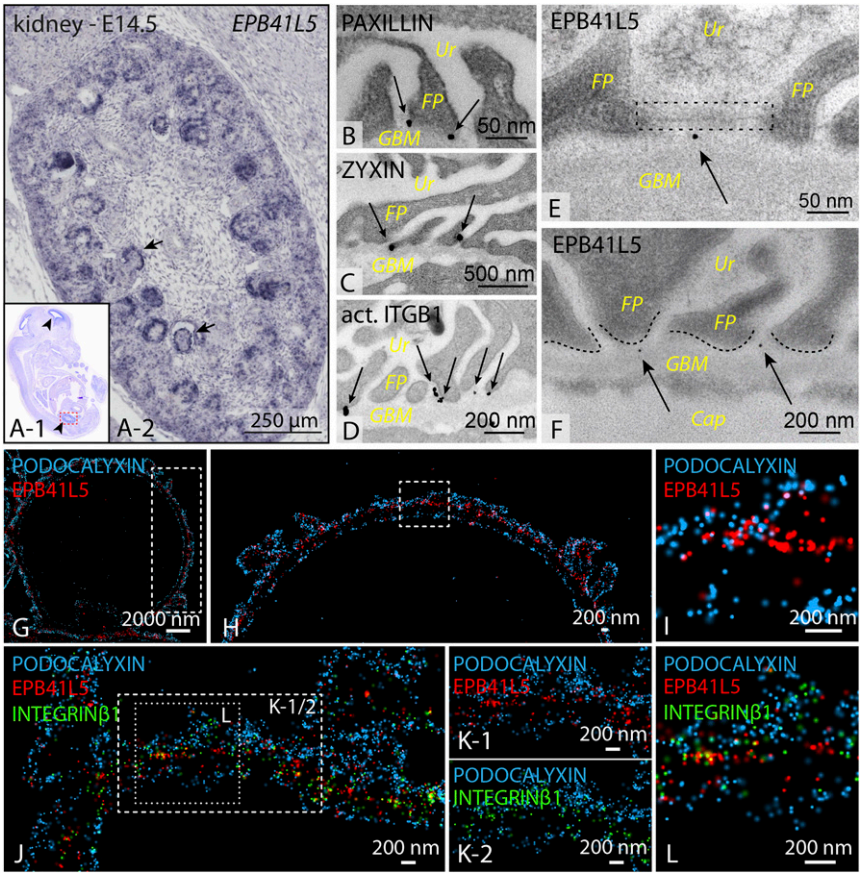

Fig. 2. EPB41L5 localizes at FAs in vivo. (*A*) In situ hybridization revealed that Epb41l5 is exclusively expressed in developing glomeruli of the kidney at embryonic stages E14.5. (*B–F*) Immunogold electron microscopy for core FA components revealed predominant basal localization toward the GBM in wild-type mice. EPB41L5 concordantly localized basally of foot processes. Ur, urinary pole; FP, foot processes; GBM, glomerular basement membrane; Cap, capillary; arrows, gold particles; dotted lines, FP morphology. (*G–L*) Stochastic optical reconstruction microscopy of glomeruli, using PODOCALYXIN (apical marker) and INTEGRIN-beta1 (basal marker) in combination with EPB41L5, demonstrated close proximity and colocalization of EPB41L5 with the FA compartment (as indicated by ITGB1; boxed regions indicate areas of zoomed details).

using standardized loxP technique (Fig. 3 *A–D* and *SI Appendix*, Fig. S7). Glomerular epithelial cells contribute to the maintenance of the kidney filtration barrier, and levels of proteinuria represent a sensitive readout system in terms of podocyte function (2). Analysis of *Epb41l5*$^{fl/fl}$**NPHS2Cre* animals revealed severe proteinuria indicated by albumin/creatinine ratios greater than 100 compared with wild-type animals. Proteinuria in those mice was already present at birth and remained at high levels for the whole observational period (Fig. 3*E*). As a result of high-grade proteinuria and progressing renal failure (as demonstrated by pronounced glomerulosclerosis; Fig. 3 *J* and *K* and *SI Appendix*, Fig. S8), respective knockout animals showed decreased weight gain compared with control animals (Fig. 3*F*). The severe phenotype in terms of proteinuria resulted in premature death of *Ebp41l5* knockout animals, reflected by dramatically reduced survival by 50% 2 wk after birth (Fig. 3*G*). Morphological analysis of kidney sections revealed dilated tubules with an accumulation of proteinaceous casts, reflecting severe proteinuria in knockout animals (Fig. 3 *H–K* and *SI Appendix*, Fig. S8). Given the basolateral localization of EPB41L5 in glomerular epithelial cells, we sought to directly determine the potential influence of EPB41L5 on podocyte cell morphology. Although in wild-type animals, interdigitating FPs were regularly separated by slit diaphragms, *Epb41l5* knockout podocytes displayed a global fusion of FPs at P0 (*SI Appendix*, Fig. S9). Furthermore, slit diaphragms were either not detectable or dislocated to a more apical position (*SI Appendix*, Fig. S9), but there were no obvious changes in apico-basal compartmentalization (*SI Appendix*, Fig. S10). Strikingly, massive podocyte detachment was detectable in *EPB41L5* knockout animals, as demonstrated by decreased numbers of podocytes per glomerulus, as well as increased levels of detached podocytes in the urine (Fig. 3 *L–O* and *SI Appendix*, Fig. S10). To test the effect of EPB41L5 in already completely maturated podocytes, the conditional EPB41L5 floxed allele was intercrossed to a podocyte-specific, doxycycline-dependent inducible *Cre*-system (*SI Appendix*, Fig. S11 and S12). Induction of *Cre*-activity was performed in 4-wk-old animals for a period of 2 wk (*SI Appendix*, Fig. S11). Remarkably, 1 wk after induction, increased levels of proteinuria already were detectable in knockout animals (*SI Appendix*, Fig. S11). In agreement with the *NPH2Cre* line, inducible knockout animals developed signs of progressive focal segmental sclerosis and foot process effacement (*SI Appendix*, Fig. S11 and S12). These alterations were accompanied by altered localization and decreased signal intensity for NEPHRIN, PODOCIN, and SNYAPTOPODIN, whereas the polarity molecule PAR3 exhibited no significant changes (*SI Appendix*, Fig. S12). Together, these findings underline the uttermost importance of EPB41L5 for developing, as well as fully maturated, podocytes in vivo.

To gain mechanistic insights into EPB41L5 function in podocytes, we used a recently established method for isolation of primary podocytes from control and EPB41L5-deficient animals (Fig. 1*C*) (23). As expected, EPB41L5 displayed on a subcellular level a typical FA localization pattern close to the cell border (Fig. 3*P*). Interestingly, a pronounced decrease in migratory function was detected in primary knockout podocytes when seeded on collagen IV coated surfaces (*SI Appendix*, Fig. S13).

EPB41L5 Controls FA Maturation and Cellular Spreading. Because primary podocytes are only of limited availability, we used CRISPR/Cas9 genome editing technology to generate *EPB41L5*-deficient

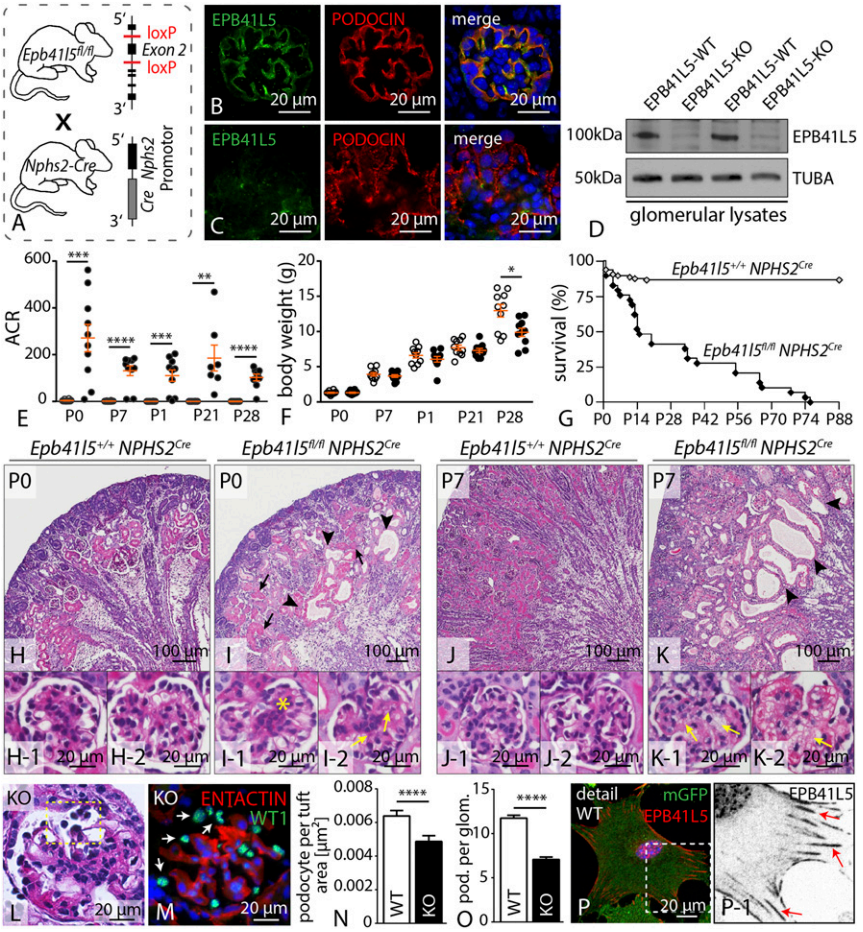

Fig. 3. Podocyte-specific knockout of *Epb41l5* causes nephrotic syndrome and lethality. (*A*) Schematic illustrating the generation of a podocyte-specific knockout mouse (*B* and *C*) Immunofluorescence staining confirmed that EPB41L5 protein is not detectable in the podocyte compartment in respective knockout mice. (*D*) Western blot on glomerular lysates from either control or respective knockout animals revealed that EPB41L5 protein is completely abolished. (*E* and *F*) Proteinuria measurements demonstrate a drastic increase of proteinuria in *Epb41l5* knockout animals beginning at P0 (at least $n = 7$; Dataset S3), accompanied by decreased body weight gain (at least $n = 10$ animals per group; *SI Appendix*, Dataset S3). (*G*) Kaplan-Meier analysis indicated premature death of *Epb41l5* knockout animals (at least n = 15; Dataset S3). (*H–K*) Histology of wild-type and *Epb41l5*$^{fl/fl}$**NPHS2*^{Cre} kidney sections revealed proteinaceous casts (black arrows), dilated tubules (black arrowheads), mesangial proliferation (yellow asterisk), and mesangiolysis (yellow arrows). (*L–O*) PAS and immunofluorescence staining for WT-1 demonstrated detachment of podocytes in *Epb41l5* knockout animals. Quantification of WT-1-positive cells in KO animals at 3 wk of age ($n = 3$ animals for each genotype; Dataset S3). (*P*) EPB41L5 localized in a typical FA pattern in primary wild-type podocytes (white box indicates zoom-in; red arrows indicate FAs). ACR, albumin to creatinine ratio.

immortalized human podocyte cell lines. After validation of specific gRNAs for the human EPB41L5 locus (targeting exon 2), we transfected immortalized human podocytes and isolated isogenetic clones. These clones were subsequently sequenced for deleterious mutations, and knockout efficiency was finally confirmed with Western blot (Fig. 4 *A* and *B* and *SI Appendix*, Fig. S13). As FAs are critically involved in dynamic cell–ECM interactions, we further tested for migration behavior and cellular adhesion in wild-type and respective knockout clones. Here, two independent *EPB41L5* knockout clones showed a pronounced defect in migration, as well as adhesion, when plated on collagen IV-coated ECM substratum (Fig. 4 *C–E* and *SI Appendix*, Fig. S13). The observation of impaired migration and adhesion implicated potential dysfunction in FA dynamics as a result of loss of EPB41L5. Therefore, we assessed cellular spreading and detected significant impairment of *EPB41L5* knockout clones, especially in early phases (Fig. 4 *F* and *G*), although there were no obvious differences under steady-state conditions (Fig. 4*G* and *SI Appendix*, Fig. S13 and S14). To validate the specificity of the observed phenotypes, we performed rescue experiments expressing full-length EPB41L5 in knockout clones. Here, we observed that reexpression of EPB41L5 leads to an amelioration of the spreading defect in EPB41L5 knockout cells (Fig. 4*H* and *SI Appendix*, Fig. S13). Analysis of FA morphology under dynamic conditions revealed a major proportion of immature FAs in *EPB41L5* knockout clones compared with wild-type controls (Fig. 4 *I–K*). Similar observations were also made in conditions of acute FA disassembly and reassembly via application of the myosin II inhibitor blebbistatin (24). Here, wild-type cells recovered faster and more efficiently, reflected by an increased amount of maturated FAs after washout of blebbistatin (*SI Appendix*, Fig. S14). These findings highlight the critical role of EPB41L5 for FA assembly and maturation. Because EPB41L5 appeared in a typical FA localization pattern in vivo and in vitro (Figs. 2 and 3*P*), we aimed to identify potential FA interaction partners of EPB41L5 via GST pull-down experiments. Here, we observed that the C-terminal part of EPB41L5 (encompassing amino acids 385–733; Fig. 4 *L* and *M*) interacted with PAXILLIN, whereas other bona fide FA components such as INTEGRIN-beta1 showed an interaction with neither the C-term nor the FERM-domain of EPB41L5 (Fig. 4*M* and *SI Appendix*, Fig. S14). In agreement with these data, localization studies demonstrated a clear colocalization of the C-terminal part of EPB41L5 with PAXILLIN at steady state and in spreading cells (Fig. 4 *N–Q*). Interestingly, a pronounced accumulation at the leading edge of spreading cells was observed for the C-terminal part of EPB41L5, together with PAXILLIN accumulating in nascent FAs (Fig. 4*Q* and *SI Appendix*, Fig. S14). In contrast, the FERM domain containing truncation showed a distinct localization pattern at the lamellum of spreading cells (Fig. 4*P*). These observations imply that the C-terminal part of EPB41L5 is not only interacting with PAXILLIN but also might be responsible for the localization toward the leading edge during cellular spreading.

EPB41L5-Mediated Cell Spreading Depends on Actomyosin Contractility. The process of cell spreading is being powered by contractile processes involving the actomyosin cytoskeleton (25). We observed that EPB41L5 predominantly accumulated at FA initiation sites, and also to the leading edge of cells in very early spreading phases (Fig. 5*A*). In addition, spreading *EPB41L5* KO cells exhibited a misconfigured cellular morphology characterized by the appearance of multiple pseudopods (Fig. 5 *B–D* and *SI Appendix*, Fig. S15), suggesting an impaired actomyosin regulation. We therefore hypothesized an active role for EPB41L5 in regulating the actomyosin machinery. In agreement with this hypothesis, preincubation of wild-type cells with inhibitors of actomyosin contractility phenocopied spreading and morphological defects of EPB41L5 KO cells (Fig. 5 *E–I* and *SI Appendix*, Fig. S15). The specificity of the pseudopod phenotype could be confirmed by rescue experiments, where reexpression of full-length EPB41L5 resulted in a significant reduction of pseudopod formation in respective knockout cells during spreading (Fig. 5*J*). Life imaging microscopy revealed that pseudopods are actively generated structures, characterized by a rather unorganized actin cytoskeleton and only small FAs (Fig. 5 *K–N* and *SI Appendix*, Fig. S15 and Movies S1–S5). In line with these observations, loss of EPB41L5 resulted in decreased levels of p-MLC specifically at the leading edge of spreading cells (Fig. 5 *O–Q*), accompanied by altered localization of MYOSIN-II (*SI Appendix*, Fig. S16). These findings were furthermore corroborated by Western blot experiments of either spreading or steady-state cells (Fig. 5 *R* and *W*). Again, reexpression of full-length EPB41L5 could reverse the reduced levels of p-MLC at the leading edge in EPB41L5 knockout cells (Fig. 5*S* and *SI Appendix*, Fig. S16). Because the activation mode of the actomyosin cytoskeleton is mainly regulated by of GTPases such as RhoA or Rac1 (26), we quantified for active levels of those. RhoA and Rac1 are either inactive (GDP-bound state) or active (GTP-bound state). Interestingly, we observed that EPB41L5 knockout cells exhibited lower levels of active RhoA during spreading, whereas at the same time, increased levels of active Rac1 were detected (Fig. 5 *T* and *U* and *SI Appendix*, Fig. S16). These findings indicate that loss of EPB41L5 results in a reciprocal activation of the GTPases RhoA and Rac1, finally leading to decreased actomyosin contractility. Remarkably, we also observed a pronounced accumulation of Rac1 in pseudopods of EPB41L5 knockout cells, potentially implying that Rac1 activation might account for this phenotype (Fig. 5*V*). Furthermore, *EPB41L5* knockout cells exhibited a much higher sensitivity toward myosin inhibition, characterized by altered cellular morphology (*SI Appendix*, Fig. S16). Together, these data indicated a clear correlation among the loss of EPB41L5, impaired actomyosin function, and defective cell spreading.

EPB41L5 Regulates Actomyosin Contractility via ARHGEF18. To understand the potential mechanisms of EPB41L5 in regulating the actomyosin machinery, we reanalyzed our initial in vivo iTRAQ proteomics approach and screened for podocyte-enriched GEFs as potential direct regulators of actomyosin contractility. Using this targeted approach, we identified the RhoGEF ARHGEF18, similar to EPB41L5, as a highly and specifically enriched podocyte candidate protein (Fig. 6 *A* and *F*). Previously, ARHGEF18 has been implicated in cell shape modulation by regulating myosin activity (27). To further characterize a potential interaction of both proteins, we performed coimmunoprecipitation assays and could demonstrate that ARHGEF18 precipitated EPB41L5 (Fig. 6*B*). Moreover, endogenous pull-down experiments using a specific antibody for ARHGEF18 revealed efficient precipitation of EPB41L5 in immortalized human podocytes (Fig. 6*C*). To better characterize this association, a set of complementary truncations for EPB41L5 was generated. Here, only the FERM domain containing truncations showed an efficient association with ARHGEF18 (Fig. 6*D* and *SI Appendix*, Fig. S17). These findings were corroborated by the use of GST-tagged recombinant protein versions for the FERM-/FERM-FA, full-length as well as C-terminal part of EPB41L5 in endogenous pull-down assays (Fig. 6*E* and *SI Appendix*, Fig. S17). In line with our iTRAQ proteomics data set, ARHGEF18 was strongly detected in podocytes in vivo, with a rather prominent perinuclear, as well as distinct basal, localization pattern (Fig. 6*F* and *SI Appendix*, Fig. S18). Similar to EPB41L5, ARHGEF18 was highly enriched at the leading edge of spreading podocytes (Fig. 6*G*). In agreement with the decreased p-MLC level (Fig. 5 *O–Q*), ARHGEF18 localization was reduced at the leading edge (Fig. 6 *H* and *I*) of *EPB41L5* KO cells. These data collectively indicated that EPB41L5 might be required to recruit ARHGEF18 to the leading edge as a prerequisite for actomyosin activation. To further corroborate the function of ARHGEF18 in podocytes, we used siRNA to generate

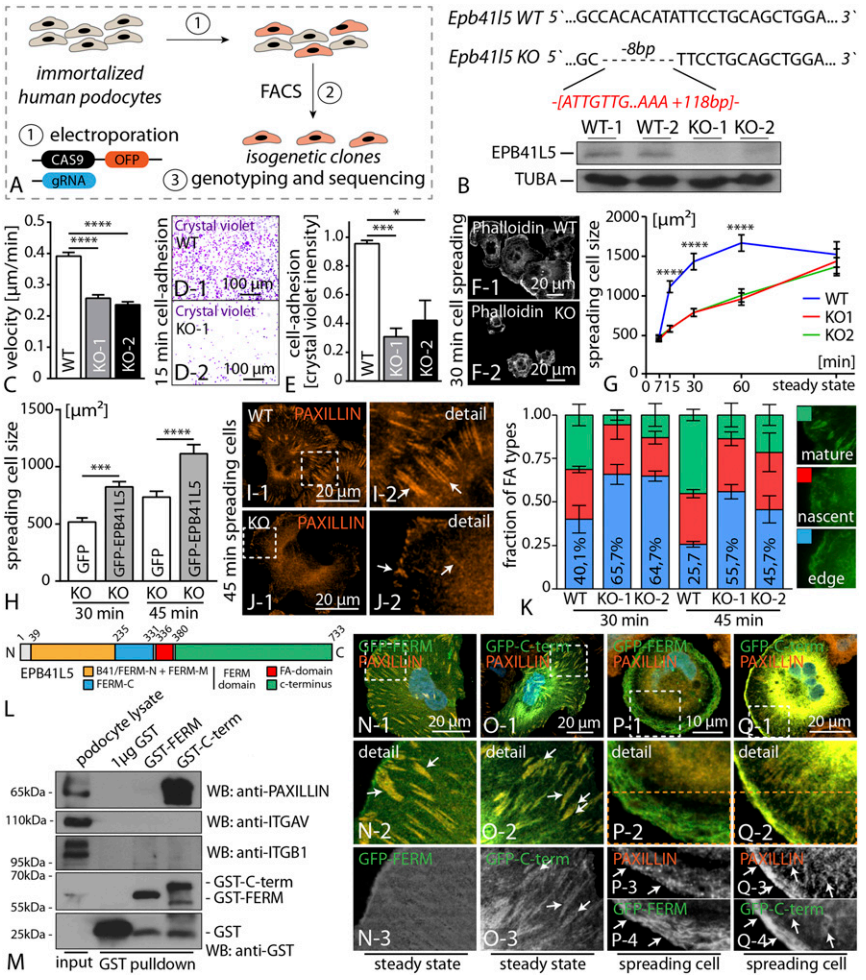

Fig. 4. EPB41L5 controls FA maturation and cellular spreading. (*A*) Schematic depicting the generation strategy of *EPB41L5* knockout using Crispr/CAS9 genome editing. (*B*) Exemplary Sanger sequencing results illustrating two different mutations in one podocyte clone. Western blot confirmed the absence of EPB41L5. (*C*) Single-cell migration analysis demonstrated a decreased migratory speed in *EPB41L5* knockout clones ($n = 86$ cells over three independent experiments; Dataset S3). (*D* and *E*) Decreased adhesion of EPB41L5 knockout cells ($n = 3$; Dataset S3). (*F* and *G*) Impaired cell spreading of knockout cells compared with wild-type controls ($n = 3$; Dataset S3). (*H*) Reexpression of full-length EPB41L5 ameliorated the spreading defect in EPB41L5 knockout cells (at least 70 cells were analyzed over three independent experiments; Dataset S3). (*I–K*) Quantification of FA subtypes in *EPB41L5* knockout cells demonstrated more immature FAs (>400 cells analyzed; Dataset S3). (*L*) Schematic depicting the domain structure of EPB41L5. (*M*) GST-pull-down experiments revealed that only the C-terminal part of EPB41L5 is required for association with the FA molecule PAXILLIN. (*N–Q*) Expression of GFP-tagged versions of C-terminal or FERM-domain truncations highlighted the FA localization pattern for the C-terminal part (Q3-4; white arrows indicate colocalization with PAXILLIN). FACS, fluorescence-activated cell sorting.

knockdown of ARHGEF18. Remarkably, loss of ARHGEF18 phenocopied the spreading defects of *EPB41L5* knockout cells and was accompanied by decreased levels of p-MLC (Fig. 6 *J–O* and *SI Appendix*, Fig. S18).

ECM Influences EPB41L5 Mediated Phenotypes. From hereditary collagenopathies, it is evidenced that podocytes rely on collagen type IV interactions to maintain their mechanical stress resistance and filter function (28, 29). Therefore, we speculated that the EPB41L5-mediated regulatory networks stabilizing cell function, cell adhesion, and contractility might be specifically influenced by the ECM composition. In fact, observed phenotypes resulting from loss of EPB41L5 were influenced by provided ECM ligands and respective concentrations. Wild-type cells showed a dose-dependent increase in cell size during spreading on either collagen IV or fibronectin. Although the spreading defects of EPB41L5 KO cells persisted on all collagen IV concentrations, high concentrations of fibronectin could ameliorate the spreading defect of EPB41L5 KO cells and prevented the hypersensitivity toward myosin II inhibitors (Fig. 7 *A–C* and *E–J* and *SI Appendix*, Fig. S19), suggesting that EPB41L5, in addition to its general effect on FA maturation, is particularly required for the execution of collagen IV-mediated outside-in signaling. In agreement, quantification of active RhoA for cells spreading on fibronectin revealed almost equalized levels of EPB41L5 KO cells compared with wild-type cells, in contrast to persistently diminished RhoA activation on collagen IV (Figs. 7*D* and 5*T*). To elucidate this phenomenon, we performed quantitative SILAC (stable isotope labeling with amino acids in cell culture)-based focal adhesome proteomics (30), in which enriched and chemically cross-linked FA complexes are analyzed using mass spectrometry (30). Strikingly, we detected that loss of EPB41L5 modulated the composition of the focal adhesome, most prominently on the level integrin receptors such as INTEGRIN-beta1 (Fig. 7 *K* and *L* and Dataset S2). Although not primarily detected in the MS data set (most probably because of sensitivity issues), we could reveal that the collagen-binding INTEGRIN-alpha2 also concordantly exhibited lower levels in the focal adhesome fraction of EPB41L5-depleted cells (Fig. 7*L*). Thus, EPB41L5 appears to be required for efficient collagen IV-mediated outside-in signaling in podocytes.

Discussion

Modulation and regulation of adhesion represents a fundamental mechanism in epithelial cell biology (9). Interaction of epithelial cells with the surrounding ECM or the underlying basement membrane is mediated by different adhesion receptors such as integrin adhesion complexes (9, 31). In this study, we focused on the adhesome of podocytes. The medical relevance of podocyte adhesion is underlined by the fact that podocyte detachment is a key factor for chronic kidney disease progression (32–34). Previous studies mainly focused on key components of the integrin adhesome, such as different integrin subunits or central signaling proteins such as ILK and TALIN (11, 12, 15). Despite those previous advances, there is still only limited knowledge about cell type-specific modulation of cell adhesion and contractility. To identify potential podocyte-inherent adhesome modulators, we performed an in vivo screening approach

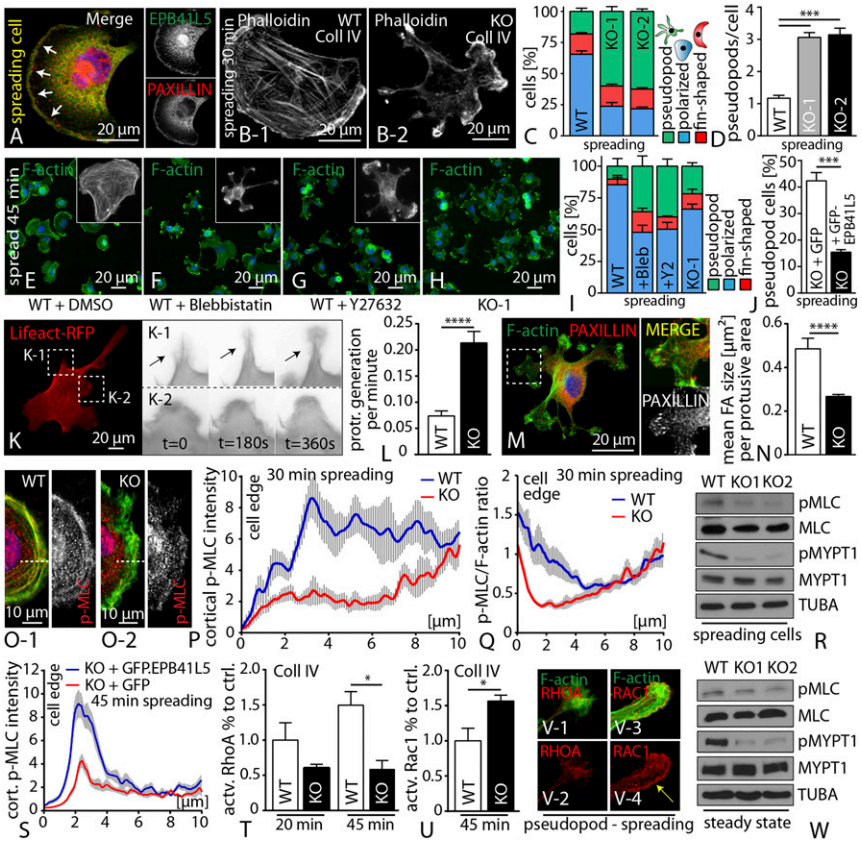

Fig. 5. EPB41L5-mediated cell spreading depends on actomyosin contractility. (*A*) During initial phases of spreading, EPB41L5 colocalized with PAXILLIN at nascent adhesion initiation sites. (*B–D*) Loss of EPB41L5 resulted in the formation of pseudopodial protrusions (>100 cells over three experiments, 30 min spreading; Dataset S3). (*E–I*) Treatment of wild-type cells with blebbistatin or Y27632 promoted the formation of pseudopods (at least n = 50 cells over three experiments, 45 min spreading; Dataset S3). (*J*) Reexpression of full-length EPB41L5 ameliorated the pseudopod phenotype in EPB41L5 knockout (>100 cells over three experiments; 30 min spreading; Dataset S3). (*K* and *L*) Life imaging of EPB41L5 knockout cells revealed pseudopod formation as an active process (Dataset S3). (*M* and *N*) FA morphology is shifted toward smaller adhesion sites in pseudopod protrusions (12 WT and 23 KO cells were analyzed; Dataset S3). (*O–Q*) Analysis for P-MLC showed decreased levels at the leading edge of spreading *EPB41L5* KO cells (n = 10 over two experiments; Dataset S3). (*R*) Western blot on spreading wild-type and EPB41L5 KO cells showed decreased levels of P-MLC as well as P-MYPT. (*S*) Reexpression of full-length EPB41L5 restores p-MLC levels at the leading. (*T* and *U*) Quantification of active GTPase levels during cell spreading showed decreased active RhoA and increased active Rac1 levels in knockout cells (n = 3; Dataset S3). (*V*) RAC1 and RHOA immunofluorescence in knockout pseudopods. (*W*) Western blot on steady state EPB41L5 KO cells showed decreased levels of P-MLC, as well as P-MYPT.

and identified the FERM domain protein EPB41L5 as a highly selectively expressed FA component of podocytes (Figs. 1 and 2). The importance of EPB41L5 for podocyte function was furthermore supported by the profound phenotype of conditional knockout mice and striking down-regulation in a series of human glomerular disease conditions, as well as experimental mouse and cell models (Fig. 3 and *SI Appendix*, Figs. S5, S6, and S20). More recently, it was demonstrated that loss of TALIN (genetic deletion and experimental stress models), a well-established core focal adhesome component, results in a dramatic podocyte phenotype characterized by massive proteinuria, as well as consecutive development of glomerular sclerosis (15). Interestingly, TALIN-deficient podocytes exhibited a mild adhesion and spreading defect, but a predominant misconfiguration of the actin cytoskeleton. In contrast, EPB41L5 mainly influenced dynamic cellular functions such as spreading and adhesion via titration of the actomyosin machinery (Figs. 4 and 5).

The EPB4.1 protein family is involved in cellular morphogenesis, and EPB41L5 was particularly investigated in terms of apicobasal polarity establishment via interaction with CRUMBS in early development (35, 36). Previous work demonstrated that EPB41L5 was required during early embryo gastrulation, which seemed to be partially a result of EPB41L5-dependent FA modulation and cell–cell contact establishment via cadherins (37). On the basis of our observations, we here propose that EPB41L5 mainly influences the maturational phase of FAs, implicating that decreased tension or traction might attribute for the detachment of podocytes, as evidenced in the EPB41L5 knockout model (Figs. 3 and 4). The actomyosin cytoskeleton is involved in multiple cellular functions ranging from migration, to cellular morphogenesis, to adhesion (38). Although ARHGEF18 was previously implicated in controlling cell migration, our data now indicate that the RhoGEF ARHGEF18 acts downstream of EPB41L5-regulated cellular spreading in the cell-specific context of podocytes (Fig. 6) (39). In agreement with the known role of ARHGEF18 as a RHOGEF activator for RhoA, we observed decreased levels of active RhoA and concomitantly increased activation of Rac1 in EPB41L5 knockout cells during spreading (Fig. 5). Although hyperactivation of Rac1 is an accepted pathogenetic model in podocyte disease verified by several independent studies (40, 41), there is an ambiguous perception regarding the role of RhoA. Nevertheless, an emerging body of evidence supports the concept of a required balance of these GTPases to maintain cellular function (42). Therefore, our findings exemplify the interdependent and reciprocal interplay of small GTPases and demonstrate their essential role for podocyte spreading and adhesion maturation (Fig. 6).

The disturbed activity of the actomyosin cytoskeleton also contributes to the prominent feature of active pseudopod formation in EPB41L5 knockout cells during spreading (Fig. 5 and Movies S1–S5). Pseudopods represent a specialized cellular protrusion type mainly observed in chemotactic cell types, and Rac1 activation has been shown to be involved in the initiation and propagation of pseudopod formation (43). In light of this, the pseudopod phenotype of EPB41L5 knockout cells might reflect the disturbed balance of GTPase activation and insufficient FA maturation, ultimately culminating in the generation of numerous unstable cellular projections. A very recent study could demonstrate that stabilization of the actin cytoskeleton via application of a small molecule affecting the DYNAMIN structure resulted in prevention of progressive proteinuria in a series of genetic and toxic podocyte stress models. These observations underlined the importance of the actin cytoskeleton as a common final pathway of podocyte injury (44, 45). Our data now extend these observations and identify with EPB41L5, a podocyte-specific upstream link from the adhesion machinery to the regulation of the cytoskeleton. As FAs are known to transmit outside-in-signals, this also raised the possibility of potential sensing

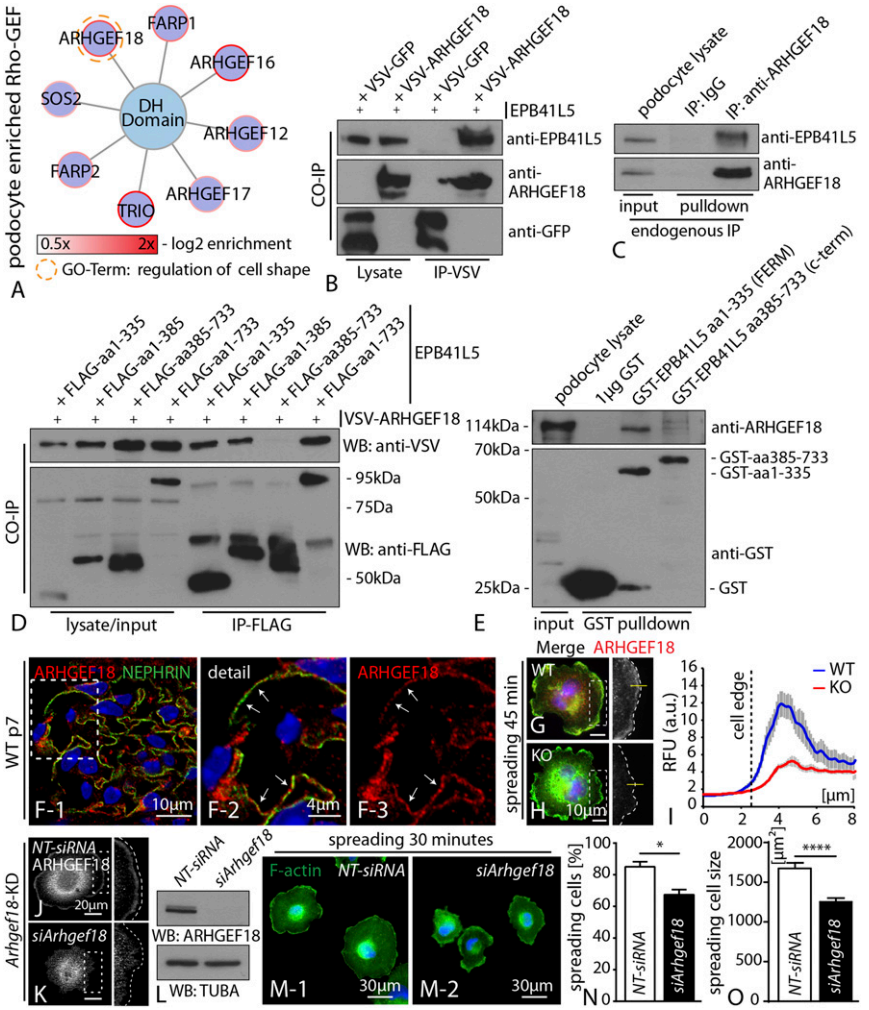

Fig. 6. EPB41L5 regulates actomyosin contractility via ARHGEF18. (*A*) Subanalysis of the in vivo iTRAQ proteomics dataset for DH domain containing small GTPases. ARHGEF18 showed a high enrichment score, as well as involvement in cell shape regulation. (*B*) Coimmunoprecipitation between epitope-tagged EPB41L5 and ARHGEF18. (*C*) Endogenous EPB41L5 was precipitated via pull-down with an antibody directed against ARHGEF18, IgG was included as a control. (*D*) A series of different EPB41L5 truncations (all epitope tagged) were used to map the association with ARHEF18; here only the FERM domain containing truncations precipitated ARHGEF18. (E) GST-tagged recombinant protein versions of either FERM domain or C-terminal truncations of EPB41L5 were used in endogenous pull-down experiments. Only the FERM domain containing truncation precipitated ARHGEF18. (*F*) Immunofluorescence staining for ARHGEF18 on murine adult glomeruli revealed colocalization with the podocyte marker NEPHRIN (boxed regions indicate zoomed-in detail). (*G–I*) Immunofluorescence staining for ARHGEF18 on cells, while spreading revealed localization toward the leading edge. Quantification of immunofluorescence intensities across the cell border indicated decreased levels ARHGEF18 in KO cells (at least 20 cells per genotype were analyzed over two independent experiments). (*J–L*) siRNA-mediated knockdown of *ARHGEF18* in immortalized human podocytes, as confirmed via immunofluorescence and Western blot. (*M–O*) Knockdown of ARHGEF18 resulted in significant impairment of early spreading on collagen IV surfaces (at least 100 cells per condition were analyzed and averaged over three independent experiments; Dataset S3).

properties of the EPB41L5 FA-associated complex. Interestingly, we detected an EPB41L5-dependent alteration of the focal adhesome composition (Fig. 7 and Dataset S2). Altogether, these changes might serve as a possible explanation for differential ECM response properties because of the loss of EPB41L5 (Fig. 7). In fact, our findings suggest the physiological GBM composition influences the EPB41L5 associated signaling response (Fig. 7), suggesting collagenopathies such as Alport syndrome specifically contribute to changes in podocyte adhesion signaling, finally leading to podocyte loss and progressive kidney disease (29).

Collectively, we describe here comprehensive adhesome mapping of podocytes in vivo as a unique model to study the requirements of FAs under enormous physical forces. On the basis of the identification of EPB41L5, we describe a cell-inherent concept of FA maturational control via integration of the actomyosin cytoskeleton and context-dependent ECM sensing, which is required to maintain the integrity of the kidney filtration barrier (Fig. 7).

Materials and Methods

Please refer to *SI Appendix* for complete details of materials and methods, as well as all supplemental figures.

Animals. EPB41L5 knockout mice were generated as described in *SI Appendix, Materials and Methods*. All animal experiments were approved by local authorities (Regierungspräsidium Freiburg, Freiburg 79106 – approval number G10/39).

MS Analysis. Detailed description of isolation and analysis is described in *SI Appendix, Materials and Methods*. All analyzed data are provided as Datasets S1 and S2.

Super Resolution Microscopy. Super resolution microscopy was performed in principle, as previously described (22). Further details are provided in the *SI Appendix, Materials and Methods*.

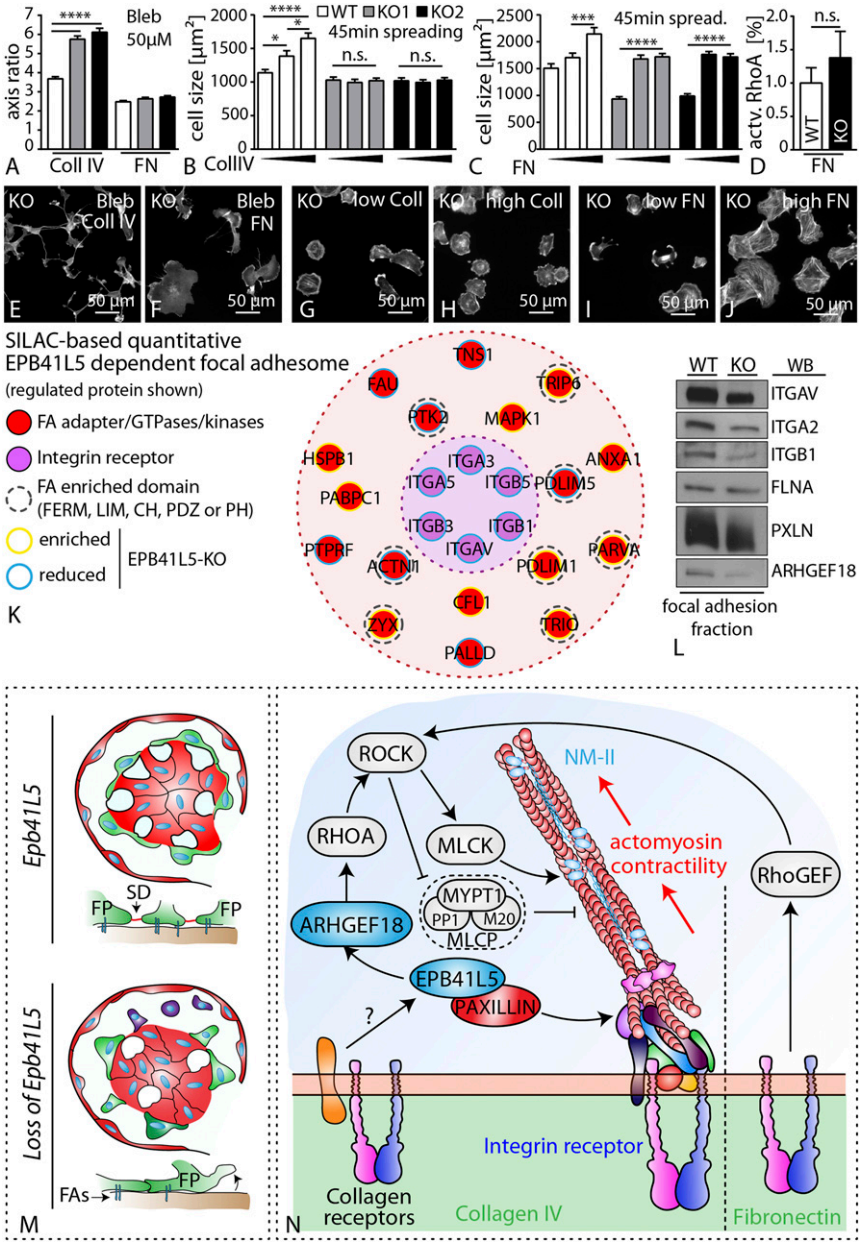

Fig. 7. ECM influences EPB41L5-mediated phenotypes. (*A*) Cell morphology assessed as major–minor axis quantification revealed altered morphological appearance of *EPB41L5* KO cells on collagen compared with fibronectin conditions (at least 145 cells were analyzed, averaged more than three independent experiments; Dataset S3). (*B*, *C*, *D–J*) *EPB41L5* KO clones show defective ECM sensing on collagen IV coated substratum. In contrast, increasing concentrations of the ECM ligand fibronectin led to improved spreading in respective KO clones (at least 100 cells per genotype and condition were analyzed, averaged over three independent experiments; Dataset S3). (*K*) Map of SILAC-based quantitative EPB41L5 dependent focal adhesome. (*L*) Western blot confirmation of focal adhesome fraction revealing balanced levels for PAXILLIN, whereas ITGB1, ITGA2, and also ARHGEF18 showed decreased intensity compared with the wild-type. (*M*) Schematic summarizing the phenotypic features of the EPB41L5 knockout characterized by foot process effacement and pronounced podocyte detachment. (*N*) EPB41L5 modulates actomyosin contractility via direct recruitment of the small GTPase ARHGEF18, and thereby influences FA maturation. This process is influenced via ECM composition and potential regulatory roles mediated by collagen receptors. Coll, collagen IV; ECM, extracellular matrix; FA, focal adhesion; FN, fibronectin, NM-II, nonmuscle myosin 2; SD, slit diaphragm; SILAC, stable isotope labeling by amino acids in cell culture.

CAS9-Mediated Knockout in Immortalized Human Podocytes. Detailed description of gRNA design, transfection, and isolation of respective clones is provided in the *SI Appendix*, *Materials and Methods*.

Statistics and Reproducibility. Data are expressed as mean ± SEM, if not stated otherwise. Based on data distribution (normal vs. nonnormal distribution), paired Student´s *t* test, one-way ANOVA (multiple comparison test, Tukey), or nonparametric two-tailed Mann-Whitney tests were performed. Experiments were not randomized or blinded. Statistical significance was defined as $*P < 0.05$, $**P < 0.01$, $***P < 0.001$, and $****P < 0.0001$; NS, not significant. Number of independent experiments and total amount of analyzed cells are stated either in the figure legends or listed in Dataset S3.

ACKNOWLEDGMENTS. We thank Charlotte Meyer, Christina Engel, Betina Kiefer, Barbara Joch, Helga Schachner, and Elisabeth Wiesner for expert technical assistance. In addition, we would like to express our gratitude to all members of our laboratories for helpful discussions and support, especially Ketan Patel for carefully reading the manuscript. We would also like to thank Ronald Roepman for generously providing antibodies and serum against EPB41L5. We thank Cristina Has for providing ITGalpha2 antibodies. This study was supported by the German Research Foundation: collaborative research

centers (CRC) 1140 (to T.B.H. and F.G.) and CRC 992 (to T.B.H.), Heisenberg program (T.B.H.), HU 1016/5-1 and HU 1016/8-1 (to T.B.H.); by the European Research Council (T.B.H.), and by the H2020-IMI2 consortium Biomarker Enterprise to Attack Diabetic Kidney Disease (BEAt-DKD) (115974 to T.B.H.); by the Bundesministerium für Bildung und Forschung, STOP Fokale Segmentale Glomerulosklerose (BMBF-STOP-FSGS) 01GM1518C (T.B.H.); by the Excellence Initiative of the German Federal and State Governments (GSC-4, Spemann Graduate School, C.S. and T.B.H.; BIOSS, T.B.H.; and the Freiburg Institute for Advanced Studies, T.B.H. and J.D.); by the Else Kröner Fresenius Stiftung, Nierenfunktionsstörungen als Komplikation von Systemerkrankungen (NAKSYS) (C.S., M.R., and T.B.H.) and Molekulare und Translationale Forschung in Freiburg – Verantwortungsvolle Ausbildung Tatkräftige Ermutigung (MOTIVATE) (D.S.); by the German Society of Nephrology (C.S.); and we gratefully acknowledge the financial support from the Ministerium für Innovation, Wissenschaft und Forschung des Landes Nordrhein-Westfalen, the Senatsverwaltung für Wirtschaft, Technologie und Forschung des Landes Berlin, and the Bundesministerium für Bildung und Forschung (to L.K., R.P.Z., and A.S.).

1. Faul C, Asanuma K, Yanagida-Asanuma E, Kim K, Mundel P (2007) Actin up: Regulation of podocyte structure and function by components of the actin cytoskeleton. *Trends Cell Biol* 17:428–437.
2. Grahammer F, Schell C, Huber TB (2013) The podocyte slit diaphragm–from a thin grey line to a complex signalling hub. *Nat Rev Nephrol* 9:587–598.
3. Simons M, Hartleben B, Huber TB (2009) Podocyte polarity signalling. *Curr Opin Nephrol Hypertens* 18:324–330.
4. Aaltonen P, Holthöfer H (2007) The nephrin-based slit diaphragm: New insight into the signalling platform identifies targets for therapy. *Nephrol Dial Transplant* 22: 3408–3410.
5. Kriz W, Lemley KV (2015) A potential role for mechanical forces in the detachment of podocytes and the progression of CKD. *J Am Soc Nephrol* 26:258–269.
6. Lennon R, Randles MJ, Humphries MJ (2014) The importance of podocyte adhesion for a healthy glomerulus. *Front Endocrinol (Lausanne)* 5:160.
7. Sachs N, Sonnenberg A (2013) Cell-matrix adhesion of podocytes in physiology and disease. *Nat Rev Nephrol* 9:200–210.
8. Hynes RO (1992) Integrins: Versatility, modulation, and signaling in cell adhesion. *Cell* 69:11–25.
9. Winograd-Katz SE, Fässler R, Geiger B, Legate KR (2014) The integrin adhesome: From genes and proteins to human disease. *Nat Rev Mol Cell Biol* 15:273–288.
10. Has C, et al. (2012) Integrin α3 mutations with kidney, lung, and skin disease. *N Engl J Med* 366:1508–1514.
11. Kanasaki K, et al. (2008) Integrin beta1-mediated matrix assembly and signaling are critical for the normal development and function of the kidney glomerulus. *Dev Biol* 313:584–593.
12. Pozzi A, et al. (2008) Beta1 integrin expression by podocytes is required to maintain glomerular structural integrity. *Dev Biol* 316:288–301.
13. El-Aouni C, et al. (2006) Podocyte-specific deletion of integrin-linked kinase results in severe glomerular basement membrane alterations and progressive glomerulosclerosis. *J Am Soc Nephrol* 17:1334–1344.
14. Sachs N, et al. (2006) Kidney failure in mice lacking the tetraspanin CD151. *J Cell Biol* 175:33–39.
15. Tian X, et al. (2014) Podocyte-associated talin1 is critical for glomerular filtration barrier maintenance. *J Clin Invest* 124:1098–1113.
16. Boerries M, et al. (2013) Molecular fingerprinting of the podocyte reveals novel gene and protein regulatory networks. *Kidney Int* 83:1052–1064.
17. Akilesh S, et al. (2011) Arhgap24 inactivates Rac1 in mouse podocytes, and a mutant form is associated with familial focal segmental glomerulosclerosis. *J Clin Invest* 121: 4127–4137.
18. Horton ER, et al. (2015) Definition of a consensus integrin adhesome and its dynamics during adhesion complex assembly and disassembly. *Nat Cell Biol* 17:1577–1587.
19. Schell C, Wanner N, Huber TB (2014) Glomerular development–shaping the multicellular filtration unit. *Semin Cell Dev Biol* 36:39–49.
20. Huber TB, et al. (2009) Loss of podocyte aPKClambda/iota causes polarity defects and nephrotic syndrome. *J Am Soc Nephrol* 20:798–806.
21. Hartleben B, et al. (2012) Role of the polarity protein Scribble for podocyte differentiation and maintenance. *PLoS One* 7:e36705.
22. Suleiman H, et al. (2013) Nanoscale protein architecture of the kidney glomerular basement membrane. *eLife* 2:e01149.
23. Schell C, et al. (2013) N-wasp is required for stabilization of podocyte foot processes. *J Am Soc Nephrol* 24:713–721.
24. Kuo JC, Han X, Hsiao CT, Yates JR, 3rd, Waterman CM (2011) Analysis of the myosin-II-responsive focal adhesion proteome reveals a role for β-Pix in negative regulation of focal adhesion maturation. *Nat Cell Biol* 13:383–393.
25. Wolfenson H, Iskratsch T, Sheetz MP (2014) Early events in cell spreading as a model for quantitative analysis of biomechanical events. *Biophys J* 107:2508–2514.
26. Lawson CD, Burridge K (2014) The on-off relationship of Rho and Rac during integrin-mediated adhesion and cell migration. *Small GTPases* 5:e27958.
27. Nakajima H, Tanoue T (2011) Lulu2 regulates the circumferential actomyosin tensile system in epithelial cells through p114RhoGEF. *J Cell Biol* 195:245–261.
28. Suh JH, Miner JH (2013) The glomerular basement membrane as a barrier to albumin. *Nat Rev Nephrol* 9:470–477.
29. Meehan DT, et al. (2009) Biomechanical strain causes maladaptive gene regulation, contributing to Alport glomerular disease. *Kidney Int* 76:968–976.
30. Schiller HB, Friedel CC, Boulegue C, Fässler R (2011) Quantitative proteomics of the integrin adhesome show a myosin II-dependent recruitment of LIM domain proteins. *EMBO Rep* 12:259–266.
31. Geiger T, Zaidel-Bar R (2012) Opening the floodgates: Proteomics and the integrin adhesome. *Curr Opin Cell Biol* 24:562–568.
32. Kriz W, Hähnel B, Hosser H, Rösener S, Waldherr R (2014) Structural analysis of how podocytes detach from the glomerular basement membrane under hypertrophic stress. *Front Endocrinol (Lausanne)* 5:207.
33. Kobayashi N, et al. (2015) Podocyte injury-driven intracapillary plasminogen activator inhibitor type 1 accelerates podocyte loss via uPAR-mediated β1-integrin endocytosis. *Am J Physiol Renal Physiol* 308:F614–F626.
34. Potla U, et al. (2014) Podocyte-specific RAP1GAP expression contributes to focal segmental glomerulosclerosis-associated glomerular injury. *J Clin Invest* 124:1757–1769.
35. Gosens I, et al. (2007) FERM protein EPB41L5 is a novel member of the mammalian CRB-MPP5 polarity complex. *Exp Cell Res* 313:3959–3970.
36. Laprise P, et al. (2009) Yurt, Coracle, Neurexin IV and the Na(+),K(+)-ATPase form a novel group of epithelial polarity proteins. *Nature* 459:1141–1145.
37. Hirano M, Hashimoto S, Yonemura S, Sabe H, Aizawa S (2008) EPB41L5 functions to post-transcriptionally regulate cadherin and integrin during epithelial-mesenchymal transition. *J Cell Biol* 182:1217–1230.
38. Salbreux G, Charras G, Paluch E (2012) Actin cortex mechanics and cellular morphogenesis. *Trends Cell Biol* 22:536–545.
39. Terry SJ, et al. (2011) Spatially restricted activation of RhoA signalling at epithelial junctions by p114RhoGEF drives junction formation and morphogenesis. *Nat Cell Biol* 13:159–166.
40. Auguste D, et al. (2016) Disease-causing mutations of RhoGDIα induce Rac1 hyperactivation in podocytes. *Small GTPases* 7:107–121.
41. Yu H, et al. (2013) Rac1 activation in podocytes induces rapid foot process effacement and proteinuria. *Mol Cell Biol* 33:4755–4764.
42. Guilluy C, Garcia-Mata R, Burridge K (2011) Rho protein crosstalk: Another social network? *Trends Cell Biol* 21:718–726.
43. Li A, et al. (2011) Rac1 drives melanoblast organization during mouse development by orchestrating pseudopod- driven motility and cell-cycle progression. *Dev Cell* 21: 722–734.
44. Schiffer M, et al. (2015) Pharmacological targeting of actin-dependent dynamin oligomerization ameliorates chronic kidney disease in diverse animal models. *Nat Med* 21:601–609.
45. Gu C, et al. (2017) Dynamin autonomously regulates podocyte focal adhesion maturation. *J Am Soc Nephrol* 28:446–451.

Supporting Information

Schell et al. 10.1073/pnas.1617004114

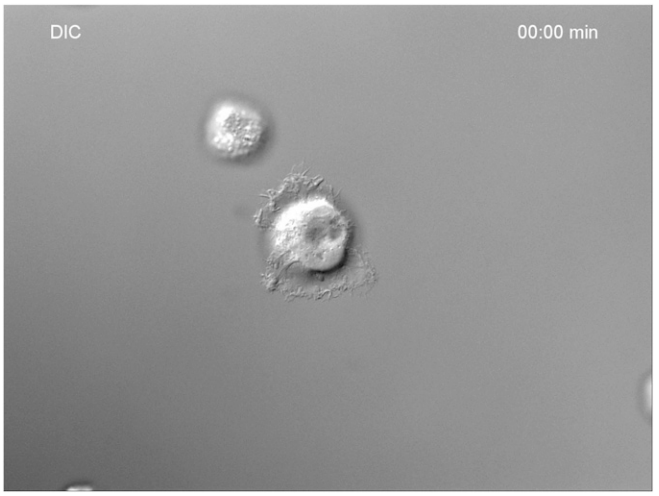

Movie S1. Spreading of EPB41L5 KO cells using differential interference contrast life microscopy.

Movie S1

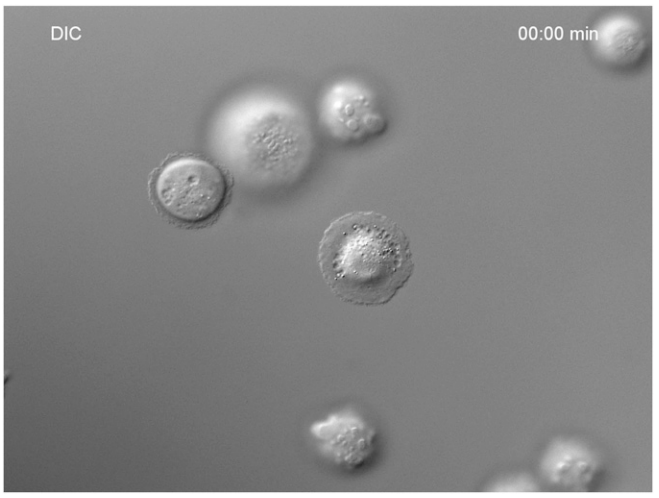

Movie S2. Spreading of wild-type cells using differential interference contrast life microscopy.

Movie S2

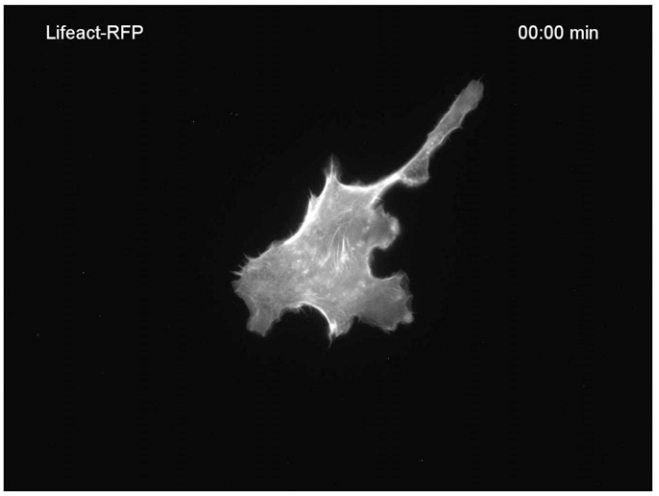

Movie S3. Life-imaging of EPB41L5 knockout cells employing Lifeact-RFP.

Movie S3

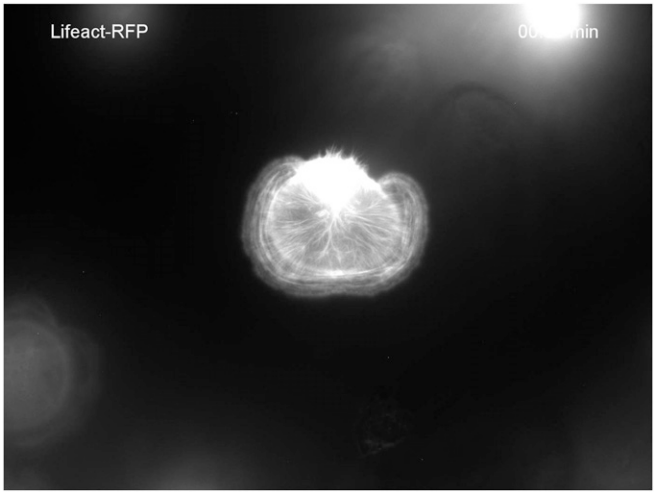

Movie S4. Life-imaging of wild-type cells employing Lifeact-RFP.

Movie S4

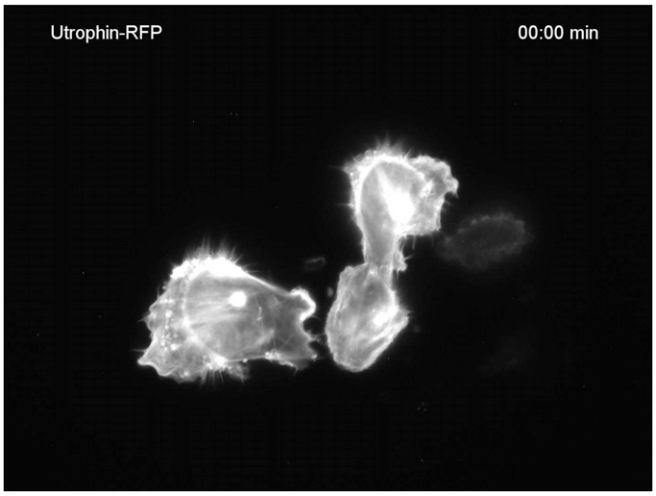

Movie S5. Life-imaging of EPB41L5 knockout cells employing Utrophin-RFP.

Movie S5

Dataset S1. iTRAQ based in vivo podocyte proteome

Dataset S1

Dataset S2. Podocyte focal adhesome

Dataset S2

Dataset S3. Statistical data

Dataset S3

Other Supporting Information Files

SI Appendix (PDF)

Supporting Information

Extendend Materials and Methods

Animals

A BAC clone, RP23-443K20, that contains the translational start site of the *Epb41l5* gene was obtained from BACPAC Resources (http://bacpac.chori.org/), and targeting and control vectors were constructed as described. Following primers were used: the 32 bp p1 (5'-CAGAAAGTCGACGCTAGATCCCCTCGCCTACC-3') and 23bp p2 (5'-GGTGTGGGGTCTGGGAATGAAGG-3') to amplify the 2.5kb 5' arm of the targeting vector, the 19bp p3 (5'-GGTCAAACAGCTCCTGTCC-3') and 36bp p4 (5'-GACTGGCTCGAGGGTAGGGTTGAGAGGGATTAGTAG-3')
sequences to amplify the 1.1kb 3' arm of the targeting vector. Their locations are indicated in Figure S7. The six underlined nucleotides in p1 and p4 sequences were converted into AccI and XhoI recognition sequences, GTCGAC and CTCGAG, respectively, to generate each primers. The amplified products were digested by each restriction enzyme: AccI and XhoI for the 2.5 kb 5' arm and SpeI and NotI for the 1.1kb 3' arm, respectively. To construct the targeting vector, the 5' 2.5kb and 3' 1.1kb arms were inserted into the AccI/NotI sites and NheI/XhoI sites of 5' and 3' cloning sites, respectively, of the LacZ/Neo-DTA vector. To generate podocyte specific knockout mice the well established *hNPHS2-Cre* allele was intercrossed to *Epb41l5* conditional mice (provided by Lawrence Holzman - Renal, Electrolyte and Hypertension Division, University of Pennsylvania School of Medicine Philadelphia, PA, USA). As an inducible podocyte specific mouse line we made use of a mouse line expressing a *rtTA* cassette under control of the *hNPHS2* promotor (1). Induction of the respective inducible mouse models was performed according to following protocol: animals at the age of 4 weeks received doxycycline hydrochloride (Fagron) via the drinking water (2mg/ml with 5% (wt/vol) sucrose, protected from light) for a periode of 14 days. For isolation of primary podocytes conditional *Epb41l5* knockout animals were crossed to *Gt(ROSA)26Sor*$^{tm4(ACTB-tdTomato,-EGFP)Luo/J}$ (purchased from JAX mice). Mice were maintained on a SV129 background. All mouse experiments were performed according to the National Institutes of Health Guide for the Care and Use of Laboratory Animals, as well as the German law governing the welfare of

animals. All studies were approved by the Regierungspräsidium Freiburg (G-10/39), Germany.

Urine analyses

Urine was collected at indicated time points and urinary albumin and creatinine were measured using Microflural™ Microalbumin Test (Progen, Heidelberg, Germany) and an Creatinine Kit (Labor+Technik, LT-Sys, Berlin, Germany) according to the manufacturer´s protocol. Proteinuria was expressed as albumin to creatinine ratio (ACR ratio: albumin mg to creatinine mg).

In situ hybridization

Whole mRNA extracts from P1 mouse kidneys served as template for RT-PCR and subsequent cloning of fragments of the coding sequence and 3′-untranslated region. For generating insitu probes against *mEpb41l5* the following primers were used:
mEpb41l Transcript variant 1+2(fp): 5´- AGT TCA GGT TTG TGC CCA TC -3´
mEpb41l Transcript variant 1+2(rp): 5´ - CGG GAT CCT AGT CGA ATG AA -3´
PCR products were cloned into pBluescript II KS (-), linearized and transcribed with T3 and T7 RNA polymerases (Promega, Mannheim, Germany) to generate sense and antisense digoxigenin-labeled probes (digoxigenin RNA labeling mix; Roche Applied Science, Mannheim, Germany). Kidneys at postnatal day 2 were fixed overnight at 4 °C in 4% paraformaldehyde, embedded in paraffin, and sectioned at 8 µm. For mRNA detection, slides were treated with proteinase K, refixed with 4% paraformaldehyde, acetylated by using acetic anhydride (0,25% acetic anhydride in 0,1M triethanolamine (T-1377; Sigma, Schnelldorf, Germany) and hybridized at 68 °C in hybridization buffer (50% formamide, 5× SSC, yeast RNA (50g/ml), 1% SDS, heparin (50g/ml), 0,1% probe). Stringency washes were performed with wash I (50% formamide, 5× SSC (pH4,5), 1%SDS) and wash II (50% formamide, 2× SSC). For detection, slides were incubated with alkaline phosphatase-conjugated anti-digoxigenin antibody 1:3000 at 4 °C overnight followed by BM purple staining (Roche Applied Science, Mannheim, Germany). Digital photographs were captured on an Axioplan2 microscope (Zeiss, Oberkochen, Germany).

SEM and TEM procedures

For scanning electron microscopy kidney samples were fixed in glutaraldehyde and dehydrated by graded ethanol series (70% ethanol, 80% ethanol, 90% ethanol and

100% ethanol), followed by incubation in 50:50 ethanol/Hexamethyldisilazane (Sigma, Schnelldorf, Germany). After incubation in 100% HMDS the solvent was allowed to evaporate. Samples were coated with Gold (Zeiss Semco Nanolab7, Polaron Cool Sputter Coater E 5100, Balzer Cpd 020) and imaged using a Leo 1450 VP scanning electron microscope. Samples for immunogold electron microscopy were fixed and subsequently embedded in Lowicryl K4M resin (Electron Microscopy Sciences). Ultrathin sections were cut and stained by indirect immunogold protocol as described before (for antibodies see supporting information antibodies list)(2).

Immunofluorescence staining of kidney sections

Kidneys were frozen in OCT compound medium immediately after dissection. 4µm sections were cut on a Leica Cryotome. Sections were subsequently fixed in 4% paraformaldehyde, blocked in PBS with 5% BSA and incubated with primary antibodies for 1h or overnight. Sections were washed for several times, then fluorophore-conjugated secondary antibodies (dilution 1:500 - Invitrogen, Karlsruhe, Germany) were applied and incubated for 45 minutes. Human kidney biopsy samples underwent an antigen retrieval step (pH citrate 6.0), and were subsequently processed as outlined above. Imaging was performed either on a Zeiss Axioscope 40FL microscope, equipped with an Axiocam MRc5 digital video camera and conventional HBO lamp (Carl Zeiss, Oberkochen, Germany) or on a LSM510 confocal microscope (Zeiss). Use of human kidney biopsy material was approved by the Scientific-Ethical Committee of the University Medical Center of Freiburg. Control kidney samples were from unaffected areas of tumor nephrectomies. Imaging was performed on a Zeiss Axioscope 40FL microscope, equipped with an Axiocam MRc5 digital video camera and conventional HBO lamp (Carl Zeiss, Oberkochen, Germany).

mRNA expression analysis of human kidney disease entities (NEPHROSEQ)

For analysis of differential mRNA expression levels in human glomerular disease entities the opensource database NEPHROSEQ was used (www.nephroseq.org). For detailed patient information and statistical data see dataset S3.

Antibodies

All antibodies used in this study are collectively described in the SI Materials and Methods (at the end of the SI appendix).

STORM – super resolution microscopy

Briefly, primary antibody diluted in 3% BSA-PBS was applied on the sections and incubated overnight at 4°C. The next day, sections were washed for 30 minutes with PBS at room temperature and then incubated with the STORM-specific secondary antibodies diluted in 3% BSA-PBS at room temperature for 2 hours. STORM image acquisition was performed using a custom-made setup as described (22). Approximately 10,000 images per channel were captured and analyzed using custom software. Further details are provided in the supplemental section. After washing the samples for 30 minutes with PBS at room temperature, immunolabeled sections were postfixed using 3% PFA and 0.1% glutaraldehyde (Electron Microscopy Sciences) in PBS and prepared for STORM imaging. The secondary antibodies were custom conjugated to Alexa647 reporter dye and either Alexa405 or Cy3 activator dyes. Coverglass with the sections on it was inverted onto a slide containing a drop of imaging buffer containing mercaptoethylamine along with an oxygen scavenger system, and coverglass edges were sealed with nail polish.

MS-procedures: Cell lysis and carbamidomethylation

Approximately 1.3 to 2.7 million GFP+ (podocytes) and RFP+ (non-podocytes) cells per individual preparation were used. Each preparation consisted of 4 individual animals, which were pooled after cell sorting. The whole analysis was performed with 4 individual and independent preparations. Snap frozen cell pellets were lysed in 50 mM Tris-HCl, pH 7.8 buffer containing 150 mM NaCl, 1% SDS and complete mini EDTA-free (Roche Diagnostics). Subsequently, 1 µL of benzonase (25 U/µL) and 2 mM $MgCl_2$ were added to the lysates and incubated at 37°C for 30 min. Samples were centrifuged at 4°C and 18,000 *g* for 30 min. Protein concentration of the supernatant was determined by BCA assay according to the manufacturer's protocol (Pierce, Thermo Scientific). Cysteines were reduced with 10 mM dithiothreitol at 56°C for 30 min followed by alkylation of free thiol groups with 30 mM iodoacetamide at room temperature (RT) in the dark for 30 min.

MS-procedures: Sample preparation and proteolysis

Samples for LC-MS analysis were prepared using filter aided sample preparation (FASP) (3, 4) with minor changes. Cell lysates corresponding to 50 µg of protein

were diluted with freshly prepared 8 M urea/100 mM Tris-HCl, pH 8.5 buffer (5). Diluted samples were placed on the Microcon centrifugal devices (30 KDa cutoff) and were centrifuged at 13,500 *g* at RT for 25 min. All the following centrifugation steps were performed under similar conditions i.e. 13,500 *g*, RT, 15 min. To eliminate residual SDS, three washing steps were carried out using 100 µL of 8 M urea/100 mM Tris-HCl, pH 8.5 buffer and finally for the buffer exchange, the devices were washed thrice with 100 µL of 50 mM triethylammonium bicarbonate (TEAB) buffer, pH 8.5. To the concentrated proteins, 100 µL of proteolysis buffer comprising sequencing grade modified trypsin (Promega) 1:25 w/w (enzyme to protein), 0.2 M GuHCl, 2 mM $CaCl_2$ in 50 mM TEAB buffer, pH 8.5 were added and incubated at 37°C for 14 h. The generated tryptic peptides were recovered by centrifugation with 50 µL of 50 mM TEAB buffer, pH 8.5 followed by 50 µL of ultra-pure water. Finally, the peptides were acidified (pH < 3.0) with trifluoroacetic acid (TFA) and the digests were quality controlled as described previously (6). Acidified peptides were completely dried under vacuum (SpeedVac), resolubilized in 0.5 M TEAB (pH 8.5) and the peptide concentration was determined using a NanoDrop 2000 UV-Vis spectrophotometer (Thermo Scientific). ,

MS-procedures: iTRAQ 8-plex labeling and reversed phase fractionation at pH 6.0

Prior to labeling with iTRAQ reagents, each sample (~ 0.5 µg) was analyzed on a LC-MS system. The sample amounts were corrected based on the comparison of total ion chromatograms (TICs) to compensate for the systematic errors such that each sample had identical starting material before labeling. After adjustment, 25 µg of tryptic peptides of each sample were labeled with iTRAQ 8-plex reagents (AB Sciex) according to the manufacturer's instructions. After incubation, the samples were pooled and the reaction was quenched by adding 100 µL of ultra-pure water. The multiplexed sample was concentrated to ~20 µL under vacuum and subsequently acidified with TFA (1% final concentration). Sample cleanup was done with a C18 SPE cartridge (15 mg, Varian) using a vacuum manifold system and the eluted peptides were dried in a SpeedVac. The dried multiplexed sample was resolubilized in buffer A (10 mM ammonium acetate, 0.4 mM formic acid (FA), pH 6.0) and 50 µg were fractionated by reversed phase chromatography at pH 6.0 on an Zorbax 300SB-C18 column, 1 x 150 mm, 5 µm particle size column (Agilent) using an UltiMate 3000

HPLC (Thermo Scientific) using a binary buffer system; buffer A: 10 mM ammonium acetate, 0.4 mM FA, pH 6.0 and buffer B: 84% acetonitrile (ACN) in 10 mM ammonium acetate, 0.4 mM FA, pH 6.0. Peptides were loaded onto the column with buffer A at a flowrate of 12.5 µL/min and separation was carried out using the following gradient: 0-3% B in 10 min, 3-50% B in 65 min, 50-60% B in 5 min, 60-95% B in 5 min, 95% B hold for 5 min, 95%-3% B in 5 min and finally re-equilibrate the column with 3% B for 20 min. In total, 24 fractions were collected at 30 sec intervals from min 15 to 70 in a concatenation mode.

LC-MS/MS analysis

Each fraction was resolubilized in 45 µL of 0.1% TFA and 1/3rd of each sample was analyzed by nano-LC-MS/MS using an Ultimate 3000 nano RSLC system coupled to a Q Exactive mass spectrometer (both Thermo Scientific). Peptides were preconcentrated on a 75 µm x 2 cm C18 trapping column for 10 min using 0.1% TFA with a flow rate of 20 µL/min followed by separation on a 75 µm x 50 cm C18 main column (both Pepmap, Thermo Scientific) with a 127 min LC gradient ranging from 3-42% of B (84% ACN in 0.1% FA) at a flow rate of 250 nL/min. The Q Exactive was operated in data-dependent acquisition mode and MS survey scans were acquired from m/z 300 to 1,500 at a resolution of 70,000 using the polysiloxane ion at m/z 371.101236 as lock mass (7). Precursor isolation window was set as 2.0 m/z and the fifteen (Top15) most intense signals were subjected to higher energy collision dissociation (HCD) with a normalized collision energy of 35% at a resolution of 17,500 taking into account a dynamic exclusion of 12 s. Automated gain control (AGC) target values and fill times were set to $3x10^6$ and 120 ms for MS and $1x10^6$ and 250 ms for MS/MS, respectively with an underfill ratio of 10%. For charge state reduction, a 10% (v/v) NH_4OH solution was placed at the nano-ESI source as previously described (8).

Protein enrichment and functional annotation analysis

Detected proteins (iTRAQ podocyte proteome) were identified as enriched/upregulated with a “log2 ratio podocytes/non-podocytes” >0.5 or as non-upregulated with a log2 ratio <0.5. Gene ontology term (GO-Term) annotation was implemented using the UniProt and MGI database (9, 10). The GO-Term: “GO:0005925 focal adhesion” (MGI database) was used to generate a list of

podocyte enriched focal adhesion proteins. These focal adhesion proteins were assembled to functional groups as previously described by Kuo JC et al. (11). To generate a network out of these proteins, the list of focal adhesion proteins found as enriched was imported into Cytoscape (version 3.2.1) (12). Protein-protein interactions were added by merging this network with a human interactome from the BioGRID (release 3.2.105) database (13). Protein and interaction duplications were removed. In order to generate an unbiased list of potential podocyte specific focal adhesion proteins, a merged focal adhesion proteome from Horton ER et al. was merged with the list of proteins enriched in podoyctes (14). This candidate list was subsequently filtered for protein domains enriched in focal adhesion proteins. This list of protein domains enriched in focal adhesion proteins was generated by analysis of the consensus integrin adhesome from Horton et al. (14) Go-Term and InterPro protein domain enrichment analysis was done using the FunRich (version 2.1.2) functional enrichment analysis software (15, 16). The mice proteome database from UniProt was chosen as a background database. For enriched Go-Terms hypergeometric uncorrected p-values are shown on the charts (Figure S2). Also Benjamini-Hochberg corrected FDR values led to significant p-values for these Go-Terms.

Isolation of focal adhesion complexes

A technique for isolation of focal adhesion complexes was described previously (11, 14). This technique was combined with a SILAC based quantitative MS approach (17). In brief, human immortalized podocytes were SILAC labeled under growth conditions at 33°C. After 14 days, podocytes were seeded to a 50µg/ml collagen IV coated 15cm cell culture dish and were cultured for 24 hours. For stabilization and linkage of focal adhesion complexes to the underlying ECM cells were incubated with two protein cross-linkers (DSP (3,3'-Dithiobis(sulfosuccinimidylpropionate); 100mM; Sigma-Aldrich) and DPPB (1,4-Bis[3-(2-pyridyldithio)propionamido]butane; 10mM; Sigma-Aldrich)) for 10 minutes. Cross-likers were removed by washing with PBS and quenched with 1M Tris-HCl (pH 7,5, 10 min). After additional washing in PBS, cell bodies were removed via cell lysis using RIPA buffer (25mM Tris-HCL, 150mM NaCl , 1% Triton-X-100, 0,2% SDS +0,5% Sodium Deoxycholic acid, pH7,5, containing proteinase inhibitors) for 3 minutes at 4°C followed by application of hydrodynamic force using a waterpik (washing 2x10s with PBS). ECM linked focal adhesion

complexes were now isolated by scraping in scraping buffer (100mM Tris-HCl (pH 7,6), 4% (w/v) SDS). Total protein concentrations were measured and samples were balanced. Laemmli buffer (with DTT) was added and focal adhesion complexes were denatured at 70°C for 10 min. MS analysis and Western blotting was performed subsequently. Data processing and annotation of external databases was performed as described above. A core focal adhesome was defined by merging the consensus integrin adhesome (14) with a literature curated adhesome(18). EPB41L5 dependent regulated components of this core adhesome were graphically shown in Figure 7. For further information see also dataset S2.

Isolation of primary podocytes for *in vitro* experiments

Kidneys were cut in small pieces and mixed in 3ml (per kidney pair) prewarmed digestion solution (digestion solution containing 1mg/ml Collagenase, 1mg/ml Proteinase, 50U/ml DNase in 1xHBSS). The solution was resuspended and incubated at 37°C for 7min. After incubation the solution was put on a cell strainer and it was rubbed through the cell strainer using the stamp of a 5ml syringe. The strainer was washed using ice cold 1xHBSS. The flow-through was filtered through a cell strainer and washed again with 1xHBSS. Glomeruli were washed from this cell strainer using 1xHBSS and collected. The obtained glomeruli were centrifuged at 4°C, 2000g for 10min, the supernatant was removed and the glomeruli pellet was dissolved in primary podocyte medium (RPMI medium supplemented with 10% FBS, Penicillin/Streptomycin, ITS). Cell culture flask were coated using Collagen IV dissolved in acetic acid solution and finally the resuspended glomeruli were seeded and cultured at 37°C and 5% $CO_{2.}$. Glomerular cells were grown out for 7 days and FACS sorted to obtain the GFP labeled podocyte fraction.

Crispr/Cas9 mediated knockout of EPB41L5

For the generation of *EPB41L5* knockout in immortalized human podocytes (generous gift from Moin Saleem, Bristol, UK) the Crispr/CAS9 genome editing technology was applied. gRNAs targeting exon 1 of the human *EPB41L5* gene were designed using a web-based platform (e-crisp.org - http://www.e-crisp.org/E-CRISP/) and further subcloned in targeting CRISPR nuclease vectors with an OFP reporter according to manufacturer´s instructions (guideRNA: 5'-GACTTAGAATCTCCAGCTGC(AGG)-3' - gene-art – Invitrogen, Karlsruhe, Germany). After initial validation in mixed cell-populations employing the nuclease

surveyor technology (Integrated DNA technologies, Leuven, Belgium), immortalized human podocytes were electroporated with CAS9 nuclease and respective gRNAs. After 48 hours, OFP positive cells were selected via FACS and single cell clones were further grown to subsequent mutation analysis. DNA of respective single cell clones was isolated and further PCR amplified and homozygous mutated clones were preselected applying a restriction enzyme digest with PstI (5'-CTGCA/G-3' New England BioLabs, Ipswich, MA, USA). These clones were subcloned and analyzed using Sanger Sequencing (primer pairs for amplification – E1 fw 5´-TCTTGAACTCCTGGCTCTA-3´; E1 rev 5´-TTTGGAGCTCAGCAAGACCT-3´). Only clones with homozygous mutations resulting in premature stop-codons were selected for further analysis. Loss of protein was furthermore confirmed using western blot.

Single cell migration assay

Cells were seeded on ibidi µ-treat dishes (ibidi, Martinsried, Germany) and cultivated in standard medium (see above). Observation of single cell migration was performed using a Nikon Biosstation IM device (Nikon, Düsseldorf, Germany). Primary podocytes were identified by *NPHS2Cre* driven podocyte specific GFP expression and phase contrast observation was performed for 12 hours. In the case of immortalized podocytes imaging was only performed using phase contrast. Further analysis was done by using the ManualTracking and ChemoTaxis plugin for NIH ImageJ 1.46.

Adhesion, cellular spreading assays and analysis of focal adhesion morphology

Adhesion assays on collagen IV coated surfaces were performed as previously described (19). In brief, cells were trypsinized, counted with an automated cell counting tool (Biorad, Munich, Germany) and equal amounts of cells (40.000 cells per genotype and technical replicate) were seed for 15 minutes on 50µg/ml collagen IV precoated 96 well plates. After standardized washing procedures, crystal violet was applied and OD as a measure of adhered cells was quantified on a photometer (TECAN, Crailsheim, Germany). For cell spreading assays equal amounts of cells were seeded on pre-coated cover-slips or ibidi 8-well dishes (if not statet otherwise precoating was performed with 50µg/ml collagen IV or fibronectin respectively, for spreading under titrated ECM concentrations 0.5µg/ml, 10µg/ml and 50µg/ml were applied for either collagen IV or fibronectin; fibronectin from BD Biosciences and

collagen IV from Sigma) for indicated time points. After brief fixation in PFA 4%, cells were stained with Phalloidin and imaged using an Axioscope 40FL microscope setup 20x magnification. Randomly chosen images were captured and analyzed using ImageJ NIH. Following binarization of images individual cell areas were measured. Circularity analysis was also performed using implemented function of ImageJ NIH. For the quantification of focal adhesion fractions cells were seeded for 30 and 45 minutes, fixed and stained. Individual cells were assessed for 3 criteria (a: only edge-staining; b: nascent adhesions; c: maturated adhesions). Focal adhesion morphology was assessed by staining for the focal adhesion component PAXILLIN. Image acquisition was performed using a Zeiss Axioscope 40FL microscope, equipped with a 63x objective. Evaluation of focal adhesion size and distribution was performed with a custom written macro embedded in FIJI NIH ImageJ 1.46. For the quantification of cellular protrusions cells were seeded for 30 minutes at 20µg/ml collagen IV coated glass cover slips, fixed and stained. Protrusions of individual cells were counted and analyzed. To assess major:minor axis ratios individual cells were analyzed using NIH ImageJ 1.46. Analysis of fluorescence intensities across the cell border were performed using the line scan function of FIJI NIH ImageJ 1.46. At least 10 representative cells per condition were measured and at least 3 biological replicates were analyzed. For treatment and washout experiments equal amounts of cells were seeded for 4 hours on collagen IV or fibronectin pre-coated glass cover-slips. Then treatment of cells using the myosin-II inhibitor blebbistatin (Sigma, Schnelldorf, Germany) and the ROCK inhibitor Y-27362 (Sigma) were performed as indicated in the individual experiments, for 40 minutes. Treatment of cells using doxorubicin and protramine sulfate (Sigma) were performed as indicated in the individual experiments. For spreading experiments under doxorubicin or protramine sulfate treatment, cells were pre-treated with 2µg/ml doxorubicin for 24 hours or 300µg/ml protamine sulfate for 10 minutes.

Live cell imaging

For analysis of pseudopod dynamics immortalized human podocytes were transfected with RFP-tagged versions of Lifeact via electroporation. After 24 hours cells were seeded on ibidi dishes (ibidi, Martinsried, Germany) and recorded on a Zeiss Cell Observer equipped with a LCI Plan-Neofluoar 63x/1.3 objective and Tokai Heat Incubator (controlled heating, controlled CO2 atmosphere). Respective imaging

sequences were analyzed using Image J NIH Version 1.47. Protrusion rate generation was calculated by counting every newly generated protrusion in a 10 minute time frame.

siRNA knockdown in immortalized human podocytes

Generation of siRNA mediated knockdown of *ARHGEF18* in immortalized human podocytes was performed using previously published siRNA sequences (siRNA p114Rhogef I - 5′-UCAGGCGCUUGAAAGAUA-3′; p114Rhogef II - 5′-GGACGCAACUCGGACCAAU-3′ (20)). Transfection was performed using Amaxa nucleofector technology (Lonza, Basel, Switzerland) according to manufacturer´s instructions. Efficiency of the knockdown was cofirmed 48 and 72 hours after transfection using western blot. Spreading experiments were performed and quantified as described above.

Analysis of activated RhoA and Rac1 levels using G-LISA

Cells were serum starved for 3 consecutive days at 1% FCS in standard RPMI1640 medium. After completion of the starvation period, cells were trypsinized and equal amounts were seeded on either collagen IV or fibronectin coated 10 cm dishes for either 20 or 45 minutes. Dishes were washed with ice-cold PBS buffer twice and lysis was performed at 4°. Lysates were equalized due to protein content and analyzed according to the manufacturers instruction (RhoA G-LISA activation assay kit – BK124; Rac1,2,3 G-LISA activation assay kit – BK125, Cytoskeleton, USA).

Immunoprecipitation and pulldown

Co-immunoprecipitation was performed as described previously (21). Briefly, HEK 293T cells were transiently transfected with 4µg DNA of the indicated constructs using the PEI (Polyethylenimin) method. After incubation for 24 h, the cells were lysed in 1% Triton X-100 lysis buffer (1% Triton X-100, 20ml Tris-HCL, 50mM NaCL, 50mM NaF, 15mM $Na_4P_2O_7$, 1mM EDTA, pH 7.4) (30 min; 4°C). Cell lysates were incubated with mouse anti-V5-tag antibody, rabbit ant-VSV-tag antibody, rabbit anti-ARHGEF18 antibody or anti-Flag M2 agarose affinity beads (Sigma Aldrich) for 1 h at 4°C. Thereafter lysates were incubated with 20 µl of protein G-Sepharose beads for mouse antibodies and with 20 µl of protein A-Sepharose beads for rabbit antibodies for 0,5 - 1 h at 4°C. Recombinant GST tagged protein was produced in a BL21(DE3)

E. coli strain. The transformation, expression and purification were performed according to standard procedures (22). GST tagged protein was pre-bound to 25µl glutathione-Sepharose beads (GE Healthcare) and subsequently incubated with lysates of human immortalized podocytes or VSV-ARHGEF18 overexpressing HEK293T cells for 1 hour at 4°. The beads were washed 5 times with lysis buffer, and bound proteins were resolved in *Laemmli sample buffer* (95°C, 5 min). Precipitated proteins were separated by standard SDS-polyacrylamide gel electrophoresis. Following constructs were used: N or C-terminal tagged constructs (either FLAG or GFP tag) for human EPB41L5 were purchased and used according to manufacturer´s instructions (Genescript, New Jersey, USA). VSV-tagged *ARHGEF18* was generously provided by K. Matter (20). N-terminal V5-, FLAG-, GFP-tagged constructs of full length and truncated EPB41L5 were created by cloning into pcDNA6 vector using standard cloning procedures. N-terminal GST-tagged constructs were created by cloning into pGEX-4T-3 vector.

Expression of *EPB41L5* constructs in immortalized human podocytes

For transfection of immortalized human podocyte cells (kindly provided by M. Saleem, University of Bristol, UK) electroporation as described above was performed. N or C-terminal tagged constructs (either FLAG or GFP tag) for human EPB41L5 were purchased and used according to manufacturer´s instructions (Genescript, New Jersey, USA). Rescue experiment in respective EPB41L5 KO cells were performed by re-expression of GFP-tagged versions of human EPB41L5 as outlined above (either full length or respective truncations). Cell size area, as well as pseudopod formation and p-MLC fluorescence intensity was recorded as indicated above and knockout cells expressing only GFP served as controls (for analysis only cells with equalized expression levels were selected).

Supplemental References

1. Shigehara T*, et al.* (2003) Inducible podocyte-specific gene expression in transgenic mice. *Journal of the American Society of Nephrology : JASN* 14(8):1998-2003.
2. Horvat R, Hovorka A, Dekan G, Poczewski H, & Kerjaschki D (1986) Endothelial cell membranes contain podocalyxin--the major sialoprotein of visceral glomerular epithelial cells. *The Journal of cell biology* 102(2):484-491.
3. Manza LL, Stamer SL, Ham A-JL, Codreanu SG, & Liebler DC (2005) Sample preparation and digestion for proteomic analyses using spin filters. *PROTEOMICS* 5(7):1742-1745.
4. Wisniewski JR, Zougman A, Nagaraj N, & Mann M (2009) Universal sample preparation method for proteome analysis. *Nat Meth* 6(5):359-362.
5. Kollipara L & Zahedi RP (2013) Protein carbamylation: In vivo modification or in vitro artefact? *PROTEOMICS* 13(6):941-944.
6. Burkhart JM, Schumbrutzki C, Wortelkamp S, Sickmann A, & Zahedi RP (2012) Systematic and quantitative comparison of digest efficiency and specificity reveals the impact of trypsin quality on MS-based proteomics. *Journal of Proteomics* 75(4):1454-1462.
7. Olsen JV*, et al.* (2005) Parts per Million Mass Accuracy on an Orbitrap Mass Spectrometer via Lock Mass Injection into a C-trap. *Molecular & Cellular Proteomics* 4(12):2010-2021.
8. Thingholm TE, Palmisano G, Kjeldsen F, & Larsen MR (2010) Undesirable Charge-Enhancement of Isobaric Tagged Phosphopeptides Leads to Reduced Identification Efficiency. *Journal of Proteome Research* 9(8):4045-4052.
9. UniProt C (2015) UniProt: a hub for protein information. *Nucleic acids research* 43(Database issue):D204-212.
10. Eppig JT*, et al.* (2015) The Mouse Genome Database (MGD): facilitating mouse as a model for human biology and disease. *Nucleic acids research* 43(Database issue):D726-736.
11. Kuo JC, Han X, Hsiao CT, Yates JR, 3rd, & Waterman CM (2011) Analysis of the myosin-II-responsive focal adhesion proteome reveals a role for beta-Pix in negative regulation of focal adhesion maturation. *Nature cell biology* 13(4):383-393.
12. Shannon P*, et al.* (2003) Cytoscape: a software environment for integrated models of biomolecular interaction networks. *Genome research* 13(11):2498-2504.
13. Chatr-Aryamontri A*, et al.* (2015) The BioGRID interaction database: 2015 update. *Nucleic acids research* 43(Database issue):D470-478.
14. Horton ER*, et al.* (2015) Definition of a consensus integrin adhesome and its dynamics during adhesion complex assembly and disassembly. *Nature cell biology* 17(12):1577-1587.
15. Hunter S*, et al.* (2009) InterPro: the integrative protein signature database. *Nucleic acids research* 37(Database issue):D211-215.
16. Pathan M*, et al.* (2015) FunRich: An open access standalone functional enrichment and interaction network analysis tool. *Proteomics* 15(15):2597-2601.
17. Kuttner V*, et al.* (2013) Global remodelling of cellular microenvironment due to loss of collagen VII. *Molecular systems biology* 9:657.

18. Winograd-Katz SE, Fassler R, Geiger B, & Legate KR (2014) The integrin adhesome: from genes and proteins to human disease. *Nature reviews. Molecular cell biology* 15(4):273-288.
19. Humphries MJ (2009) Cell adhesion assays. *Methods in molecular biology* 522:203-210.
20. Terry SJ*, et al.* (2011) Spatially restricted activation of RhoA signalling at epithelial junctions by p114RhoGEF drives junction formation and morphogenesis. *Nature cell biology* 13(2):159-166.
21. Huber TB*, et al.* (2003) Nephrin and CD2AP associate with phosphoinositide 3-OH kinase and stimulate AKT-dependent signaling. *Molecular and cellular biology* 23(14):4917-4928.
22. Huber TB*, et al.* (2003) The carboxyl terminus of Neph family members binds to the PDZ domain protein zonula occludens-1. *The Journal of biological chemistry* 278(15):13417-13421.

Supporting Information

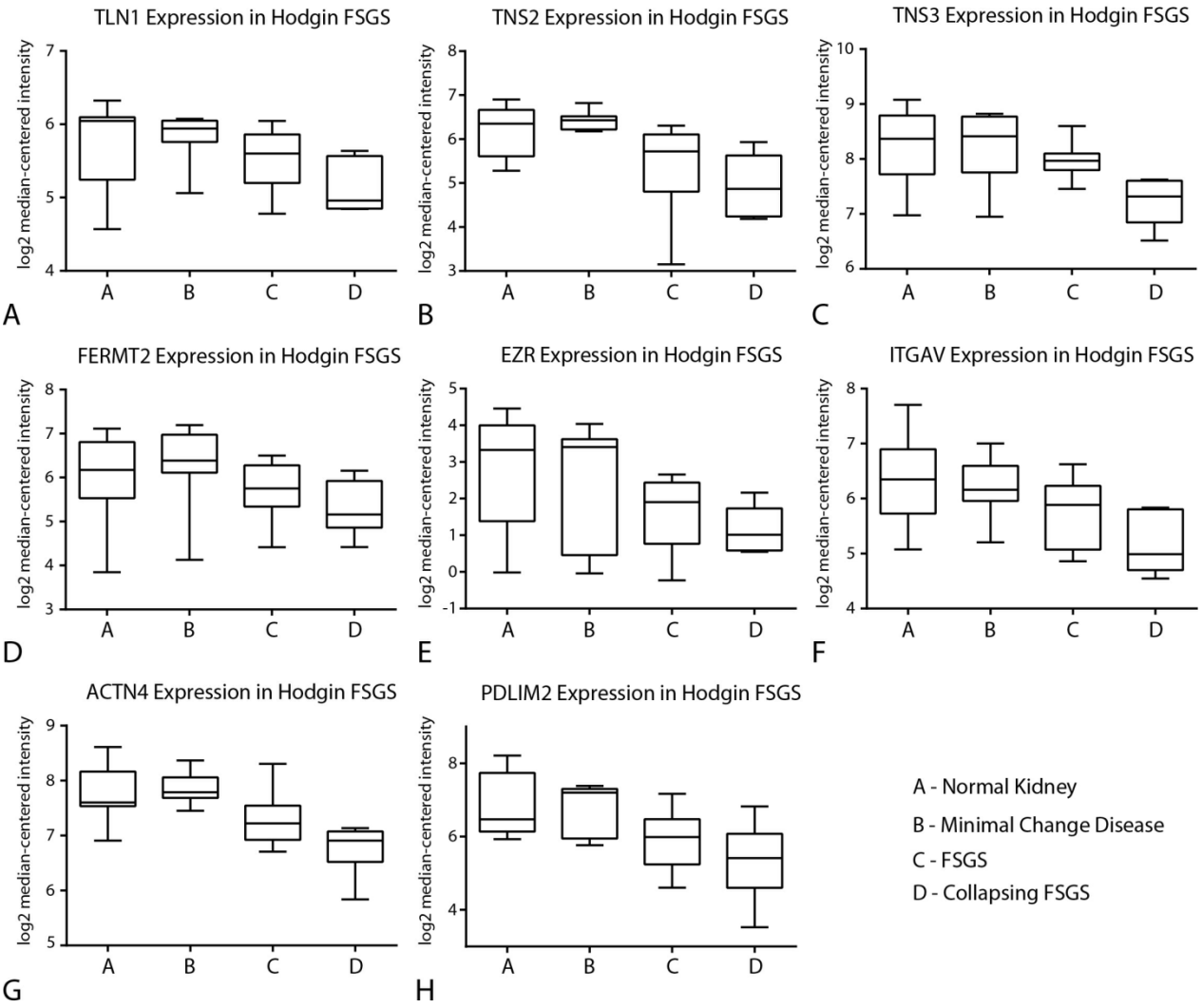

<u>Supplemental Figure 1</u>: Analysis of mRNA expression levels of focal adhesion proteins in human glomerular disease entities

(A-H) Expression values of respective focal adhesion proteins (TALIN-1, TENSIN-2, TENSIN-3, FERMT2, EZRIN, INTEGRIN-alphaV, ACTININ-4, PDLIM2) were analyzed using the open source database NEPHROSEQ. As disease entities minimal change disease, focal segmental sclerosis and collapsing focal segmental glomerular sclerosis were analyzed (for statistical data see dataset S3). All FA proteins showed a diminished expression level in respective disease entities when compared to controls (human nephrectomy samples).

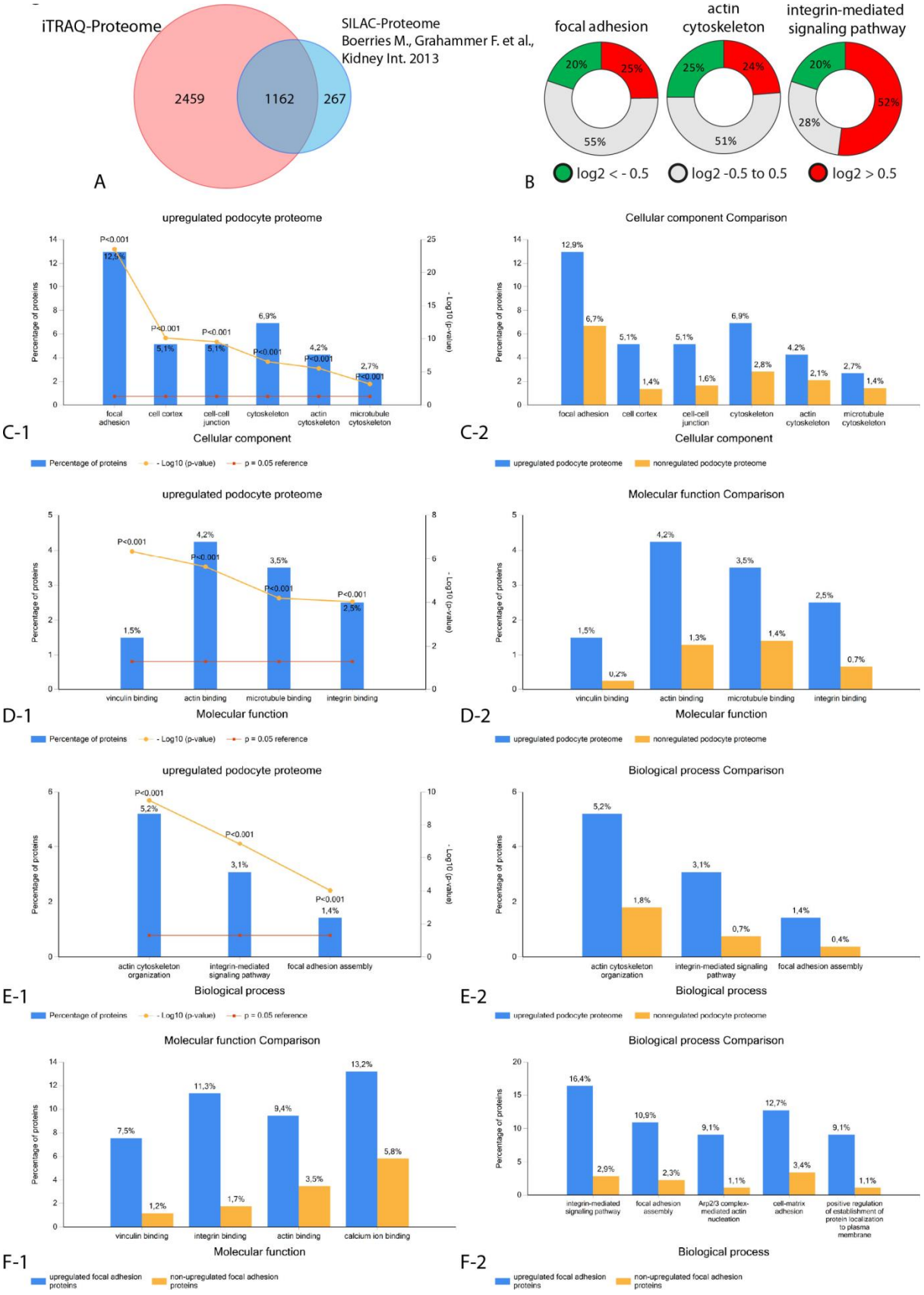

<u>Supplemental Figure 2</u>: Analysis of mapped podocyte adhesome

(A) Venn diagram comparing the coverage of detected proteins between a previous SILAC labeled podocyte proteomics approach [19] and the actual iTRAQ labeled

proteomics approach. **(B)** Sub-analysis of the focal adhesome data set revealed enrichment of integrin-mediated signaling pathways **(C-F)** Analysis of cellular component, molecular function and biological process of respective enriched FA components (see also dataset S1): B1, C1 and D1 GO-Term analysis for log2 fold >0.5 enriched proteins; B2, C2 and D2 GO-Term comparison between log2 fold >0.5 versus log2 fold <0.5 proteins; E1 and E2 selected FA-proteins with log2 fold change >0.5 were analyzed again for GO-term enrichment.

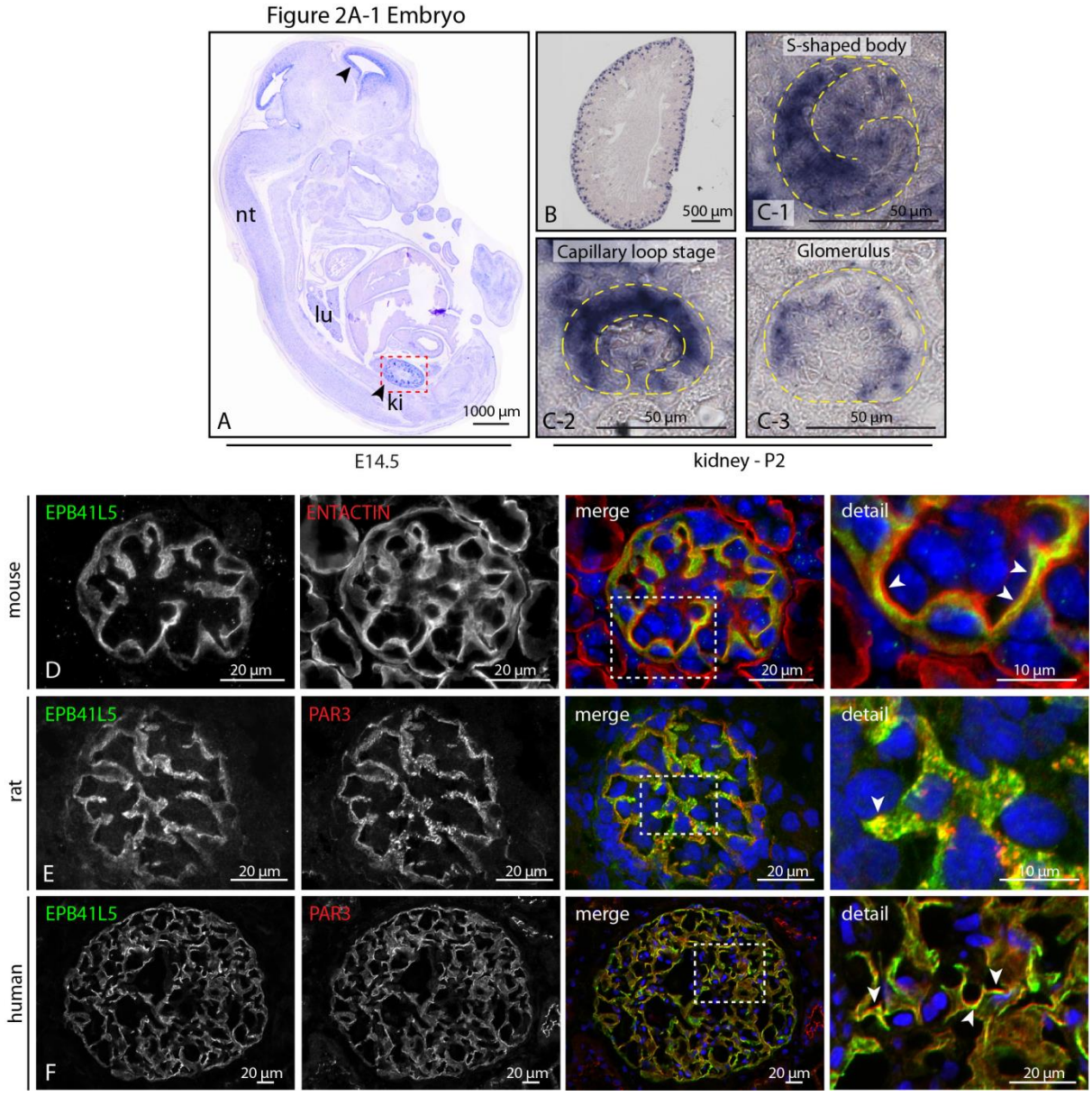

<u>Supplemental Figure 3</u>: Expression of *Epb41l5* in murine development and localization in glomeruli

(A) In situ hybridization on E14.5 murine embryo revealed strongest expression in the kidney (nt= neural tube, lu= lung, ki=kidney; black arrowhead indicates expression in the developing CNS, red boxed area highlights developing kidney). **(B-C)** During glomerular development (C1-C3: comma shaped body, capillary loop stage and glomerulus) *EPB41L5* was specifically detected in podocytes (glomerular structures are highlighted by yellow dotted lines). **(D-F)** Immunofluorescence for EPB41L5 on murine, rat and human glomerular sections (white arrowheads indicate enrichment in the podocyte compartment).

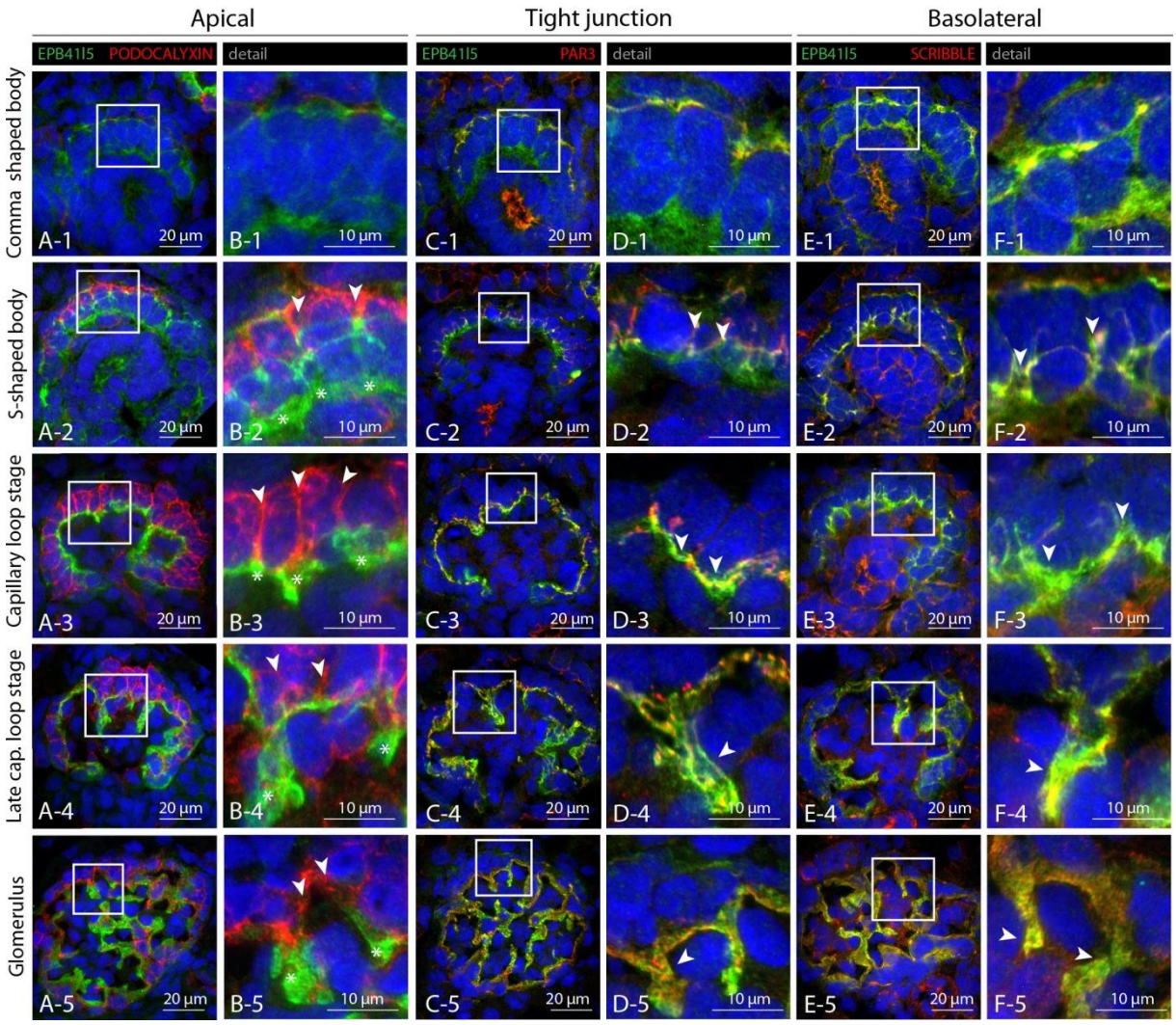

<u>Supplemental Figure 4:</u> Apico-basal polarization of podocytes while glomerular maturation

(A-F) Antibody staining on cryo-sections of P0 murine kidneys: EPB41L5 together with the apical marker PODOCALYXIN showed mutually exclusive staining (B-1-B-5). When EPB41L5 was co-stained together with the tight junction marker PAR3 overlap could be visualized at the comma shaped stage (D-3), but at later stages EPB41l5 located more basal than PAR3(D-4 & D-5). The basolateral marker SCRIBBLE perfectly co-localized with EPB41L5 in every developmental stage of the glomerulus (F-1 – F-5).

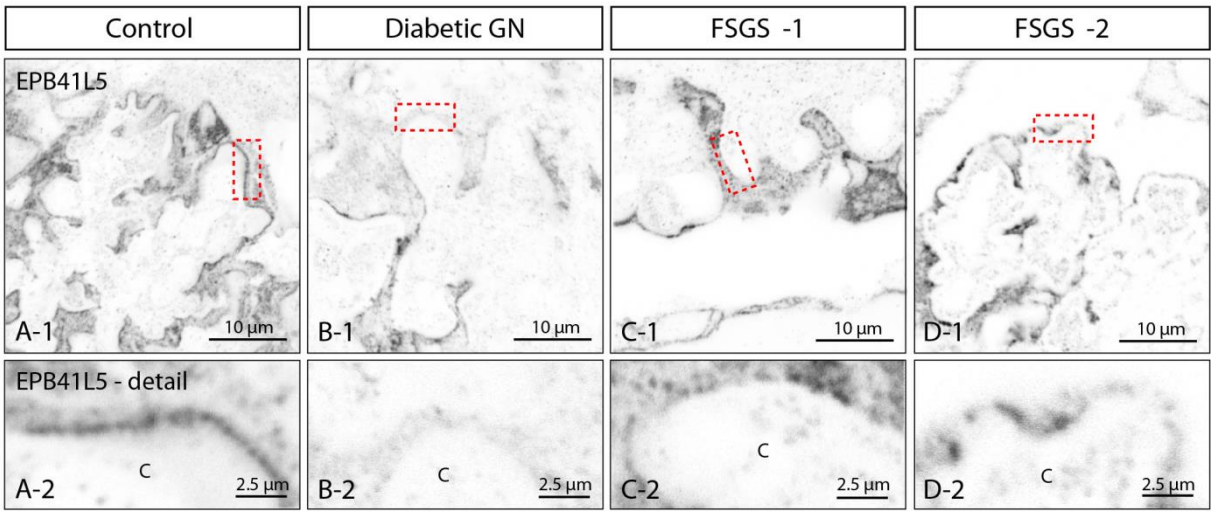
Control
Diabetic GN
FSGS -1
FSGS -2
EPB41L5
A-1
B-1
C-1
D-1
10 µm
EPB41L5 - detail
A-2
B-2
C-2
D-2
C
2.5 µm

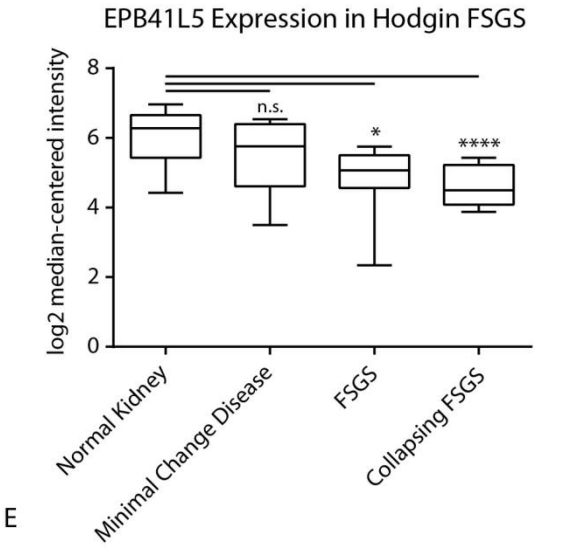
EPB41L5 Expression in Hodgin FSGS
log2 median-centered intensity
n.s.
*
****
Normal Kidney
Minimal Change Disease
FSGS
Collapsing FSGS

E

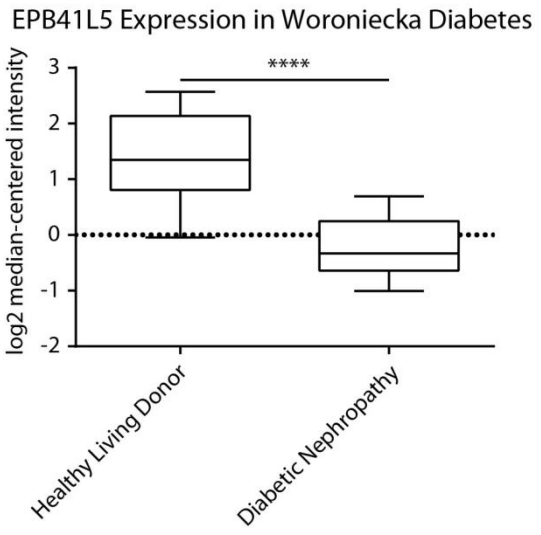
EPB41L5 Expression in Woroniecka Diabetes
log2 median-centered intensity
****
Healthy Living Donor
Diabetic Nephropathy

F

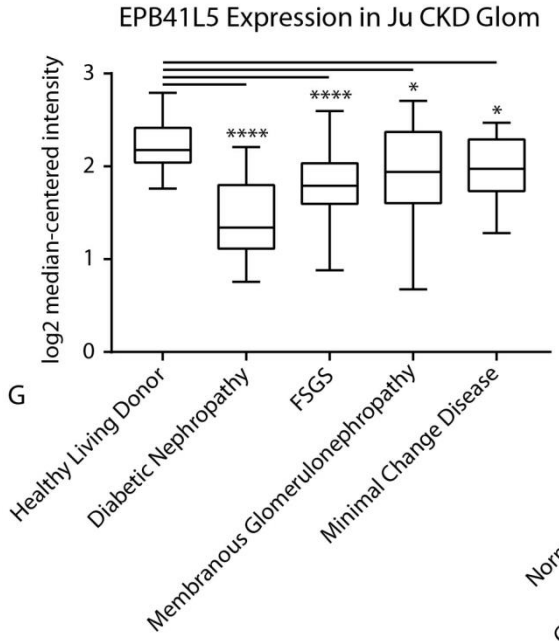
EPB41L5 Expression in Ju CKD Glom
log2 median-centered intensity
****
****
*
*
Healthy Living Donor
Diabetic Nephropathy
FSGS
Membranous Glomerulonephropathy
Minimal Change Disease

G

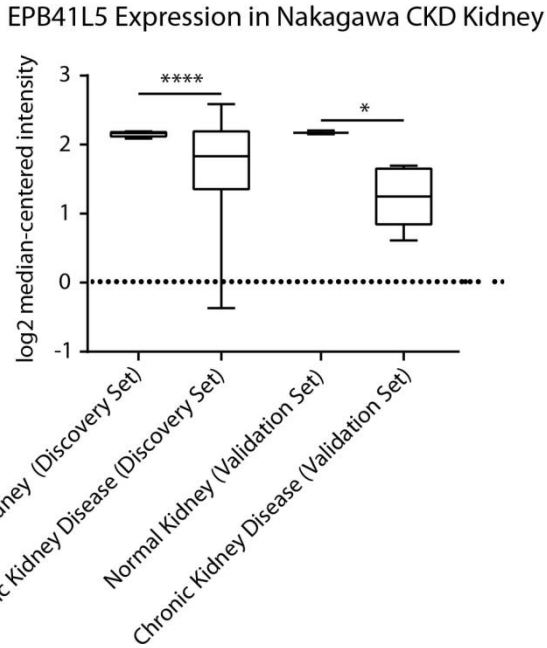
EPB41L5 Expression in Nakagawa CKD Kidney
log2 median-centered intensity
****
*
Normal Kidney (Discovery Set)
Chronic Kidney Disease (Discovery Set)
Normal Kidney (Validation Set)
Chronic Kidney Disease (Validation Set)

H

<u>Supplemental Figure 5:</u> EPB41L5 shows decreased expression levels in human glomerular diseases

(A-D) Immunofluorescence studies on human biopsy samples (Diabetic nephropathy and focal segmental glomerulosclerosis) revealed a diminished and granular signal intensity of EPB41L5, predominantly at the basal compartment of glomerular podocytes (red boxes indicate zoom-in areas). (E-H) Analysis of expression levels for EPB41L5 in different glomerular disease entities shows decreased expression compared to control or healthy donors (for statistical data see dataset S3).

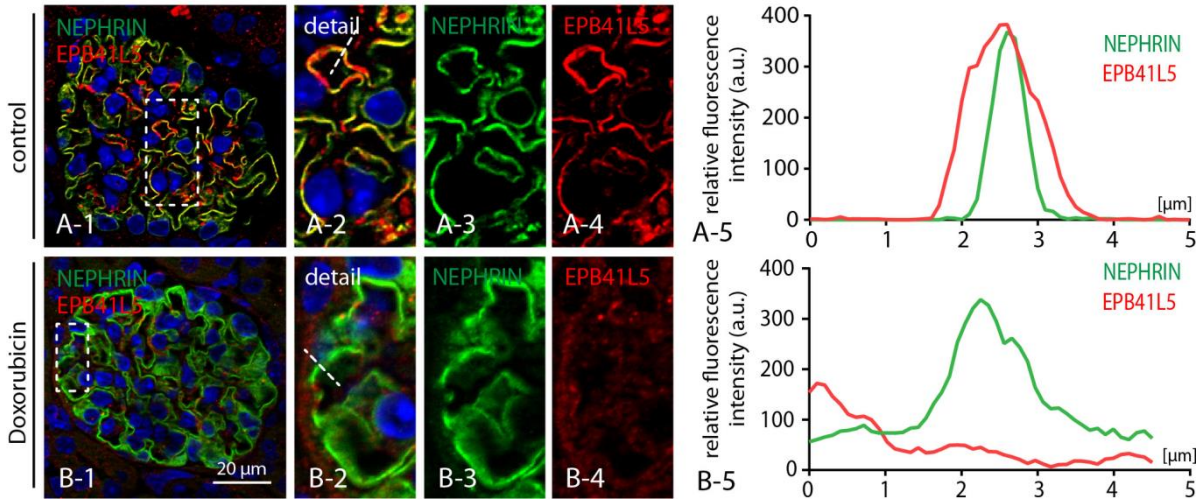

<u>Supplemental Figure 6</u>: EPB41L5 shows altered localization pattern in experimental murine doxorubicin mediated glomerulopathy

(A-B) Immunofluorescence studies of doxorubicin treated animals revealed diminished signal intensity EPB41L5. Respective line scans across the glomerular filtration barrier (white dotted lines) reflect the altered signal intensities for NEPHRIN and EPB41L5.

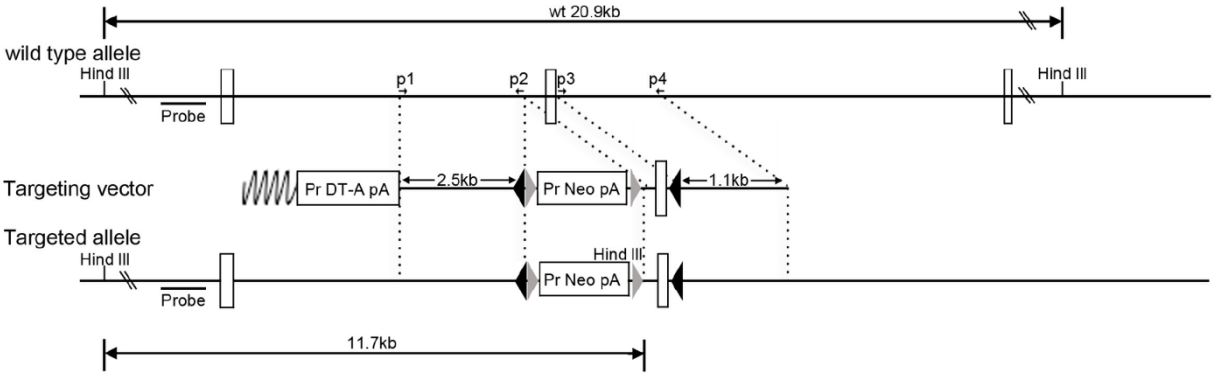

A

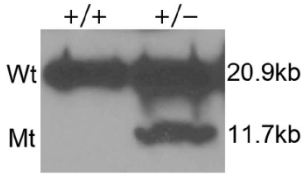

B

<u>Supplemental Figure 7</u>: Targeting strategy and generation of a conditional *Epb41l5* allele

(A) Schematic representation of the wild type *Epb41l5* allele (top), the targeting vector (middle), and the predicted mutant allele (bottom). Black triangles, *loxP* sequence; Gray triangles, *frt* sequences; Neo, neomycine resistant gene; DT-A, diphtheria toxin A-fragment gene. Probe indicates the location of the probe used for Southern blot analysis. **(B)** An example of Southern blot analysis for F1 offspring with the probe indicated in **(A)**.

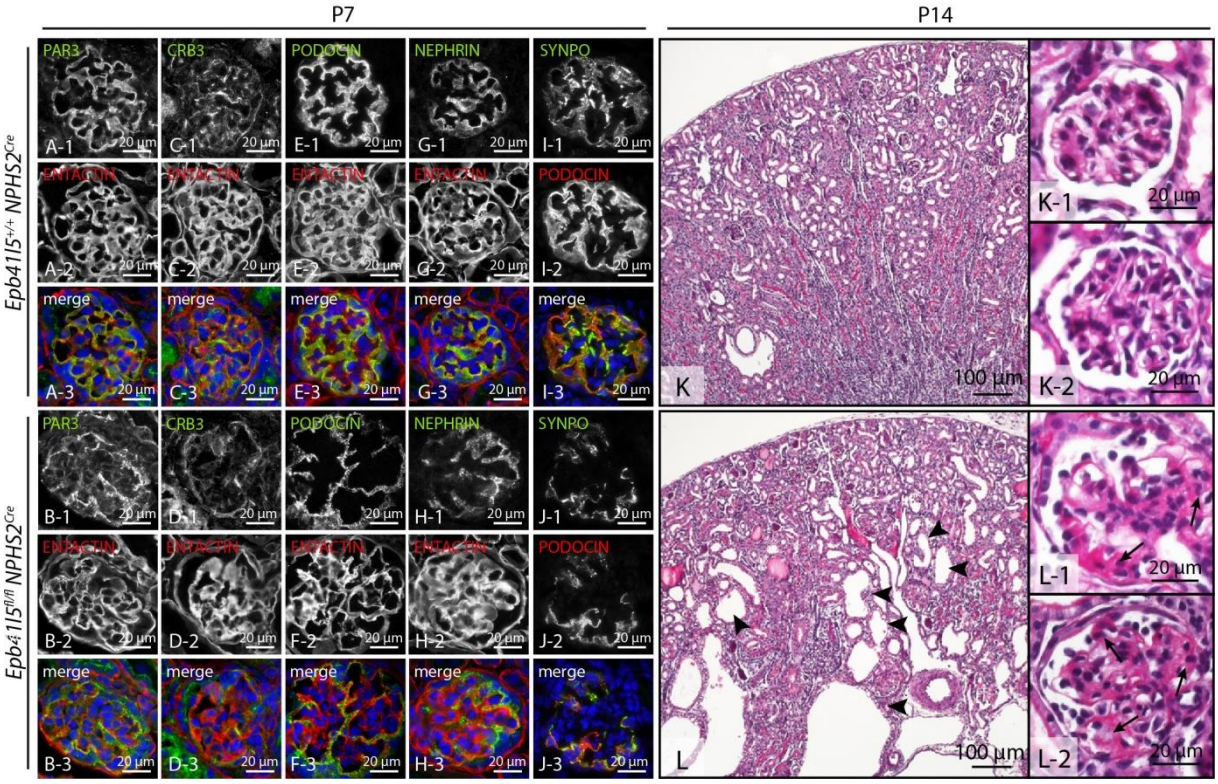

<u>Supplemental Figure 8</u>: Podocyte specific knockout of *Epb41l5* leads to glomerulosclerosis

(A-J) Analysis of podocyte marker proteins showed altered expression and localization patterns in respective *Epb41l5* knockout podocytes compared to wild type animals at P7. **(K-L)** Histological evaluation at P14 demonstrated prominent cystic tubular degeneration (L - black arrowheads) and pronounced glomerulosclerosis (L-1 and L-2; black arrows) in *Epb41l5* knockout animals.

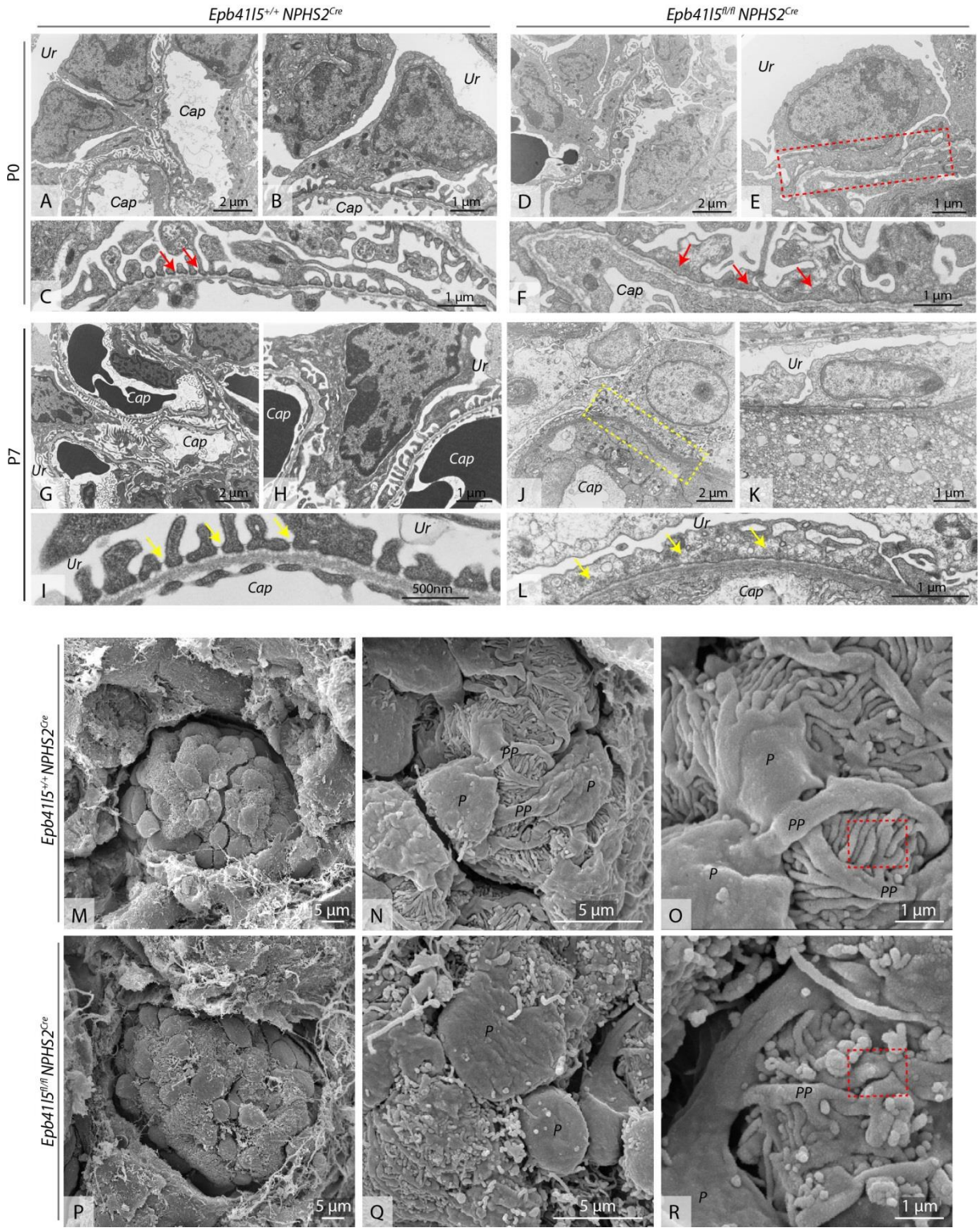

<u>Supplemental Figure 9</u>: *Epb41l5* knockout animals show severe signs of foot process effacement

(A-L) Electron microscopy revealed severe signs of global foot process fusion in *Epb41l5* knockout animals already at birth. One week after birth discrete vacuolization is noticed and slit diaphragms are not discernible any more (red arrows indicate fused areas of podocyte FPs; yellow arrows highlight slit diaphragms in wild type animals and electron dense accumulations in knockout animals; boxed regions

indicate zoomed details, Ur: urinary space; Cap: capillaries). **(M-R)** Scanning electron microscopy of glomeruli from wild type and *Epb41l5* knockout animals: while wild type animals showed a regular pattern of interdigitating foot processes, these structures were simplified and retracted in *Epb41l5* knockout animals (P = podocyte cell body, PP = primary processes; boxed regions indicate areas of disturbed FP architecture).

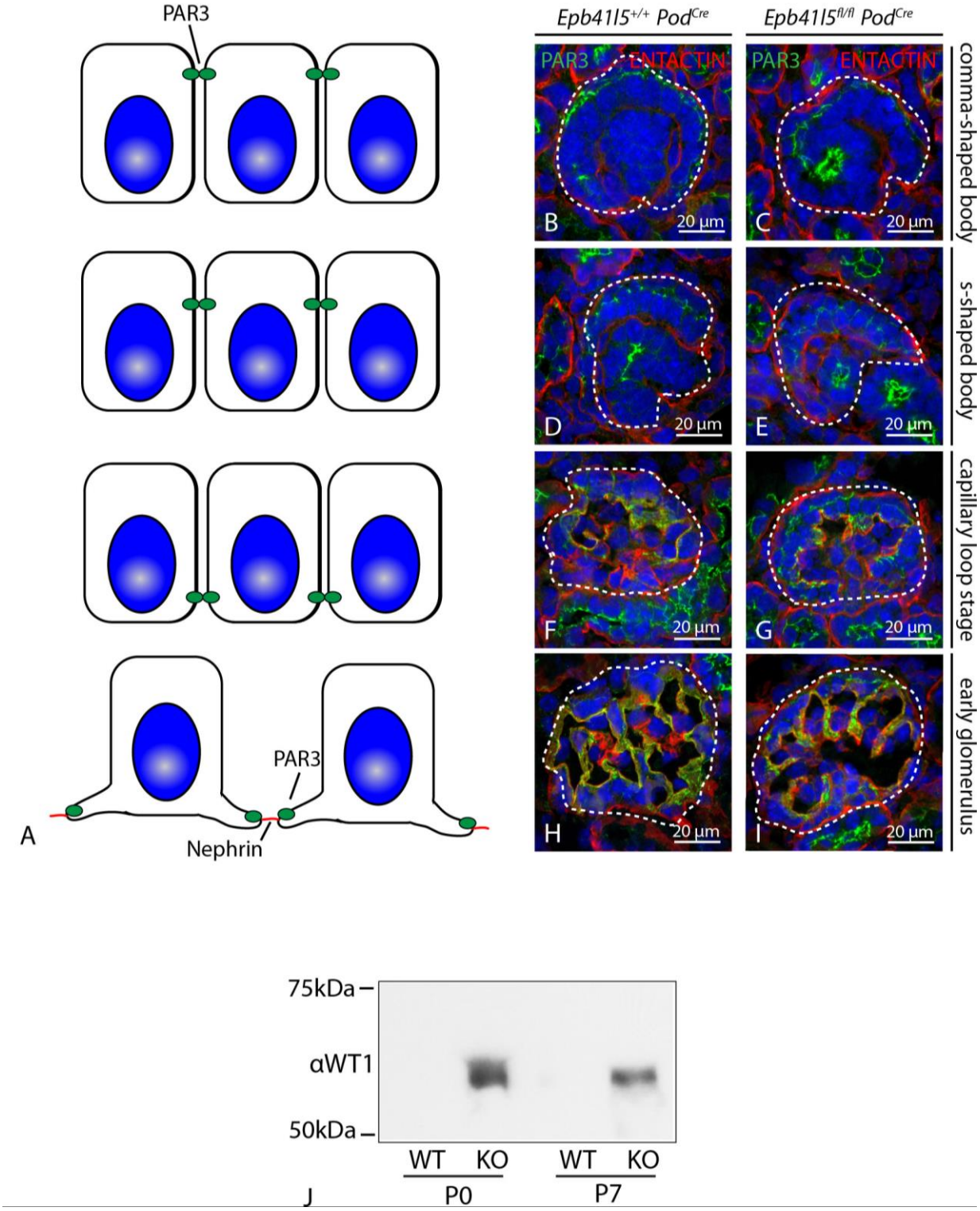

<u>Supplemental Figure 10</u>: Apico-basal migration of PAR3 is not influenced by EPB41L5 deficiency

(A) Schematic illustration of podocyte development: while transition from cuboidal epithelial cell morphology towards extensive basal specification and generation of podocyte foot processes certain marker proteins indicate the shift in polarization. PAR3 and slit diaphragm proteins like NEPHRIN migrate from the apical domain towards the basal compartment of podocytes. **(B-I)** The apico-basal migration of

PAR3 is not impaired in *Epb41l5* knockout mice. At the comma and s-shaped stage PAR3 is pre-dominantly apically localized (B-E). During further glomerular maturation PAR3 undergoes a change in localization towards the more basal compartment. No major alterations between wild type and respective knockout animals were observed at any developmental stage (*PodCre* was used synonymously used for *hNPHS2Cre*). **(J)** Western blot of urine samples detected a WT-1 positive band only in *Ebp41l5* knockout animals.

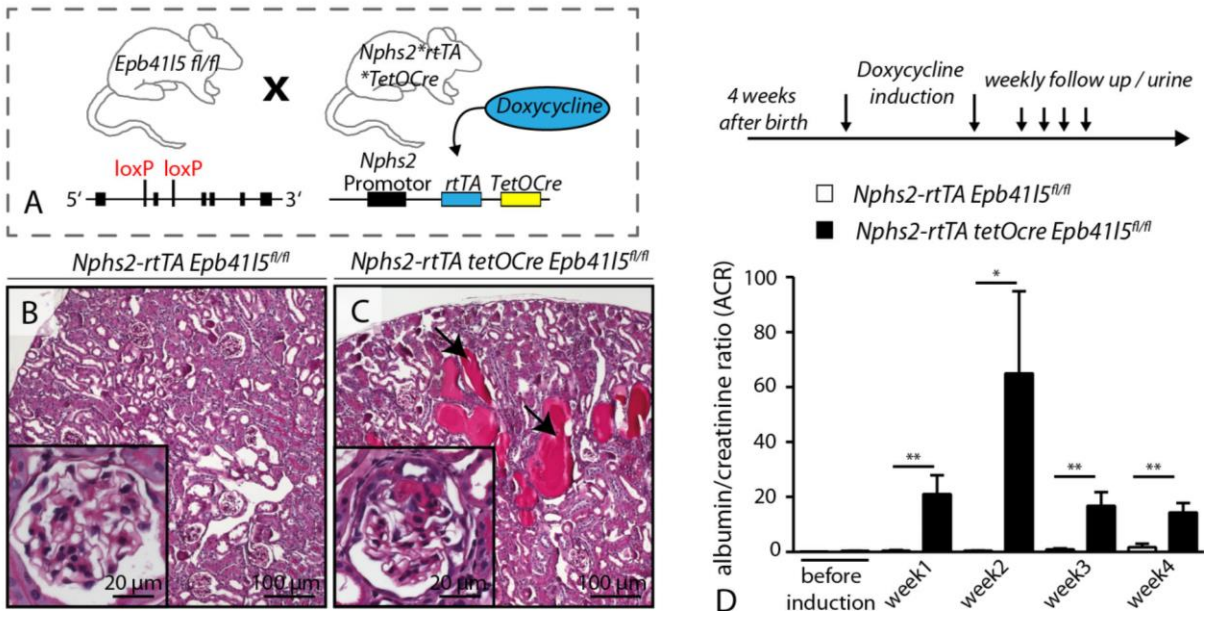

<u>Supplemental Figure 11</u>: Inducible deletion of *Epb41l5* in podocytes leads to nephrotic syndrome

(A) Schematic for the breeding strategy to generate inducible podocyte specific *Epb41l5* knockout mice (left panel). With the age of 4 weeks mice were induced with doxycycline via drinking water and after a 2 week induction protocol, weekly follow up monitored for levels of proteinuria (right panel). **(B-C)** Histology of induced *Epb41l5* knockout mice revealed accumulation of proteinaceous casts, dilated tubuli and segmental sclerosis in glomeruli (arrows and inserts). **(D)** Measurement of albumin/creatinine ratio revealed early onset of proteinuria already at 1 week after induction, further increasing at week 2 (after initial induction period at least 6 animals per genotype and time point were analyzed; for statistics see the material and methods section).

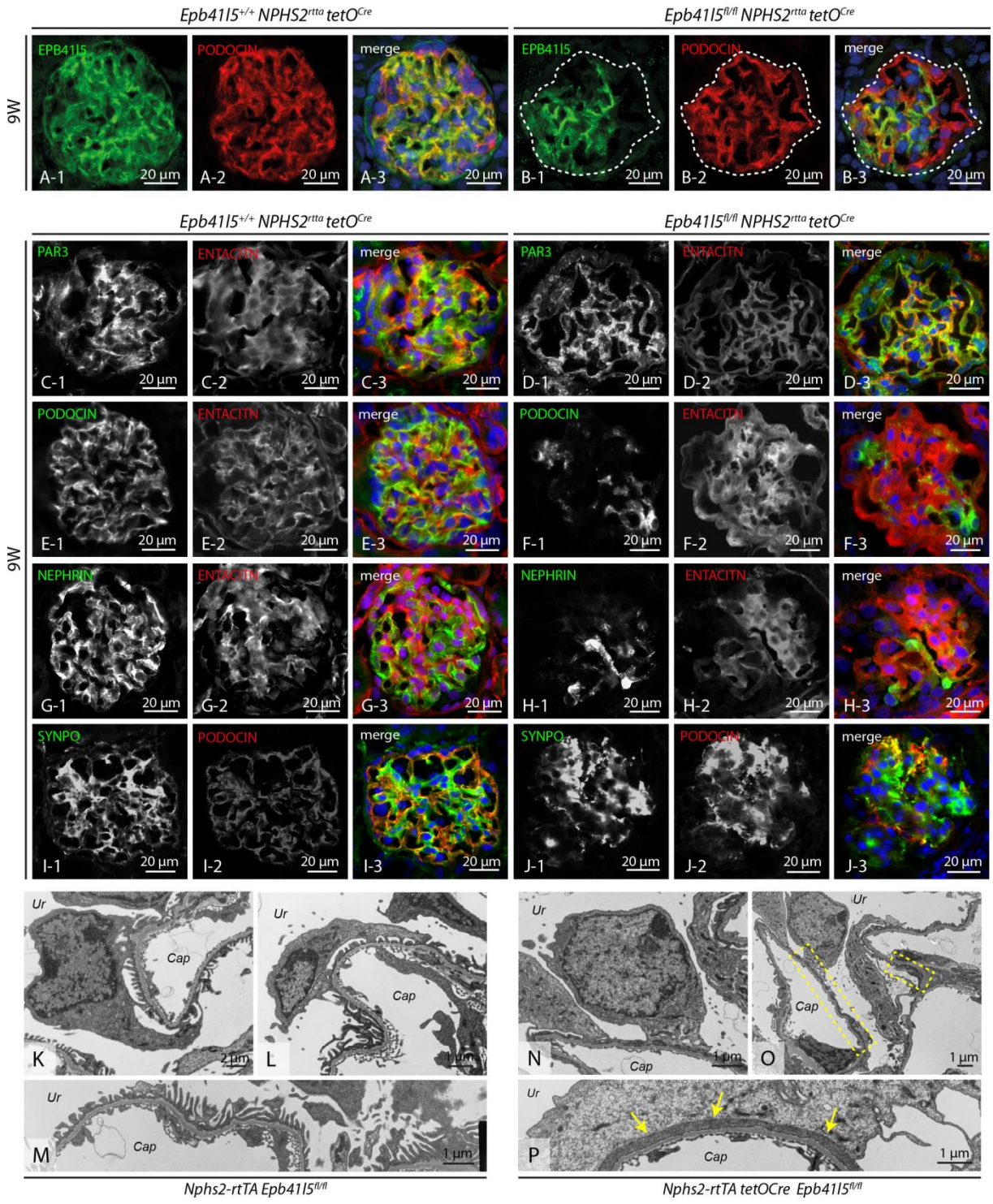

<u>Supplemental Figure 12</u>: Inducible deletion of *Epb41l5* in podocytes results in altered expression patterns of podocyte marker proteins.
(A&B) Immunofluorescence staining confirmed that EPB41L5 protein is reduced in *hNPHS2^{rtTA} tetO^{Cre} EPB41L5$^{fl/fl}$* animals. Due to incomplete recombination residual EPB41L5 protein was detectable in some podocytes. **(C-J)** After 5 weeks of induction typical slit diaphragm markers like PODOCIN and NEPHRIN showed a severely altered localization pattern, most likely due to heavy proteinuria in respective knockout animals **(E-H)**. In contrast, PAR3 showed only modest changes in localization and staining intensity **(C-D)**. In accordance with the massively disturbed

slit diaphragm proteins, also the cytoskeletal component SYNAPTOPODIN showed altered localization patterns **(I-J)**. **(K-P)** Electron microscopy revealed drastic alterations of FP morphology in respective induced knockout animals (boxed areas indicate zoomed details; yellow arrows highlight fused foot processes; Cap – capillaries; Ur – urinary space).

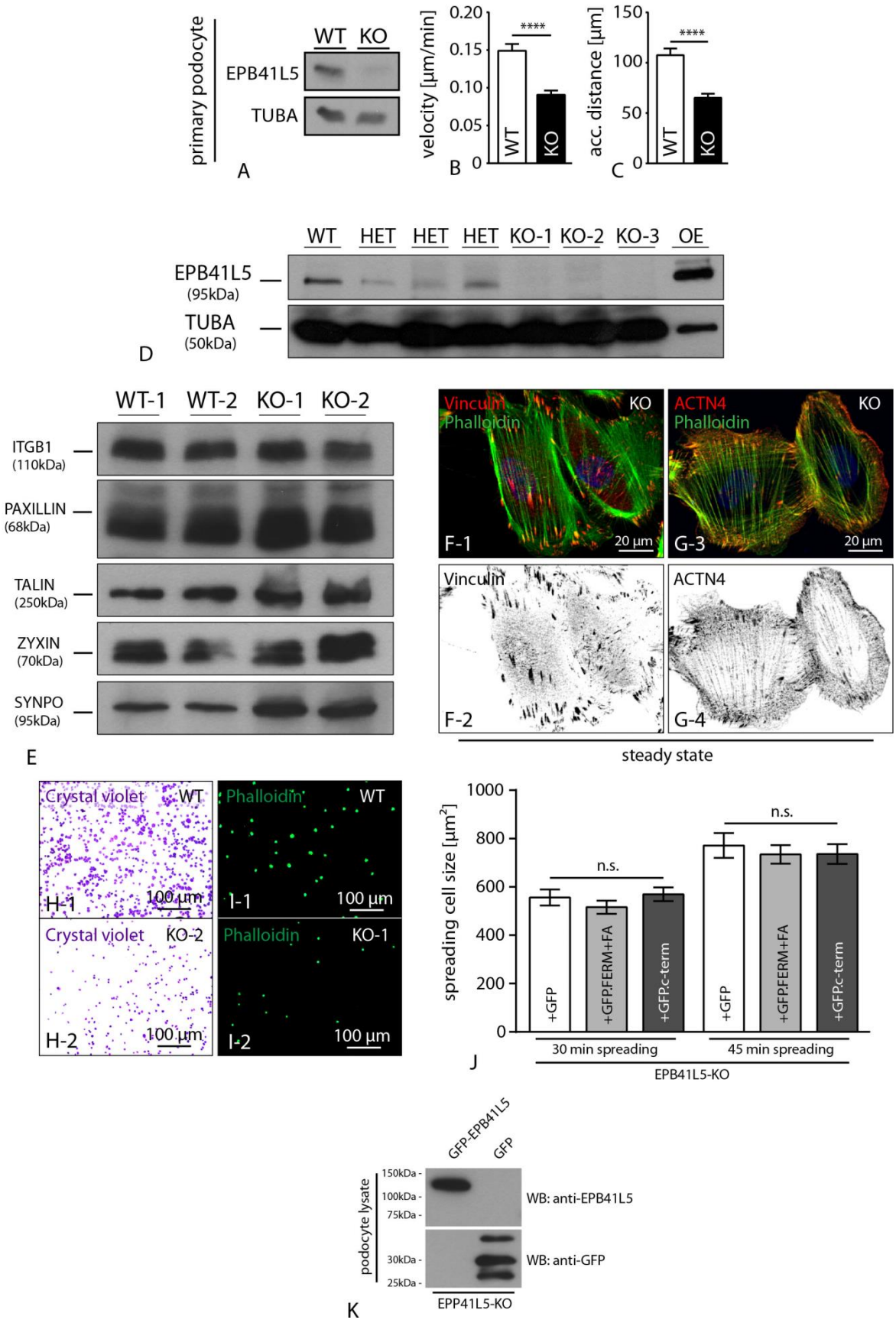

<u>Supplemental Figure 13</u>: Characterization of EPB41L5 knockout cell clones
(A-C) Western blot confirmed loss of EPB41L5 protein in primary podocytes from *Epb41l5* knockout animals. Epb41l5 knockout podocytes exhibited a decreased

migratory speed compared to wild type cells (at least n=50 cells over 3 independent experiments; dataset S3). **(D)** Western blot on different wild type, heterozygous and knockout CRISPR/CAS9 clones confirmed loss of protein in respective knockout podocytes (OE = overexpression of *EPB41L5*). **(E)** Western blot of wild type and *EPB41L5* knockout clones for different FA components did not detect major differences. **(F, G)** Staining for FA components VINCULIN and ACTININ-4 in *EPB41L5* knockout clones revealed normal morphology and no obvious alterations in terms of localization and intensity. **(H, I)** Overview images highlighting the different adhesion properties of respective EPB41L5 knockout clones compared to wild type controls. **(J)** Re-expression of FERM-domain as well as C-terminal EPB41L5 truncations were not capable of rescuing the spreading defect in EPB41L5 knockout cells (at least 87 cells were analyzed at both time points, for statistical data see dataset S3). **(K)** Western blot experiments confirm the efficient expression of GFP-tagged versions of EPB41L5 in transfected podocytes 48 post-transfection.

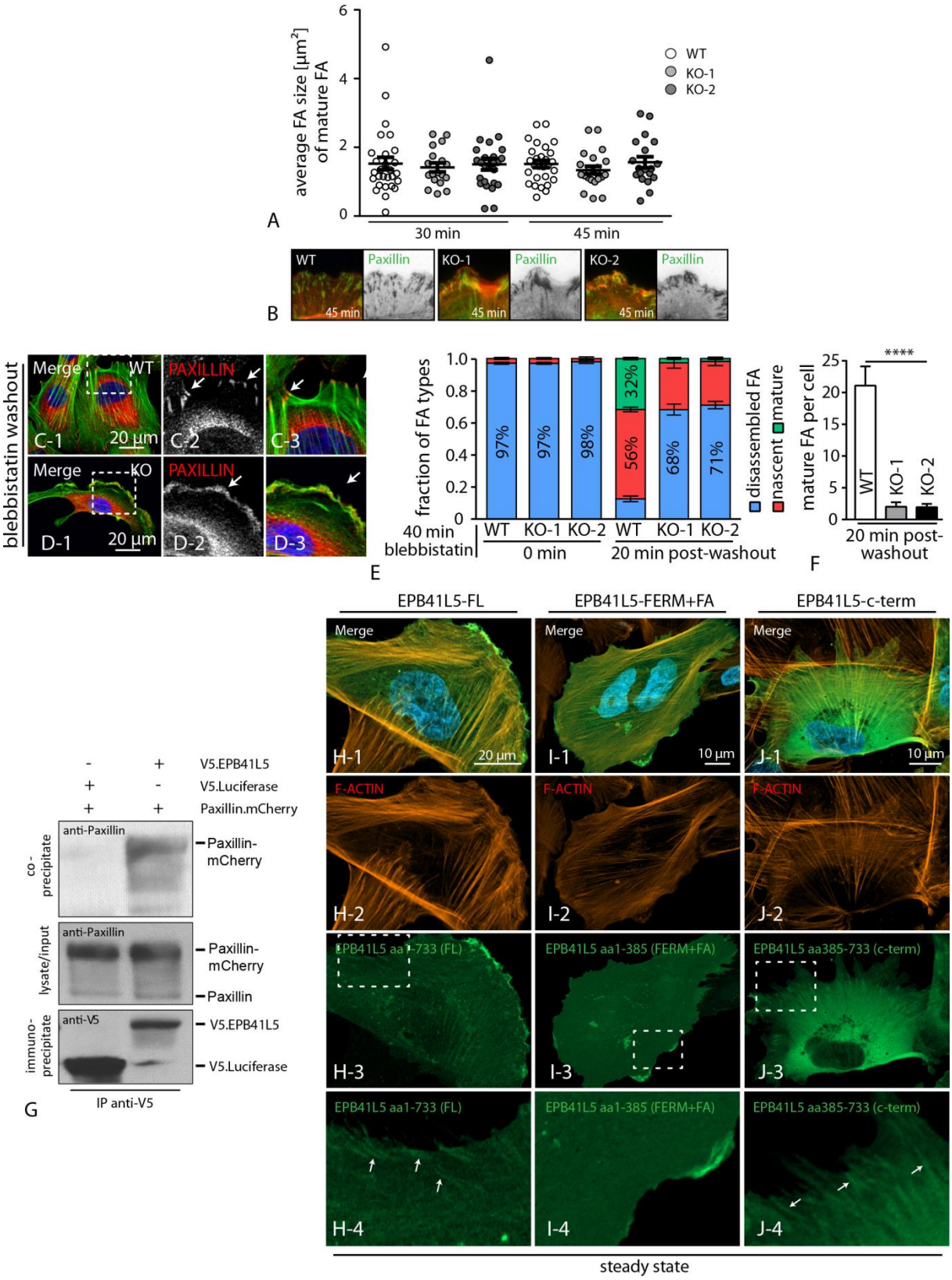

<u>Supplemental Figure 14</u>: EPB41L5 interacts with PAXILLIN

(A) Morphological analysis of focal adhesions at two different time points while cellular spreading detected no major differences between wild type and respective knockout clones (n=28, 18 and 25 at time point 30 minutes for WT, KO1 and KO2 respectively; n=28, 22 and 19 cells at time point 45 minutes for respective genotypes; averaged from 2 independent experiments, for statistical see dataset S3). **(B)**

PAXILLIN morphology at the leading edge of spreading cells at 45 minutes after spreading. **(C-E)** Impaired FA recovery after blebbistatin washout in knockout cells (more than 400 cells were analyzed; dataset S3). **(F)** Decreased number of mature FAs in *EPB41L5* KO cells after blebbistatin washout (n=20 cells, dataset S3). **(G)** Co-immunoprecipitation assay using epitope tagged versions of EPB41L5 and Paxillin in HEK293T cells, tagged luciferase was included as a control. **(H-J)** Expression of either full length, or FERM-domain as well as C-terminal truncations of EPB41L5 revealed that only the C-terminal part and the full-length version of EPB41L5 result in a FA localization pattern (white arrows). In contrast, the FERM-domain containing truncation showed a more membranous localization pattern (Phalloidin was used as a co-labeling; boxed areas indicate zoomed details).

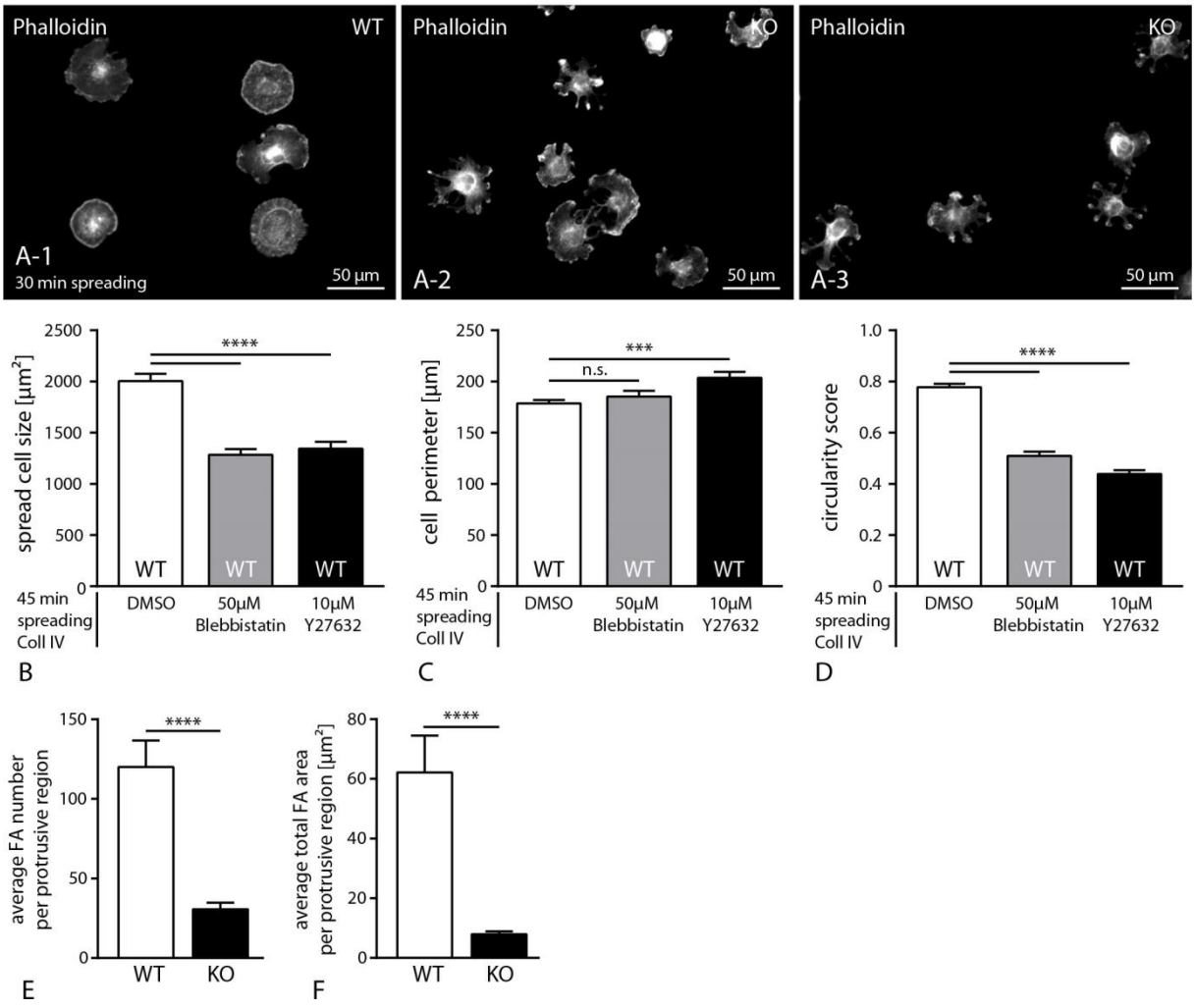

<u>Supplemental Figure 15</u>: Inhibition of the actomyosin machinery during dynamic cellular processes leads to a phenocopy of *Ebp41l5* knockout in wild type cells

(A) Representative images illustrating morphological difference between wild type and knockout cells while cellular spreading (30 min spreading on collagen IV coated glass cover slips; representative low magnification images from at least 5 independent experiments). **(B-D)** Quantification of cellular spreading size, perimeter and circularity of wild type cells pretreated with either blebbistatin or Y27632 during spreading (more than 150 cells per condition were quantified over 3 independent experiments; for statistics see the material and methods section). **(E, F)** Quantification of FA in pseudopods of spreading EPB41L5 knockout cells demonstrating lower FA numbers as well as decreased average total FA area (n=12 WT and 23 KO cells were analyzed, for statistics see dataset S3)

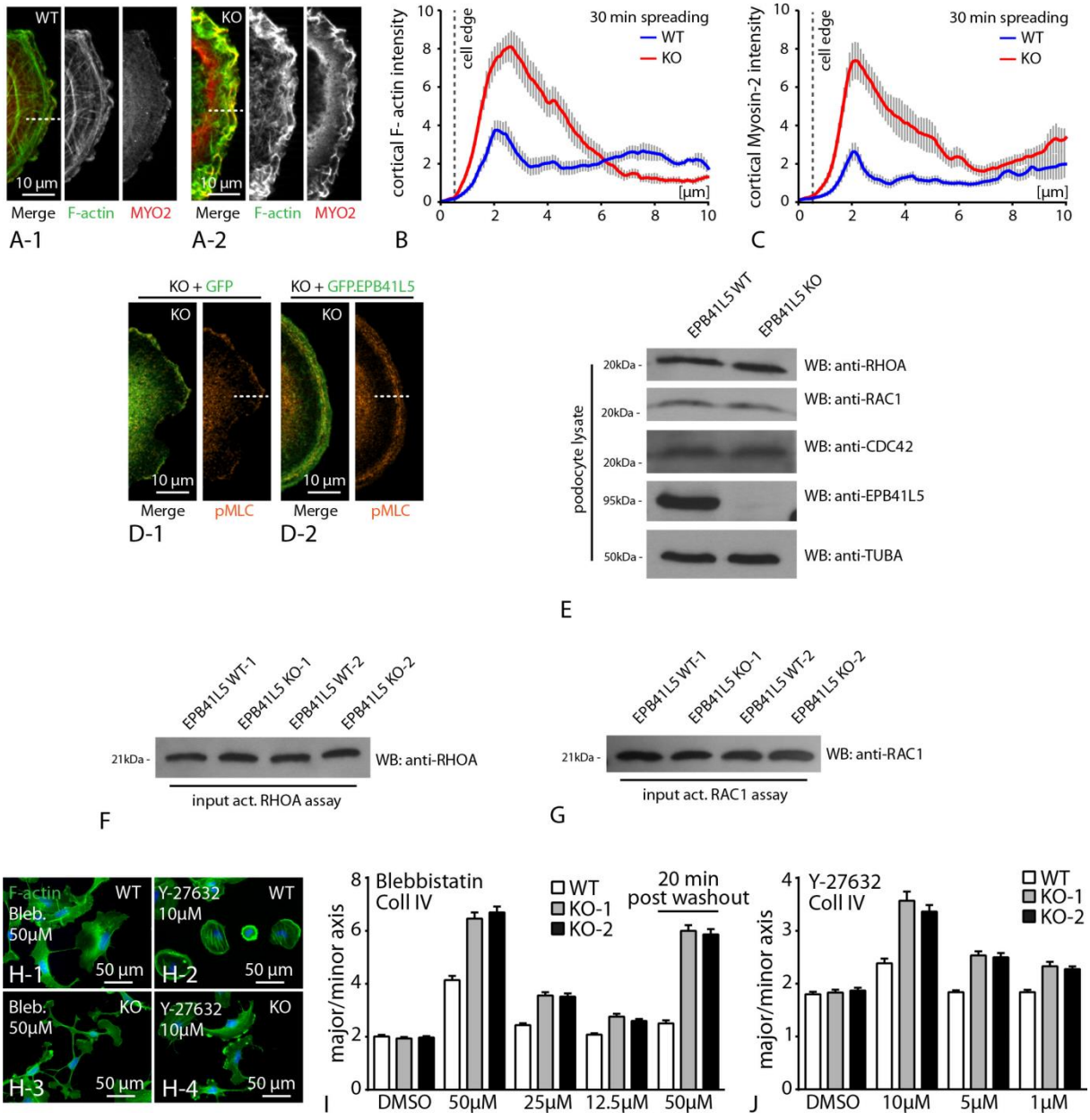

<u>Supplemental Figure 16</u>: Equal total levels of RhoA and RAC1 in EPB41L5 knockout cells

(A) Representative immunofluorescence for MYOSIN-II at the leading edge of wild type and EPB41L5 KO cells: accumulation of F-actin and MYOSIN-II was detected at the leading edge of KO cells. **(B-C)** Representative line scans for MYOSIN-II and F-actin across the cell edge (grey lines indicate respective SDs; at least 10 cells per condition). **(D)** Immunofluorescence for pMLC in EPB41L5 knockout cells with re-expression of full length EPB41L5 (white dotted line indicates area at the leading edge, selected for measurements represented in the main figures). **(E)** Western blot for various GTPases demonstrating equalized total levels between wild type and knockout cells. (**F, G)** Representative western blot for RhoA and Rac1 total levels out of equalized input lysates in G-Lisa assay. **(H-J)** Treatment with blebbistatin or Y-27632 led to pronounced morphological alterations in EPB41L5 KO cells when compared to wild type cells. (at least n=89 cells over 3 independent experiments; dataset S3).

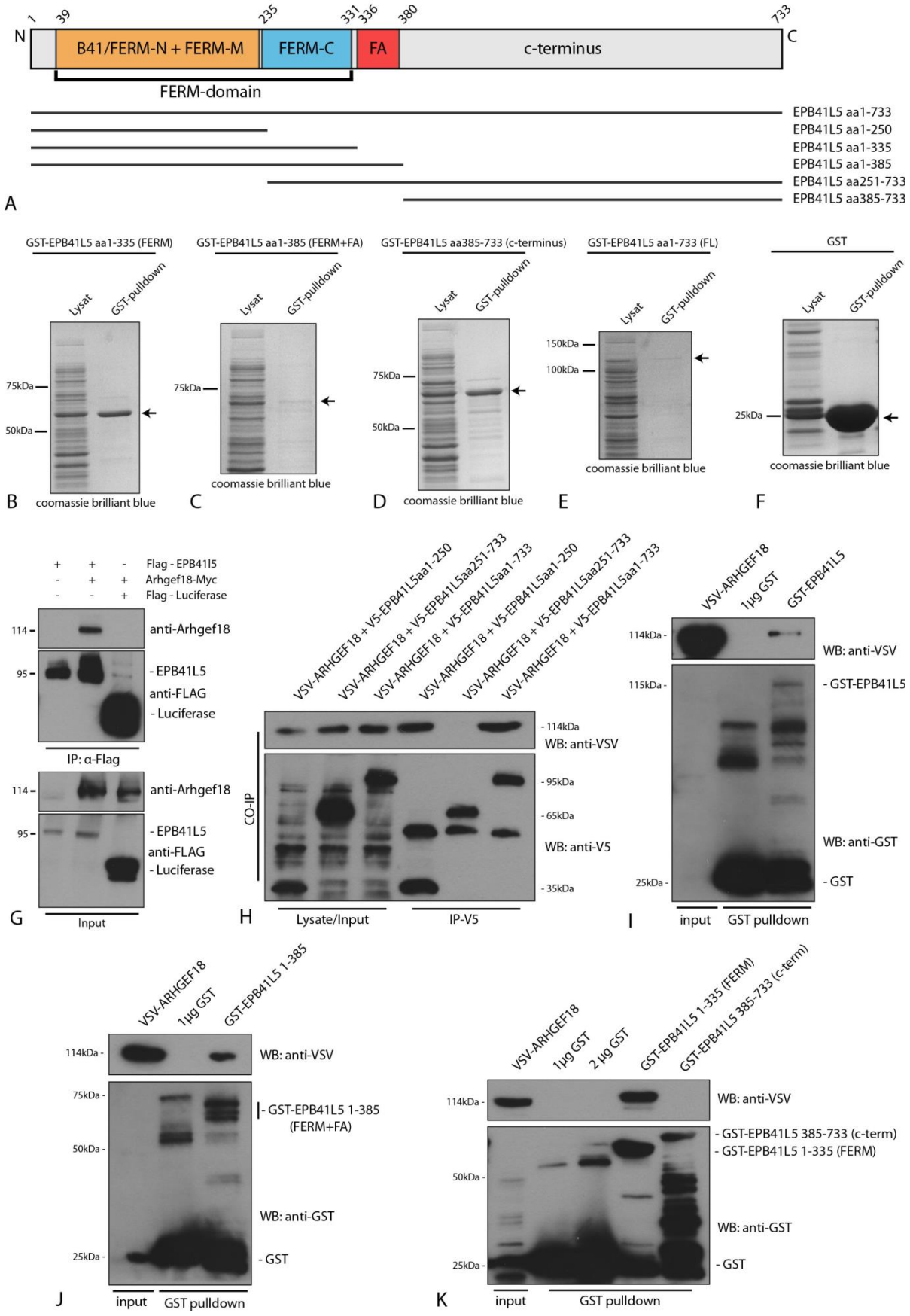
1
39
235
331
336
380
733
N
C
B41/FERM-N + FERM-M
FERM-C
FA
c-terminus
FERM-domain
EPB41L5 aa1-733
EPB41L5 aa1-250
EPB41L5 aa1-335
EPB41L5 aa1-385
EPB41L5 aa251-733
EPB41L5 aa385-733
A
GST-EPB41L5 aa1-335 (FERM)
GST-EPB41L5 aa1-385 (FERM+FA)
GST-EPB41L5 aa385-733 (c-terminus)
GST-EPB41L5 aa1-733 (FL)
GST
Lysat
GST-pulldown
75kDa
50kDa
150kDa
100kDa
25kDa
coomassie brilliant blue
B
C
D
E
F
+ + - Flag - EPB41l5
- + + Arhgef18-Myc
- - + Flag - Luciferase
114
95
anti-Arhgef18
- EPB41L5
anti-FLAG
- Luciferase
IP: α-Flag
Input
G
VSV-ARHGEF18 + V5-EPB41L5aa1-250
VSV-ARHGEF18 + V5-EPB41L5aa251-733
VSV-ARHGEF18 + V5-EPB41L5aa1-733
- 114kDa
WB: anti-VSV
- 95kDa
- 65kDa
WB: anti-V5
- 35kDa
CO-IP
Lysate/Input
IP-V5
H
VSV-ARHGEF18
1µg GST
GST-EPB41L5
114kDa -
115kDa -
25kDa -
WB: anti-VSV
- GST-EPB41L5
WB: anti-GST
- GST
input
GST pulldown
I
VSV-ARHGEF18
1µg GST
GST-EPB41L5 1-385
114kDa -
75kDa -
50kDa -
25kDa -
WB: anti-VSV
- GST-EPB41L5 1-385
(FERM+FA)
WB: anti-GST
- GST
input
GST pulldown
J
VSV-ARHGEF18
1µg GST
2 µg GST
GST-EPB41L5 1-335 (FERM)
GST-EPB41L5 385-733 (c-term)
114kDa -
50kDa -
25kDa -
WB: anti-VSV
- GST-EPB41L5 385-733 (c-term)
- GST-EPB41L5 1-335 (FERM)
WB: anti-GST
- GST
input
GST pulldown
K

<u>Supplemental Figure 17</u>: ARHGEF18 and EPB41L5 interaction studies
(A) Schematic depicting the domain structure of EPB41L5 and including the various used truncations. **(B-F)** Coomassie blue staining of respective GST-tagged truncated protein versions indicated different efficiencies in protein expression due to protein size (note FERM-domain and C-terminal truncations showed the best expression efficiency). **(G)** Co-immunoprecipitation assay with epitope tagged versions of EPB41L5 and ARHGEF18 in HEK293T cells, FLAG-tagged Luciferase was included as a control. Precipitated ARHGEF18 was detected using antibody directed against ARHGEF18. **(H)** Mapping studies using additional truncations of EPB41L5 together with overexpressed ARHGEF18; only full length EPB41L5 and the FERM-domain (FERM A+B/B41 domain) containing truncation was able to precipitate ARHGEF18. **(I-K)** GST-pulldown experiments using either full-length EPB41L5 recombinant protein, or respective truncations (FERM, FERM+FA, or C-terminal domain) in combination with epitope tagged ARHGEF18. Note: only the FERM-domain containing truncated protein versions showed successful pulldown of ARHGEF18.

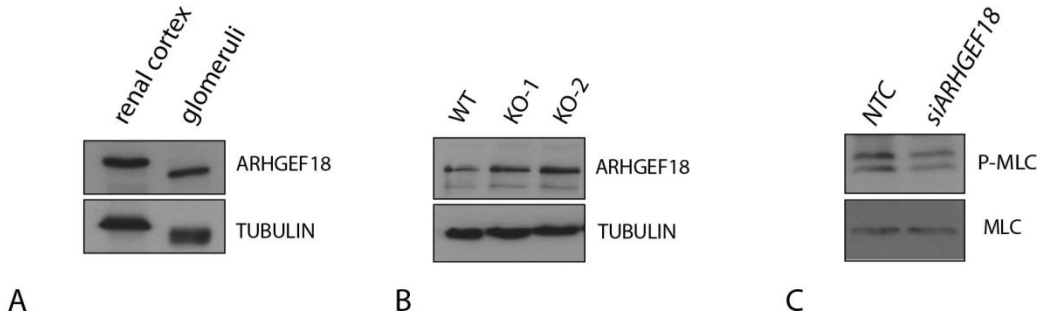

<u>Supplemental Figure 18</u>: ARHGEF18 expression in wild type murine kidneys and EPB41L5 knockout cells

(A) Western blot for ARHGEF18 in adult murine renal cortices and isolated glomeruli; TUBULIN was used as a loading control. **(B)** Western blot experiments for ARHGEF18 in EPB41L5 and wild type control cells revealed equal levels for ARGEFH18. **(C)** Decreased levels of p-MLC upon knockdown with ARHGEF18 siRNA; MLC total levels were used as input controls.

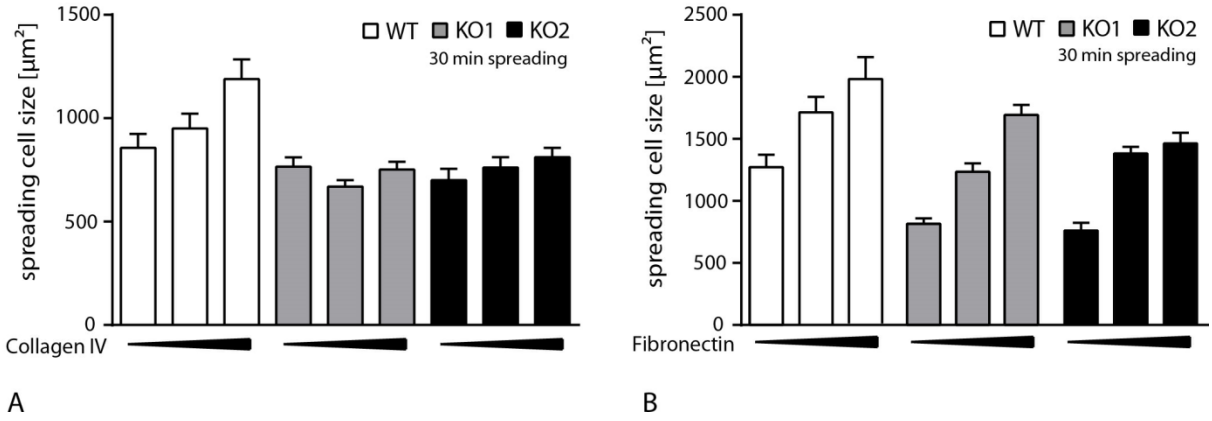

<u>Supplemental Figure 19</u>: ECM composition and concentration differentially influences EPB41L5 dependent spreading defect

(A, B) Analysis of cell spreading depending on ECM coating and concentration (collagen IV and fibronectin): A clear response to increasing fibronectin concentrations was observed in wild type cells as well as knockout clones. This response was partially observed also on collagen IV, but here solely in wild type cells (one representative experiment out of 3 independent experiments, for statistics see dataset S3).

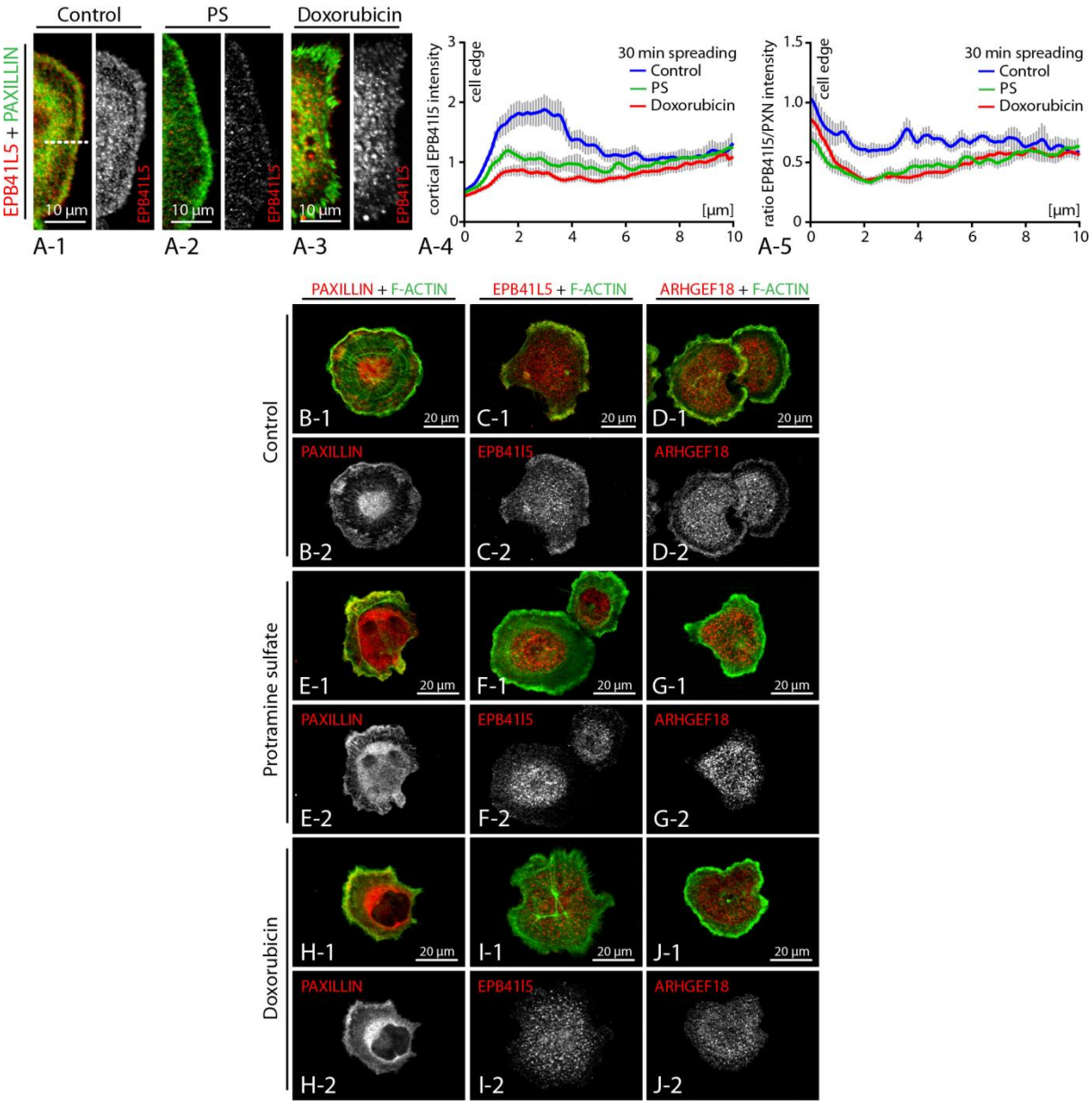

<u>Supplemental Figure 20</u>: EPB41L5 is sensitive towards podocyte toxic substances

(A) Immortalized human podocytes were treated with either protamine sulfate or doxorubicin and stained for EPB41L5 and PAXILLIN. Compared to control cells EPB41L5 exhibited a decreased signal intensity at the leading edge of either PS or doxorubicin treated cells as highlighted in depicted line scans (A4 and A5). **(B-J)** EPB41L5 as well as ARHGEF18 localize towards the leading edge in spreading podocytes. Treatment with podocyte toxic substances such as protamine sulfate or doxorubicin resulted in diminished signal intensity for both proteins, whereas F-actin was still present at the leading edge zone.

Supplemental Movies S1-S5

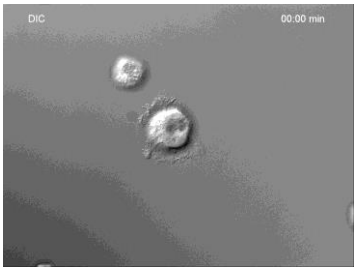

Movie S1 – EPB41L5 KO – DIC

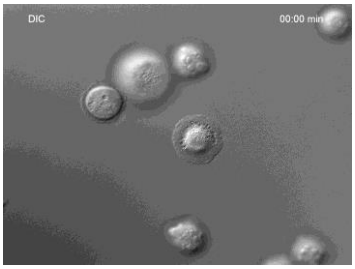

Movie S2 – Wild type podocyte – DIC

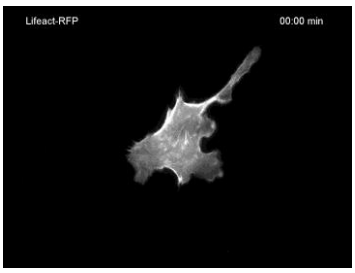

Movie S3 – EPB41L5 KO – Lifeact-RFP

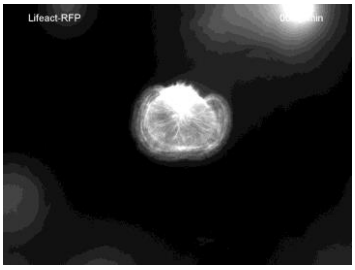

Movie S4 – Wild type podocyte – Lifeact-RFP

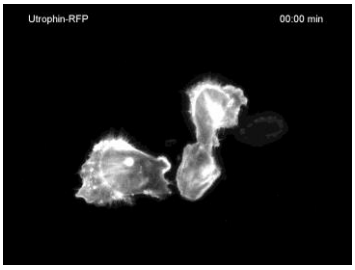

Movie S5 – EPB41L5 KO – Utrophin-RFP

<u>Supplemental Movies S1-5</u>: Visualization of spreading EPB41L5 KO and wild type cells, using DIC, Life-Act-RFP and Utrophin-RFP

Live cell imaging of spreading EPB41L5-KO and WT cells was performed using differential interference contrast (*DIC*) microscopy or fluorescence microscopy employing either Life-Act-RFP or Utrophin-RFP as actin probes.

Supporting Information -
Antibodies

Protein	Clone	Species	Manufacturer	Application
act. INTEGRIN-beta1	9EG7	rat	BD Transduction Lab.	WB (1:1000)
ACTININ-4		rabbit	Abcam	IF (1:200), WB (1:1000)
ARHGEF18		rabbit	Origene	IF (1:100)
ARHGEF18	HPA042689	rabbit	Atlas Antibodies	IF (1:100), WB (1:1000), IP (1:100)
B-ACTIN		mouse	Sigma	WB (1:1000)
CDC42	sc-87	rabbit	Santa Cruz	WB (1:1000)
CRUMBS3		rabbit	Sigma	IF (1:100)
EPB41L5	HPA037563	rabbit	Atlas Antibodies	IF (1:100), WB (1:500)
EPB41L5	HPA037564	rabbit	Atlas Antibodies	IF (1:50)
EPB41L5		rb,gp	gen. gift R. Roepman	IF (1:100), WB (1:1000)
FLAG	M2	mouse	Sigma	WB (1:1000)
FLNA	sc-28284	rabbit	Santa Cruz	WB (1:1000)
GFP	sc-9996	mouse	Santa Cruz	WB (1:1000)
GST	27-4577-01	goat	amersham pharmacia biotech	WB (1:1000)
INTEGRIN-beta1	M-106	rabbit	Santa Cruz	WB (1:1000)
ITGA2	AB1936	rabbit	Millipore	WB (1:1000)
ITGAV	ab179475	rabbit	Abcam	WB (1:1000)
MLC	3672	rabbit	Cell Signaling	WB (1:1000)
MYOSIN-II		rabbit	Covance	IF (1:100)
MYPT1	8574	rabbit	Cell Signaling	WB (1:1000)
NEPHRIN	gp-N2	gp	Progene	IF (1:300)
NIDOGEN	MAB1946	rat	Millipore	IF (1:300)
PAR3		rabbit	Millipore	IF (1:100)
PAXILLIN		mouse	BD Transduction Lab.	IF (1:300),WB (1:1000)
P-MLC	3674	rabbit	Cell Signaling	IF (1:100), WB (1:500)
P-MLC	3671	rabbit	Cell Signaling	IF (1:100), WB (1:500)
pMYPT1	5163	rabbit	Cell Signaling	WB (1:500)
PODOCALYXIN		mouse	gift from Tsilibary E	IF (1:100)
PODOCIN		rabbit	Sigma	IF (1:200)
P-PAXILLIN	2541	rabbit	Cell Signaling	WB (1:1000)
RAC1	240106	mouse	Cell Biolabs	IF (1.100) WB (1:1000)
RHOA	ARH03	mouse	Cytoskeleton	IF (1:100), WB (1:500)
SCRIBBLE		rabbit	Santa Cruz	IF (1:125)
SYNAPTOPODIN		mouse	Progene	IF (1:300)
TALIN		mouse	Sigma	IF (1:100)
TUBULIN		mouse	Sigma	WB (1:1000)
V5	MCA1360	mouse	Serotec	WB (1:1000), IP(1:2000)
VINCULIN	SPM227	mouse	Abcam	IF (1:100), WB (1:1000)
VSV	ab18612	rabbit	Abcam	WB (1:1000), IP(1:1000)
WT-1	clone 6F-H2	mouse	Millipore	IF (1:200), WB (1:1000)
ZYXIN	HPA004835	rabbit	Atlas Antibodies	IF (1:100)

Anti-Flag M2 Agarose Affinity beads			Sigma	IP (25µl/1ml Lysate)
Glutathione Sepharose			GE Healthcare	IP (25µl/1ml Lysate)

Supporting Information – uncropped Western Blots

F3D
WB: EPB41l5

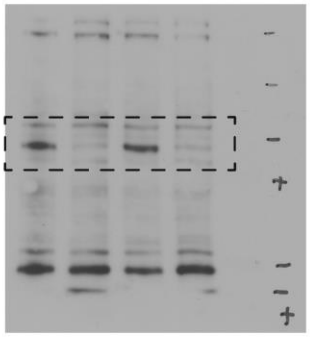

F3D
WB: TUBA

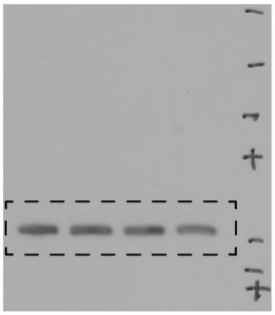

F3P
WB: WT1

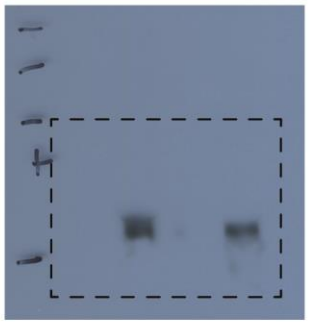

F3R
WB: EPB41L5

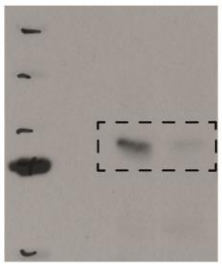

F3R
WB: TUBA

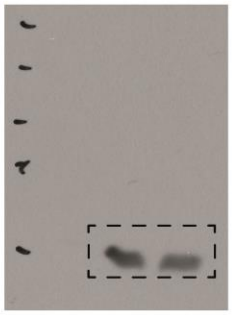

F4B
WB: EPB41L5

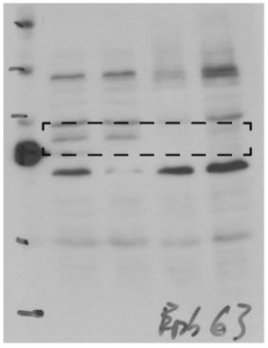

F4B
WB: TUBA

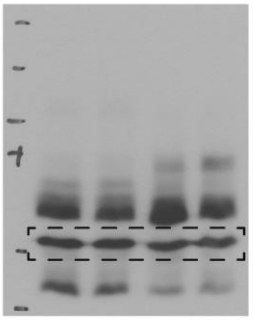

F4Q
WB: GST

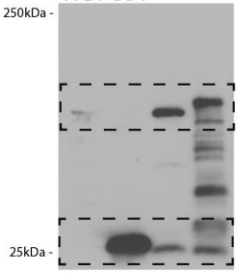

F4Q
WB: PAXILLIN

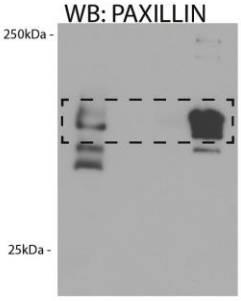

F4Q
WB: ITGB1

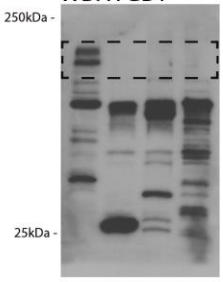

F4Q
WB: ITGAV

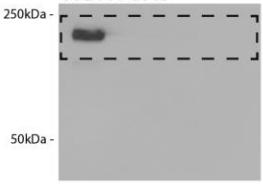

F5R
WB: p-MLC

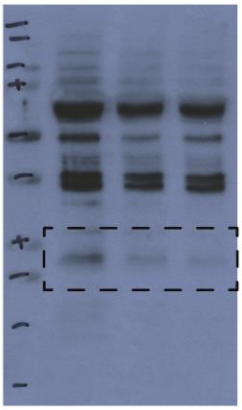

F5R
WB: MLC

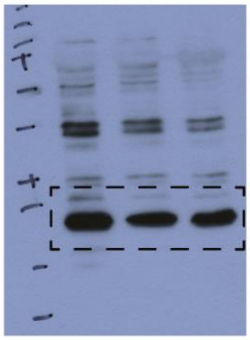

F5R
WB: TUBA

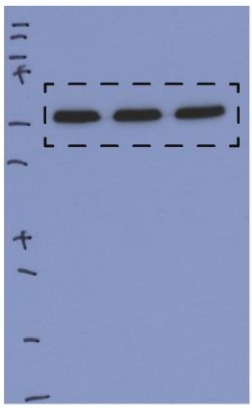

F5R
WB: p-MYPT1

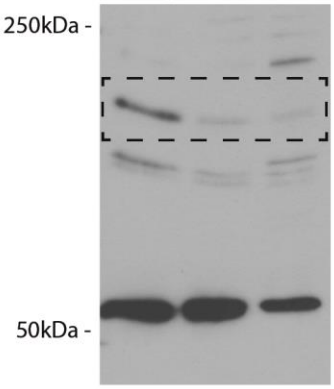

F5R
WB: MYPT1

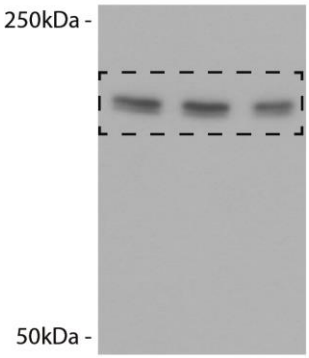

F5W
WB: p-MLC

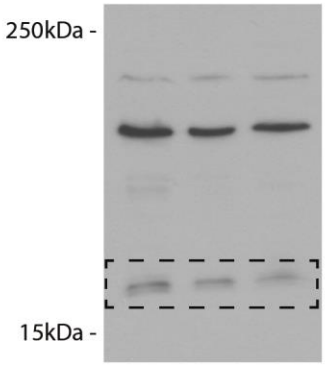

F5W
WB: MLC

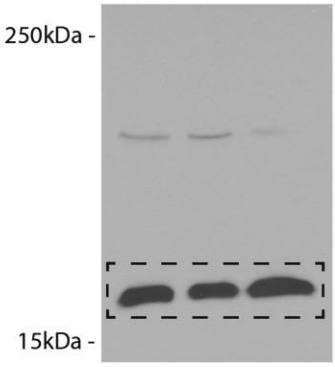

F5W
WB: p-MYPT1

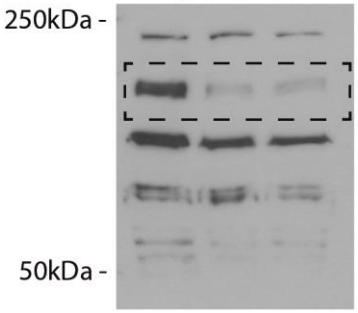

F5W
WB: MYPT1

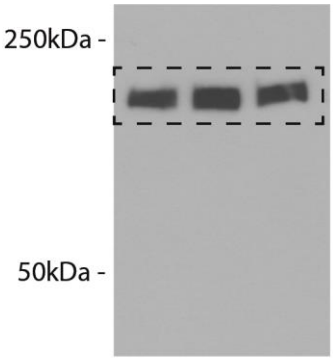

F5W
WB: TUBA

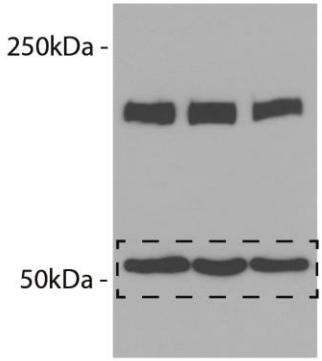

F6B
WB: EPB41L5

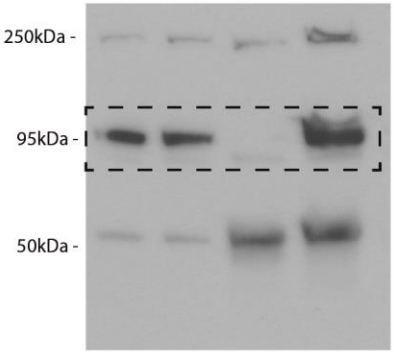

F6B
WB: ARHGEF18

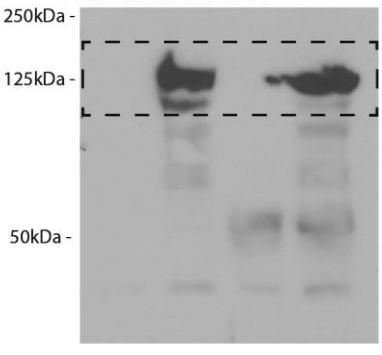

F6B
WB: GFP

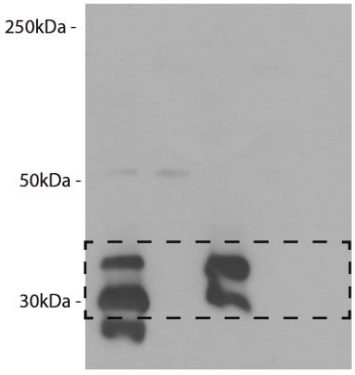

F6C
WB: ARHGEF18

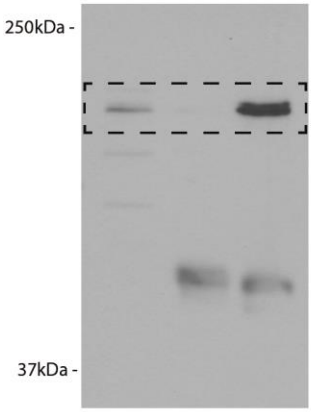

F6C
WB: EPB41L5

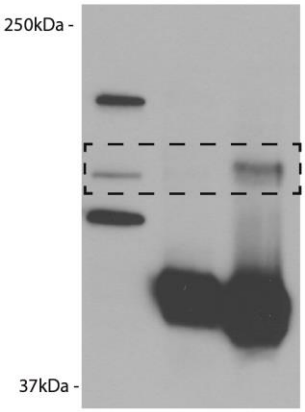

F6D
WB: VSV

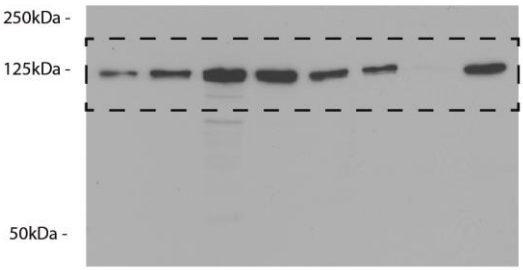

F6D
WB: FLAG

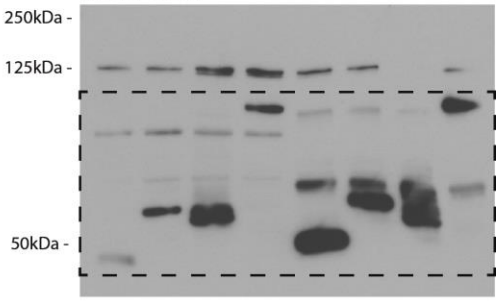

F6E
WB: ARHGEF18

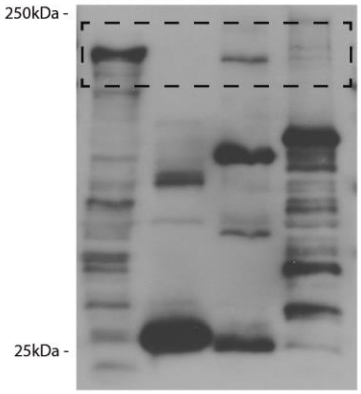

F6E
WB: GST

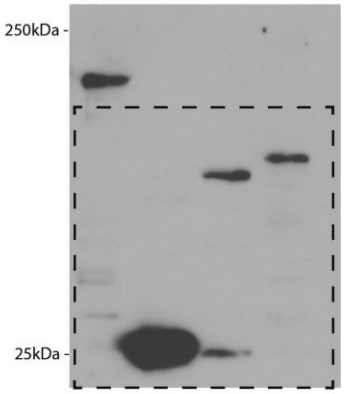

F6F
WB: ARHGEF18

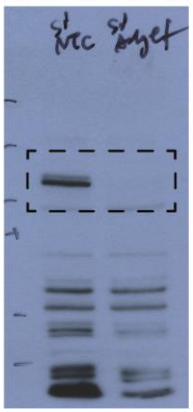

F6F
WB: TUBA

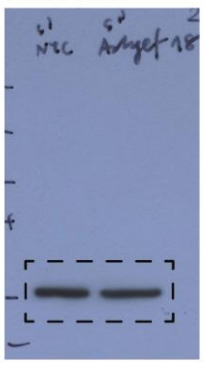

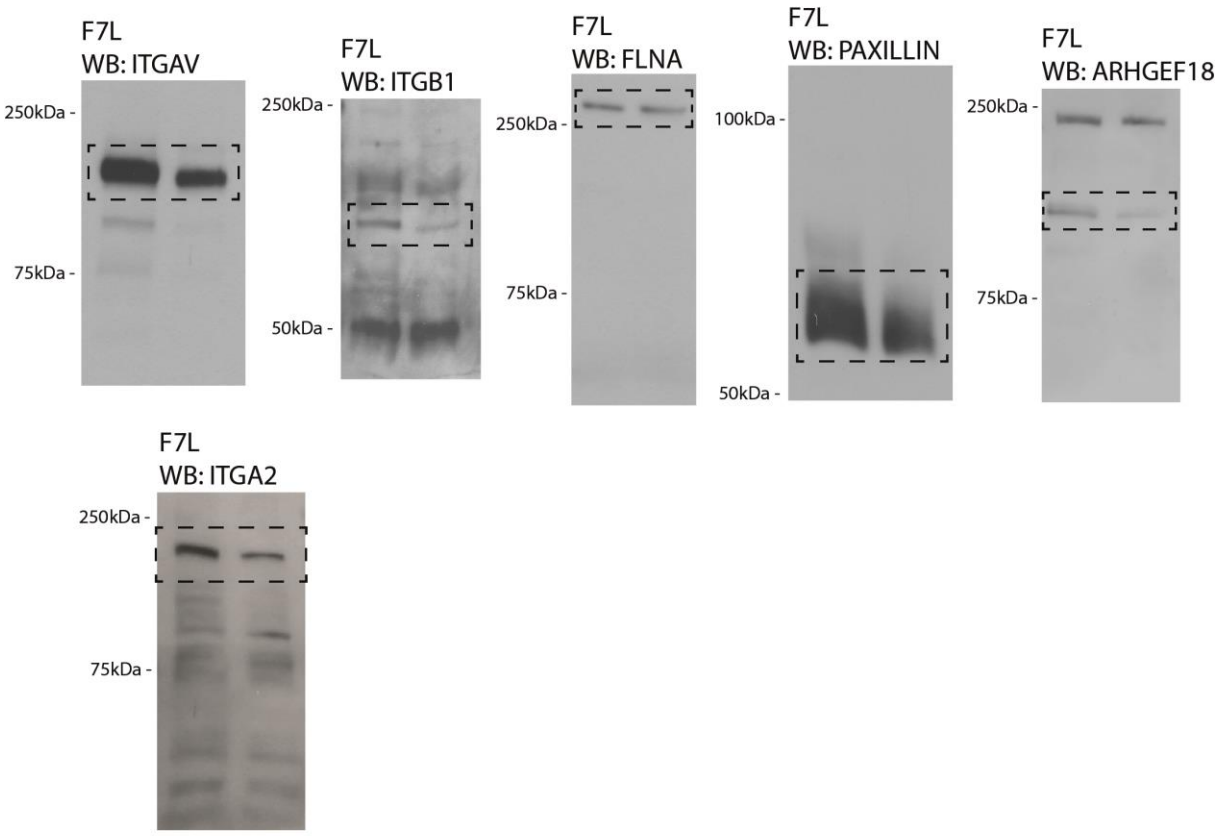
F7L
WB: ITGAV
250kDa -
75kDa -
F7L
WB: ITGB1
250kDa -
50kDa -
F7L
WB: FLNA
250kDa -
75kDa -
F7L
WB: PAXILLIN
100kDa -
50kDa -
F7L
WB: ARHGEF18
250kDa -
75kDa -
F7L
WB: ITGA2
250kDa -
75kDa -

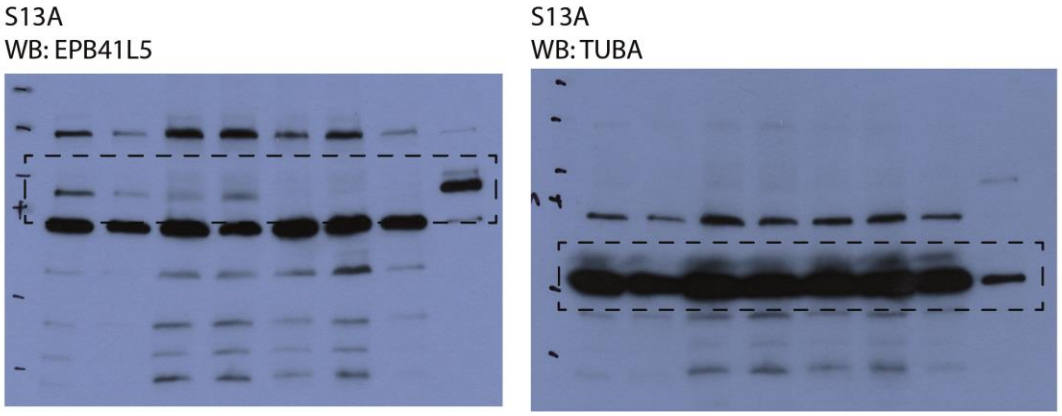
S13A
WB: EPB41L5
S13A
WB: TUBA

S13B
WB: SYNPO

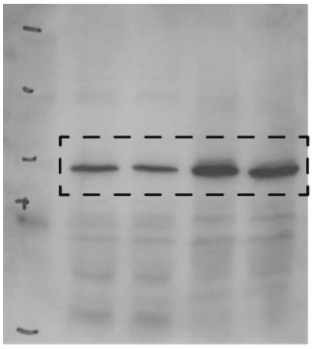

S13B
WB: Talin

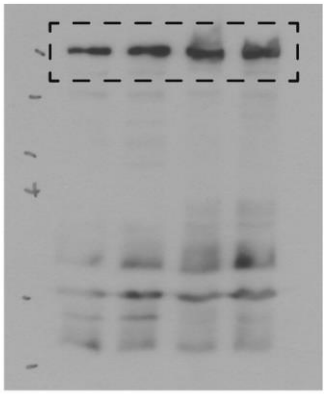

S13B
WB: Paxillin

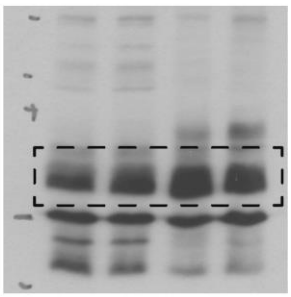

S13B
WB: ITGB1

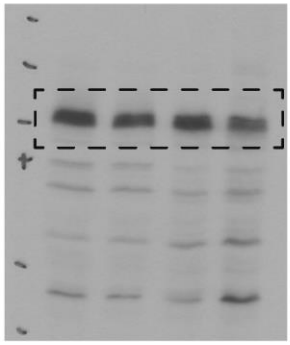

S13B
WB: Zyxin

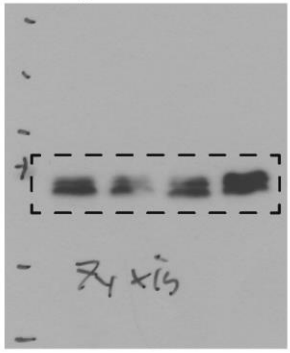

S13G
WB: EPB41L5

S13G
WB: GFP

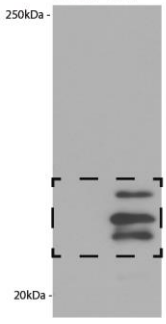

S14A
WB: Paxillin

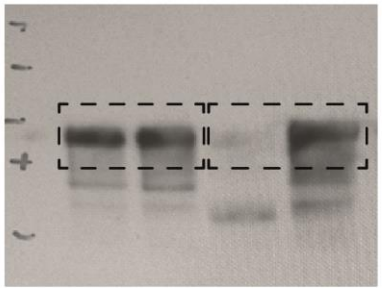

S14A
WB: V5

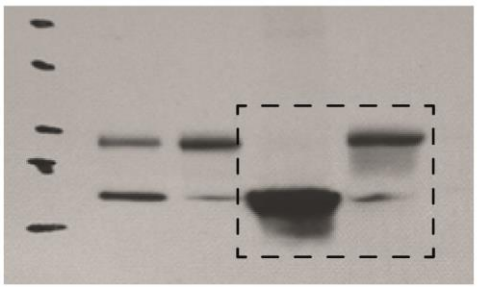

S16E
WB: RAC1

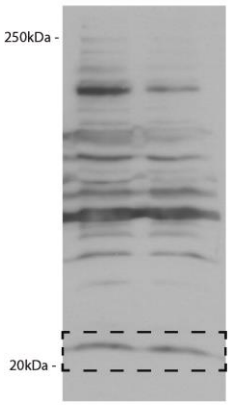

S16E
WB: CDC42

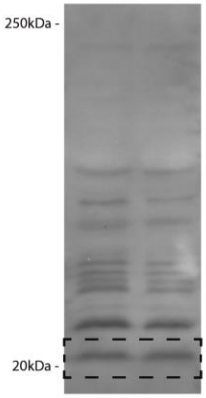

S16E
WB: RHOA

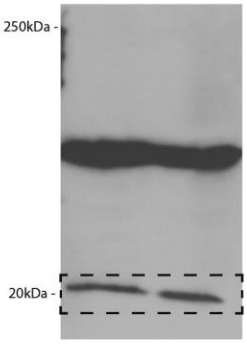

S16E
WB: TUBA

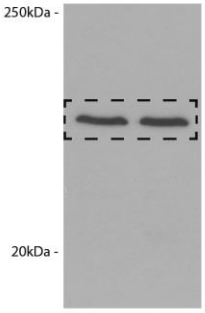

S16E
WB: EPB41L5

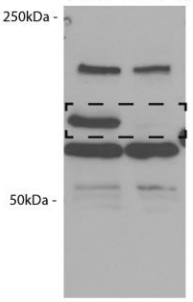

S16F
WB: RHOA

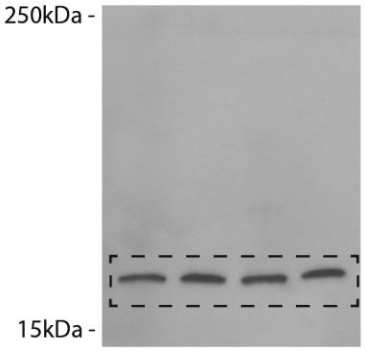

S16G
WB: RAC1

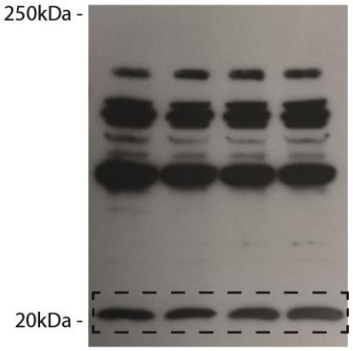

S17G
WB: ARHGEF18

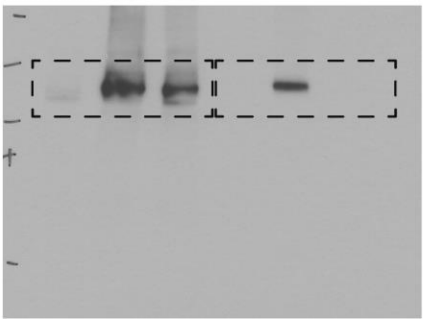

S17G
WB: FLAG

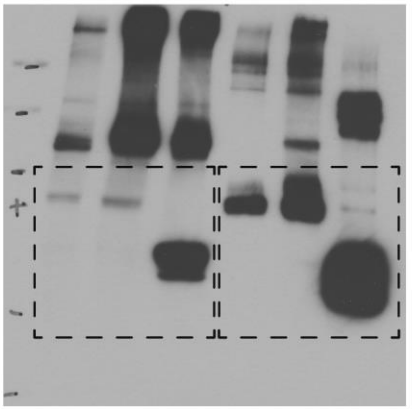

S17H
WB: V5

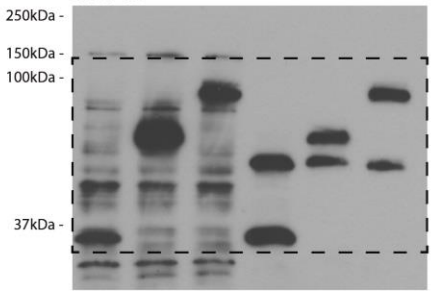

S17H
WB: VSV

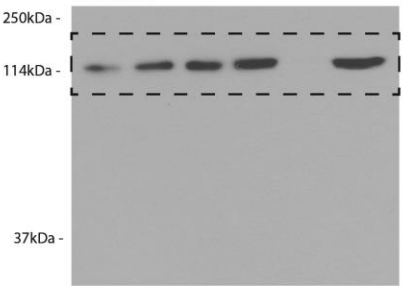

S17I
WB: VSV

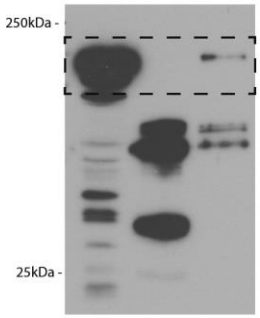

S17I
WB: GST

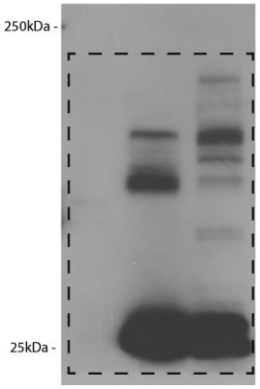

S17J
WB: GST

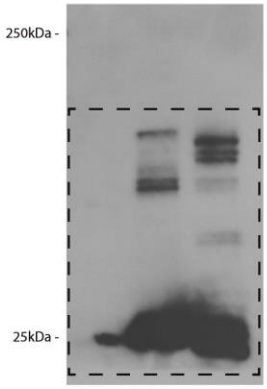

S17J
WB: VSV

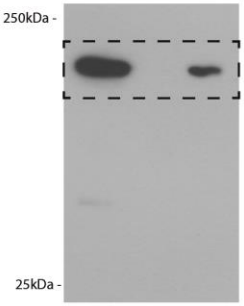

S17K
WB: VSV

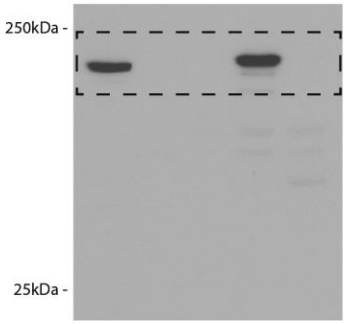

S17K
WB: GST

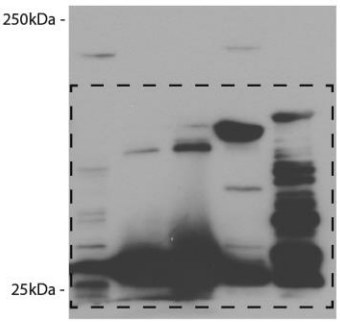

S18A
WB: ARHGEF18

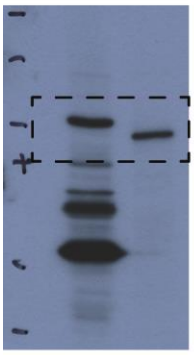

S18A
WB: TUBA

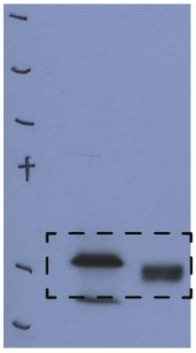

S18B
WB: ARHGEF18

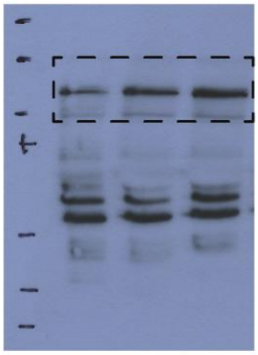

S18B
WB: TUBA

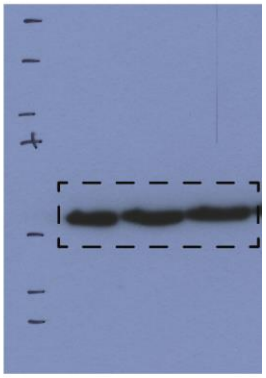

S18C
WB: p-MLC

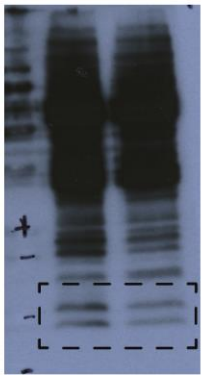

S18C
WB: MLC